Delft University of Technology

# Direct Current Power Flow

## Computational methods and low voltage applications

**MSc Thesis**

Dario Chaifouroosh Mamagany

TU Delft

# Direct Current Power Flow

## Computational methods and low voltage applications

by

**Dario Chaifouroosh Mamagany**

in partial fulfillment of the requirements for the degree of

**Master of Science**
in Sustainable Energy Technology

at Delft University of Technology
to be defended publicly on Monday June 25th, 2018 at 13:00

| | | |
|---|---|---|
| Supervisor: | Prof. dr. ir. Pavol Bauer | DCE&S |
| Thesis committee: | dr. ir. Laura Ramírez Elizondo | DCE&S |
| | dr. ir. José Rueda Torres | IEPG |
| | Nils van der Blij | DCE&S |



TU Delft

DCE&S
DC systems, Energy conversion & Storage

# Acknowledgements

Conducting for the first time research on my own, for this thesis, has been a challenging but enriching experience that I would not have been able to complete without the precious help of the people around me. I would like to thank my daily supervisor Nils for guiding me through the tough but exciting topic that is developed in this thesis. Thanks also to Laura for reading my content and supervising me in my student assistant job for the microgrids MicroMaster: it allowed me to better understand the topic of my thesis.

Next, I want to thank my crew at Frank van Borselenstraat (first and second edition!) and all of my super international and amazing friends for the unforgettable time spent together. Thanks to my parents for supporting me always and always believing in me, often way more than I have believed in myself. Last but not least, thanks to Karolina, who has constantly been there with me and for me. *Dziękuję bardzo*.

I would not have completed my Masters without all of you.

Delft,
June 20th, 2018

# Abstract

Technical developments in generation and demand of energy will motivate significant change in the electric power grid, both on the transmission and the distribution level. A major innovation would be the successful transformation of the current passive power grid towards an active and ICT-based smart grid. Among the technical efforts that will help to pursue this goal, the renewed interest in DC (direct current) distribution and transmission applications is playing an important role. In particular, the interest in the DC universal distribution networks is renewed since most of the renewable energy generation technologies (e.g. PV modules, fuel cells) and loads (e.g. LED lighting, electric vehicles) are DC-native. Their direct connection would allow to skip conversion steps, thus providing higher efficiency.

The focus of this thesis lies on the steady-state power flow analysis, a numerical study used in electrical engineering to assess the flows of power in the network. The aim of the thesis is to review the state of the art in computational methods for AC and DC power flow analysis and to determine a suitable method to develop a power flow tool for the DC framework.

The literature study revealed that most algorithms aim to solve the non-linear power flow problem without taking into account characteristics typical of future DC networks, such as highly meshed topologies and constant power converters. An innovative power flow method has therefore been developed in order to include different node behaviours, such as constant voltage, constant current, constant impedance, constant power and I-V droop control. A case study based on the IEEE European Low-Voltage Test Feeder is analysed to provide an example of the application of the power flow tool.

The thesis shows that it is possible to linearize the system equations considering the constant power node either as a current source or as a parallel of current source and impedance. Both methods allow very fast convergence for complex meshed networks, and can therefore be adopted for diverse studies such as market analysis and N-1 redundancy analysis, among others.

# Table of Contents

# List of Figures

# List of Tables

# Chapter 1

# Introduction

## Table of Contents



This chapter provides the background of the thesis and its structure. In section 1.1 the motivation of the thesis is given. In section 1.2 the scope and goals of the thesis are defined. Then, in section 1.3 the research questions are provided with a detailed explanation of what the thesis topic is about and what is the perspective chosen to pursue the research goal. Section 1.4 presents the research methodology used along the thesis work. Finally, section 1.5 provides the reader with the outline of the thesis and the chapter division.

## 1.1 Motivation

Research on DC has earned attention among academics and companies in the last decade. Several reasons can be addressed to explain this renewed interest on the topic.

First of all, an energy transition towards renewable sources appears to be inevitable, due to environmental concerns on global warming and depletion of traditional energy sources such as coal, oil and gas [1]. Nonetheless, this transition will require efforts on multiple levels, among which the most important are markets, policies and technological advancement. The latter aspect has rapidly become crucial in the field of electrical energy, which is experiencing a massive implementation of distributed sources such as solar PV, fuel cells and wind [2].

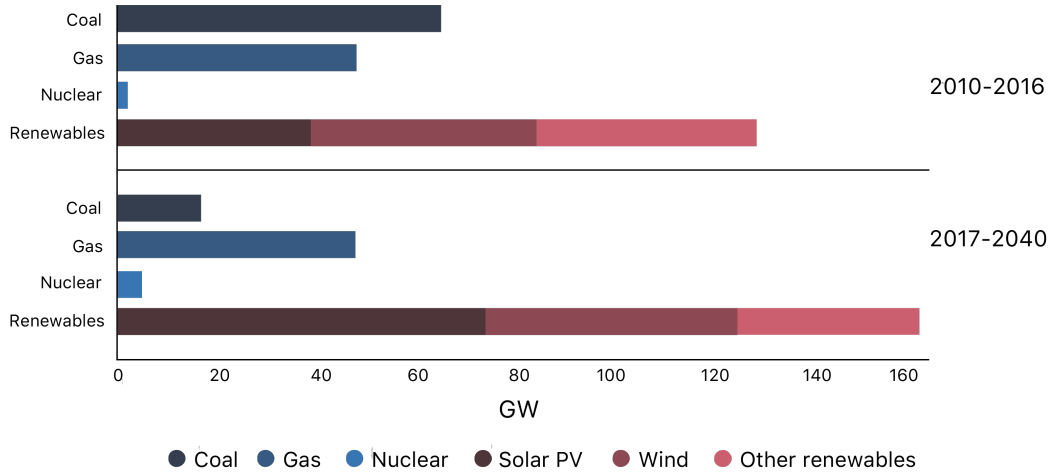


Figure 1.1: Global average annual net capacity additions by generation type [2]

Figure 1.1 shows the new net energy capacity on the global scale. In the last decade renewables have started playing an important role, which is expected to consolidate in the next 20 years. Since the three above mentioned technologies produce a DC output [3], the implementation of a DC grid at medium and low voltage level becomes technically and economically viable [4].

In second place, in many developed countries a process of electrification has started in the past years [3]. In the Netherlands, for example, some projects have been developed in order to enhance the presence of electrical energy - in particular, in DC - in airports, public offices and greenhouses [5]. Moreover, EVs are likely to increase the use of electrical energy in urban contexts in which the AC grids are at their maximum capacity. In this case it becomes interesting, economically and technologically speaking, to adopt DC at distribution level in parallel to the AC grid, with the two grids connected through AC/DC converter [6]. This process of electrification of energy supply translates into the need for better performance in long distance electricity transport. In this direction it is possible to explain the new developments in HVDC voltage source converters, especially the multi-level modular converter [7].

Besides, at consumption level, several DC based loads are becoming more important in different applications: LEDs for low power lighting; laptops and smartphones that can be charged through USB connection; electric vehicles with charged batteries; internet servers and data centers; marine and naval shipboard power systems [8]. All these appliances can efficiently work in direct current and it is expected that an even more massive *dc-fication* of society will take place in the next decades [4].

The reasons listed above, among others, led researchers all over the world to put their focus on DC technology once again after the almost one century of research and development on alternating current [9]. In parallel with industrial and academic interest on HVDC, in particular related to off-shore wind technology, research focus is also put onto lower voltage applications of DC grids. Smart grids in DC or AC/DC hybrid concepts are being tested and studied in order to set standards for transportation, households and industries [10]. Figure 1.2, presented below, shows the concept of DC microgrids and nanogrids and the connection to a medium voltage (MV) direct current grid. In this sense, the distribution grid acts as interconnection between microgrids [4].

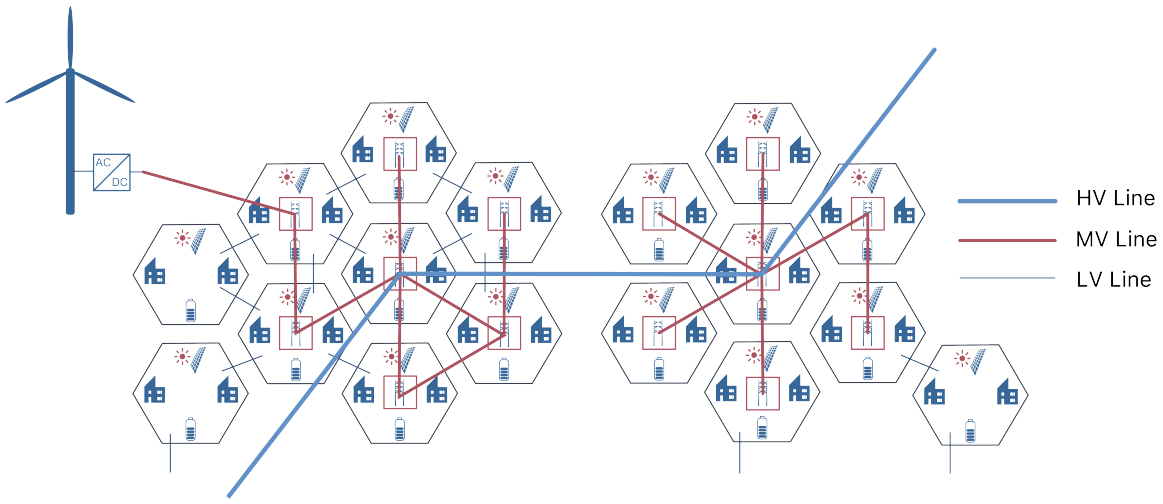


Figure 1.2: DC distribution system as interconnection of clusters of nano and microgrids [4]

Since a microgrid has the potential to be extremely interesting as a power and ancillary services provider in a broader way rather than as an island concept, low-to-medium voltage distribution DC networks can be imagined and investigated. In past years plenty of literature has been produced on the topic, but the focus is mainly on the issues related to control and protection of such grids. Among the main challenges in the design and operation of DC distribution systems there is the issue of protection. Due to the absence of a zero-crossing in direct current, fast speed fault protection, including protection coordination and interruption, is a fundamental requirement for robust DC protection architectures, together with the availability of reliable and efficient low and medium voltage equipment [8, 11]. Another issue often discussed in literature is standardization, seen as a way to reduce market inertia of AC in favour of DC [10].

This thesis addresses and investigates the topic of power flow analysis in DC networks as a tool. Similar to AC power flow analysis, the tool developed can be used for power distribution calculations. The high non-linearity of the problem gives room for improvement of the algorithms that are classically used in this field of research. Among the uses and application of the mathematical tool, a distribution system operator can benefit from network analysis and planning, redundancy analysis (N-1), stress analysis and market analysis.

## 1.2 Thesis scope and goals

This thesis aims to research current studies and developments in power flow analysis methods for future direct current distribution grids. As stated in the previous section, research focus is nowadays mainly put on medium and low voltage applications such as microgrids and very high voltage applications, i.e. HVDC connections for offshore wind energy farms. In this framework, many academics figure that in the next future also transmission and distribution levels of electrical energy dispatch will be turned into DC [11]. It is thus necessary to provide DSOs with an analytical tool in order to solve the power flow problem, as currently performed for traditional AC grids [12].

The second aim of this thesis is to create an innovative mathematical tool which is able to solve in an efficient way the power flow problem for a DC distribution power grid. In order to do so, different methods available in literature will be considered and compared. Also, great focus will be put onto grid modeling.

In both cases, some assumptions will be taken into account:

- Power flow calculation describes only the steady state of the grid and physics involved. This means that voltage, current and power are described only in their steady behaviour, thus neglecting all transients. It is shown in literature that for time frames of more than one second this assumption is completely valid [13].
- Since steady state is considered, the effects of capacitance and inductance along the lines are not considered. As a result, power lines of the networks are assumed to behave like pure resistive branches. A more extensive explanation of this point can be found in section 3.1.

## 1.3 Research questions

The main research question of this thesis can be expressed as follows:

**"What is a suitable computational method, in terms of speed, accuracy and network adaptability, to perform steady-state power flow calculations in DC distribution grids?"**

The following sub-questions are then addressed to develop the topic:

- *Why is a power flow calculation tool needed for DC distribution grids?*

Power flow analysis as an engineering tool for TSOs and DSOs is here presented for classic AC grids. Besides, the need for a power flow calculation tool, specifically for direct current distribution systems, is researched and demonstrated. Different applications can be found both in current AC applications and in future developments on DC distribution grids.

- *What are the different methods shown in literature to perform AC and DC power flow calculations?*

Literature research on the most used methods, nowadays employed, for AC power flow analysis. In particular, the non-linear nature of the power equations is investigated. Furthermore, the research focus is put onto DC power flow methods to solve linear and non-linear power flow equations, both in radial and meshed networks.

- *What is a suitable method in terms of network adaptability?*

The methods found are analyzed and compared. The aim is to identify the best method, among the ones found, in terms of performance and computational speed.

- *How can this method be applied to simple network topologies?*

One or more methods from previous research are adapted and applied to simple - radial or meshed - network topologies. The performance is determined and compared between the different methods.

- *How can this method be generalized for any kind of network?*

Once the methods are found to be applicable to DC networks with different nodes behaviors, these can be generalized for any kind of network. A generalized network features any number of node, any type of node, and any topology.

- *How can this method be applied to a standardized IEEE European low-voltage test feeder?*

The already implemented methods are finally used to test some standardized neighborhoods networks in low voltage, to which different nodes can behave as loads, generators, etc. according to the IEEE European low-voltage test feeder standards.

- *What are the applications of such tool once implemented?*

Further research on which applications such tool can give room to. In specific, steady-state flow analysis could likely be used for network development, congestion analysis, voltage level analysis, N-1 analysis and the development of new market frameworks.

## 1.4 Research approach and methodology

The research approach for this thesis involves literature review and paper research as a fundamental step to investigate the power flow computational methods currently adopted for AC grids and recommended for DC grids. Power flow computation for AC system is a type of analysis normally employed by TSOs and DSOs for grid planning and congestion analysis, among other activities. Therefore, many commercial software adopt one or more of the mathematical methods reported in the literature review. For instance, the software PowerFactory allows the user to choose between the Newton-Raphson and the DC power flow [14] - where DC, as it will be explained in a later stage, is here only indicating the fact that the AC power equation is linearized. A software like GridLab-D, on the other hand, is focused on distribution grids and offers computational methods that take into account unbalanced three-phase networks [15].

Once the state of the art in computational methods is researched, a number of missing features that appear to be very relevant in the power grids of the future are found. Among those, the different behaviours of the nodes with high penetration of power electronic interfaces, and the more complex highly meshed networks that might be applied also for distribution networks. Therefore, a subsequent step includes modeling of an innovative power flow model for DC systems. First, the solver has been implemented for linear systems (i.e. not including a constant power behaviour). Then, two linearization methods have been investigated and compared in order to include the non-linear behaviour of the constant power flow converters. Ultimately, the algorithm has been generalized in order to accept any network parameter input. The modeling has been performed using the software MATLAB.

Finally, the model has been tested through an IEEE standard neighbourhood in order to see if the solver can provide fast solutions for a larger and more complex network. A case study with different scenarios has been performed in order to provide the reader an example of how the power flow method for DC systems can be applied in the grid planning and strategic design of the universal low voltage DC distribution grids.

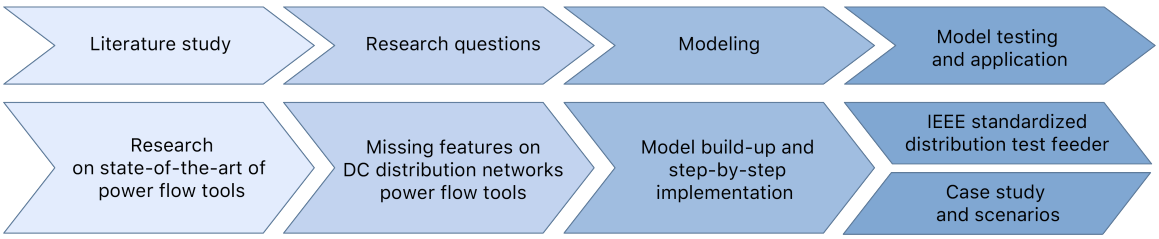


Figure 1.3: Research approach and methodology

## 1.5 Thesis outline

The previous sections have introduced the framework in which direct current networks are expected to find new interest from industry and academia in the next years. In particular, DC is already employed for high voltage transmission (point-to-point) and it is expected to be implemented also in meshed clusters of offshore wind turbines (multi-terminal). Moreover, the research questions are presented and further explained. In this section the thesis outline is provided with a brief description of the chapters.

- **Chapter 2** presents the literature review for the specific topic developed in this thesis: the power flow problem. First, the power flow problem is described in general. Then, a number of different methods found in literature for AC systems, AC distribution networks and DC systems are extensively reported. The various methods have been selected if quoted or used by several references in order to present only those methods that have an actual impact in the literature. In the conclusion of the chapter, three methods selected for DC systems are applied to a simple network and their results and performance are compared.
- **Chapter 3** focuses on the physical modeling of the universal DC distribution grid. First, the line model is given. After that, the behaviour of the nodes, divided into generation, load and hybrid nodes, is presented. The behaviour is given either by the nature of the node (e.g. resistive heating) or by the control strategy employed by the power converters that interface the different components to the grid.
- **Chapter 4** describes how the power flow tool for a direct current network is modeled, starting from the basic equations that govern the power grid. The model is subsequently tested on a simple meshed network and validated against the steady-state result of a dynamic model present in literature.
- In **chapter 5** the power flow method previously described is applied to one IEEE Low-Voltage test feeder in order to evaluate the adaptability of the tool and the ability to handle complex standardized networks.
- **Chapter 6** features one possible application of the power flow tool for grid planning and operation. A case scenario that includes the effects of distributed generation (photovoltaic modules), high power loads (fast DC electric vehicle charging) and resistive heating is built up. Additionally, the effects of droop-controlled storage units is evaluated.
- **Chapter 7** ultimately provides the conclusions and recommendations for the thesis. Moreover, the research questions are answered with the results of the thesis and indications on further work are provided.

# Chapter 2

# Power Flow Methods

## Table of Contents



This chapter outlines the literature study of the thesis and it provides the state of the art for both commercial methods and methods developed in academia for power flow computations. Given the great variety of methods reported in literature, only the most implemented and used in industry and academia have been selected.

The structure of the chapter is the following. Section 2.1 defines and describes the power flow problem, its use and field of application. Section 2.2 reports and describes two computational methods that are commonly used in commercial software for load-flow analysis: the Gauss-Seidel and the Newton-Raphson methods, focusing also on the variations of the latter. Section 2.3 points out the differences between transmission and distribution networks and shows some of the methods developed in order to perform calculations in this specific type of systems. Section 2.4 presents models treated in literature for power flow analysis in DC systems, with methods that are mainly adapted from the AC tools already seen in the previous sections. Finally, in section 2.5 a comparison between the aforementioned mathematical models is carried out and conclusions are drawn.

## 2.1 The power flow problem

Many power system problems give rise to systems of nonlinear equations that must be solved. Probably the most common nonlinear power system problem is the power flow or load flow problem [16]. The principle of a power flow problem is that given the system loads, generation, and network configuration, the system bus voltages and line currents can be found by solving the nonlinear power flow equations. This is accomplished by using Kirchhoffs law at each power system bus or node in the system. In this context, Kirchhoffs law can be interpreted as the sum of the powers entering a bus must be zero, or that the power at each bus must be conserved. Since complex power has two components, active power and reactive power, each bus gives two equations one for active power and one for reactive power [16].

The power flow problem consists in finding the steady-state operating point of an electric power system. More specifically, given the load demanded at consumption buses and the power supplied by generators, the goal is to obtain all bus voltages and complex power flowing through all network components [17].

The power flow tool is the most widely used application both in operating and in planning environments, either as a stand-alone tool or as a subroutine within more complex processes such as stability analysis, optimization problems, training simulators, among others.

During the daily grid operation, the power flow tool is the basic mathematical tool for security analysis, by identifying unacceptable voltage deviations or potential component overloading, as a consequence of both natural load evolution and sudden structural changes. It also allows the planning engineer to simulate different future scenarios that may arise for a forecast demand.

An important aspect in the problem is represented by the choice of the initial guess of the iteration process. It is in fact possible to enhance the possibilities of convergence by choosing an initial guess as close as possible to the solution [16]. It is possible to have a good guess when, for example, the solution of a particular set of conditions is already known. A new power flow analysis may involve the same network with only slight difference in topology or load and generation levels. The initial guess would then be the previously found solution. In this case the guess is referred to as hot start. When a previous solution is not known, it is always possible to undergo a flat start profile, for which voltage at 1 pu and zero degree angle is chosen. This represents often a good choice because, in per-unit analysis, we do not expect the value of the voltage to differ radically from the unitary value.

Power flow analysis is faster and easier than dynamic simulations for complex multi-terminal DC networks. This tool allows for flow-based market simulations, wind integration cost-benefit analysis, design of high-level control strategies and N-1 security assessments [18].

The power flow problem should not be confused with the optimal power flow problem (OPF). While the former aims at giving as a result the current situation in a power network, the latter determines instead power generation and demand that optimize - more specifically, minimize - particular objective functions such as cost or power losses along the transmission lines [17, 19].

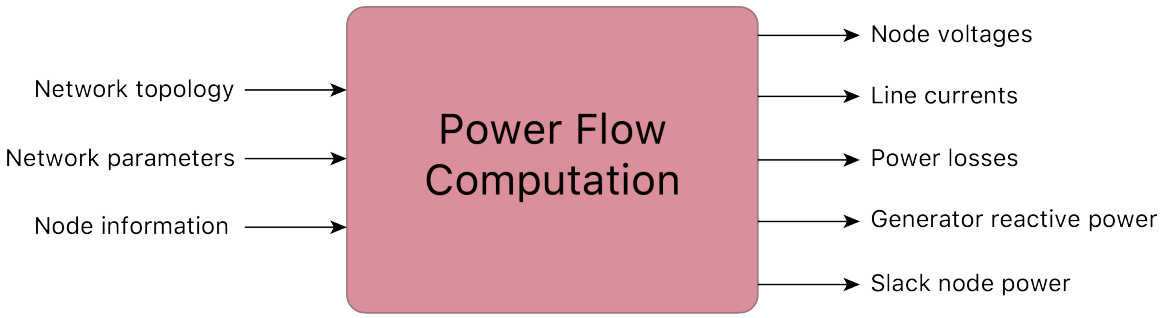


Figure 2.1: Power flow algorithm input and output scheme [20]

In figure 2.1 the inputs and outputs of the power flow problem are shown. Network topology is generally provided as *incidence matrix*, showing therefore the connections between lines and nodes. An *oriented incidence matrix* is defined as an incidence matrix that takes into account the verse of the currents in the system [21]. Network parameters are input in the computation via admittance matrix $\mathbf{Y}$, which gives information over the line physical characteristics. The network admittance matrix is often combined with the incidence matrix. State of the art methods model the grid in matrix form and, since the matrix is updated at each simulation time step, this implies an instantaneous effect of the state variables over the whole system [22]. Finally, the node information tells more about the behaviour and state of node. As explained in the next sections and chapters, the node can carry information on power, voltage or current of the system.

The outputs of the power flow problem are (complex) node voltages, found solving sets of non-linear equations. The non-linearity is given by the active and reactive power equations, that are specified as binding constraints [17]. Once the voltages are known at all buses, the second step is computing other magnitudes such as line currents, ohmic losses on the lines, and, for AC systems, generator reactive power and the power at the slack node.

## 2.2 Computational methods in traditional power systems

The load flow computation is in fact the calculation of the voltage magnitude and angle at each bus of the power system under specified conditions of system operation. Other system quantities such as the current values, power values and power losses can be derived when the voltages are known. Speaking in mathematical terms, the load flow problem is nothing more than a system consisting of as many non-linear equations as there are variables to be determined. In traditional power systems, it is possible to differentiate between three types of nodes [17, 20], as shown in table 2.1.

Table 2.1: Traditional network node types [20]

| **Node type** | **Number of nodes** | **Specified** | **Unknown** |
|---|---|---|---|
| Slack | 1 | $\lvert V_i \rvert$, $\delta_i$ | $P_i$, $Q_i$ |
| Generator (PV) | $N_g$ | $P_i$, $\lvert V_i \rvert$ | $Q_i$, $\delta_i$ |
| Load (PQ) | N - $N_g$ - 1 | $P_i$, $Q_i$ | $\lvert V_i \rvert$, $\delta_i$ |

The slack node is one single node, arbitrarily chosen in the system. The voltage of the slack node is taken as a reference for the per-unit analysis and it is known in both magnitude and phase angle. The unknown variables for this type of node are both active and reactive power.

A generator or PV node type is responsible for the injection of active and reactive power into the system. The number of PV nodes is herein defined as $N_g$, which is the number of generators in the system. Known the characteristics of the generator, it is always possible to know the active power generated and the voltage magnitude at the node end. The unknown quantities are therefore reactive power and phase angle.

Finally, the load nodes retrieve both active and reactive power from the grid. Since the quantity of power is well determined for each load, the unknown quantities are both magnitude and phase angle of the voltage at the node. The number of load nodes is thus equal to the total number of nodes N, minus the number of generator nodes and the single slack node of the system. In a network topology of N nodes, Kirchhoff's current law (in matrix form) imposes that:

$$\mathbf{I} = \mathbf{Y} \cdot \mathbf{V} \tag{2.2.1}$$

where $\mathbf{I}$ is the vector of the complex currents in the network lines, $\mathbf{V}$ is the vector of the complex node voltages and $\mathbf{Y}$ is the admittance matrix of dimension N x N. By conservation of power, at each node $i$, the complex power $S$ is the difference between generation (G) and consumption by loads (L):

$$S_i = S_{Gi} - S_{Li} = V_i I_i^* \tag{2.2.2}$$

Here the current computed $I^*$ is taken as the complex conjugate value - which means, the opposite sign of the imaginary part is taken. This conventional choice results in a negative reactive power when the load has capacitive behaviour [20]. In matrix form:

$$\mathbf{S} = \text{diag}(\mathbf{V}) \cdot \mathbf{I}^* \tag{2.2.3}$$

where $\mathbf{I}^*$ is the vector of the conjugate line currents and $\text{diag}(\mathbf{V})$ is the diagonal matrix with the components of the node voltage vector. By explicitly writing active and reactive components of the power and real (conductance, G) and imaginary (susceptance, B) part of the admittance, the power equation can be rewritten as:

$$P_i = |V_i|^2 G_{ii} + \sum_{\substack{n=1 \\ \neq i}}^{N} |V_i V_n Y_{in}| \cos(\theta_{in} + \delta_n - \delta_i) \tag{2.2.4}$$

$$Q_i = -|V_i|^2 B_{ii} + \sum_{\substack{n=1 \\ \neq i}}^{N} |V_i V_n Y_{in}| \sin(\theta_{in} + \delta_n - \delta_i) \tag{2.2.5}$$

The above equations are also called power flow equations. P and Q are the active and reactive power, respectively, at node $i$. Since in traditional power systems active and reactive power at each node are most of the times known (PQ nodes), the power flow problem exploits iteration to compare P and Q results to the specified (also *scheduled* [16, 17]) values in order to determine magnitude and phase angle of $\mathbf{V}$ at every node.

It is important to highlight the fact that, in traditional power systems, the power generation and consumption are well known variables of the system. Generation, in fact, is determined by economic dispatch of power plants in order to meet the demand according to market clearing routines [17].

### 2.2.1 Gauss-Seidel method

The Gauss-Seidel method is based on simple iterations and it is considered to be easy to implement. On the other hand, the convergence is linear and therefore very slow, compared to other methods

[17]. In fact, although the computational effort per iteration is low, the number of iterations in order to fall into the desired tolerance value is high. Hence, the computation time increases considerably when the network dimension increases. The basic assumption is that a non-linear equation of the type:

$$f(\mathbf{x}) = \mathbf{0} \tag{2.2.6}$$

can be rewritten as:

$$\mathbf{x} = F(\mathbf{x}) \tag{2.2.7}$$

The power flow equation is rewritten so that it is possible to update the value of the node voltage, starting from the value of the previous iteration ($k$):

$$V_i^{(k+1)} = \frac{1}{Y_{ii}} \left[ \frac{P_{i,\text{sp}} - jQ_{i,\text{sp}}}{V_i^{(k)*}} - \sum_{j=1}^{i-1} Y_{ij} V_j^{(k+1)} - \sum_{j=i+1}^{n} Y_{ij} V_j^{(k)} \right] i = 1, 2, ..., n-1 \tag{2.2.8}$$

The iteration process can be stopped once the result converges within the desired tolerance $\varepsilon$:

$$|V_i^{(k+1)} - V_i^{(k)}| \leq \varepsilon \tag{2.2.9}$$

The Gauss-Seidel method is often offered in software with an accelerator factor $\alpha$ which can considerably reduce the computation burden. The accelerator has usually a value between 1.4 and 1.6 [17] and it is implemented as follows in order to have faster convergence:

$$V_i^{(k+1)}\Big|_{\text{acc}} = V_i^{(k)} + \alpha(V_i^{(k+1)} - V_i^{(k)}) \tag{2.2.10}$$

The flowchart in figure 2.2 shows the steps of the solving algorithm for this iterative method.

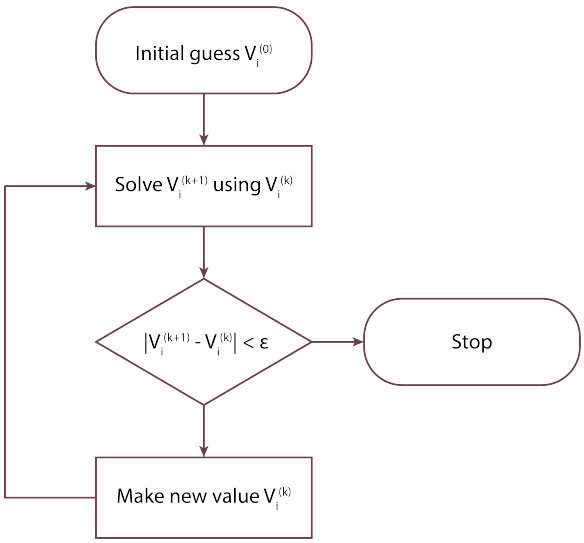


Figure 2.2: Flowchart of the Gauss-Seidel computation method

In any case, Gauss-Seidel method is used nowadays in few practical applications. However, it still comes useful as a starter for the the Newton-Raphson method, in those cases in which convergence is not guaranteed from the flat start profile, which corresponds to voltage magnitude at 1 p.u. and zero voltage angle [17].

### 2.2.2 Newton-Raphson method

The Newton-Raphson method, and its variations, are probably the most used computational methods in industry [16, 17, 20]. Since the objective of the power flow problem is to determine phase and magnitude of the voltage at the network nodes, the unknown vector can be expressed as:

$$\mathbf{x} = \begin{bmatrix} \delta \\ |\mathbf{V}| \end{bmatrix} = \begin{bmatrix} \delta_2 \\ \vdots \\ \delta_{\mathrm{N}} \\ |V|_{\mathrm{N_g}+2} \\ \vdots \\ |V|_{\mathrm{N}} \end{bmatrix} \tag{2.2.11}$$

where $\delta_1$ and $V_1$ (slack bus), and the voltages $V_i$ from $i = 2$ to $i = \mathrm{N_g} + 1$ (PV buses) are known. The power flow equations for active and reactive power at node i are:

$$P_i = |V_i|^2 G_{ii} + \sum_{\substack{n=1 \\ \neq i}}^{N} |V_i V_n Y_{in}| \cos(\theta_{in} + \delta_n - \delta_i) \tag{2.2.12}$$

$$Q_i = -|V_i|^2 B_{ii} + \sum_{\substack{n=1 \\ \neq i}}^{N} |V_i V_n Y_{in}| \sin(\theta_{in} + \delta_n - \delta_i) \tag{2.2.13}$$

The state variables (vector $\mathbf{x}$) must be determined such that the power mismatches, being the difference between the specified (sp) and computed power injections, are as close as possible to zero:

$$\mathbf{\Delta P}(\mathbf{x}) = \begin{bmatrix} P_{2,\mathrm{sp}} - P_2(\mathbf{x}) \\ \vdots \\ P_{\mathrm{N,sp}} - P_{\mathrm{N}}(\mathbf{x}) \end{bmatrix} = \mathbf{0} \tag{2.2.14}$$

$$\mathbf{\Delta Q}(\mathbf{x}) = \begin{bmatrix} Q_{2,\mathrm{sp}} - Q_2(\mathbf{x}) \\ \vdots \\ Q_{\mathrm{N,sp}} - Q_{\mathrm{N}}(\mathbf{x}) \end{bmatrix} = \mathbf{0} \tag{2.2.15}$$

If the mismatches are in one vector:

$$\mathbf{h}(\mathbf{x}) = \begin{bmatrix} \mathbf{\Delta P}(\mathbf{x}) \\ \mathbf{\Delta Q}(\mathbf{x}) \end{bmatrix} = \mathbf{0} \tag{2.2.16}$$

When the above equality cannot be achieved, a correction factor $\Delta x$ must be added so that the power mismatches factor can actually be equal to zero. In order to do that, a Taylor approximation is applied to the power equations (2.2.4) and (2.2.5) to linearize at the first order. The problem is multi-dimensional, first derivative component in the Taylor approximation is represented by the jacobian matrix. The result is the iterative formula:

$$\mathbf{J\Delta x} = \mathbf{h}(\mathbf{x}) \tag{2.2.17}$$

The jacobian matrix, in explicit terms, is formed by the first partial derivatives of $\mathbf{P}$ and $\mathbf{Q}$ over $\delta$ and $|\mathbf{V}|$. For practical reasons, the matrix is generally divided into four sub-matrices:

$$[\mathbf{J_{11}}] = \begin{bmatrix} \frac{\partial P_2}{\partial \delta_2} & \cdots & \frac{\partial P_2}{\partial \delta_N} \\ \vdots & \ddots & \vdots \\ \frac{\partial P_N}{\partial \delta_2} & \cdots & \frac{\partial P_N}{\partial \delta_N} \end{bmatrix} \tag{2.2.18}$$

$$[\mathbf{J_{12}}] = \begin{bmatrix} \frac{\partial P_2}{\partial |V_{Ng+2}|} & \cdots & \frac{\partial P_2}{\partial |V_N|} \\ \vdots & \ddots & \vdots \\ \frac{\partial P_N}{\partial |V_{Ng+2}|} & \cdots & \frac{\partial P_N}{\partial |V_N|} \end{bmatrix} \tag{2.2.19}$$

$$[\mathbf{J_{21}}] = \begin{bmatrix} \frac{\partial Q_{Ng+2}}{\partial |V_{Ng+2}|} & \cdots & \frac{\partial Q_{Ng+2}}{\partial |V_N|} \\ \vdots & \ddots & \vdots \\ \frac{\partial Q_N}{\partial |V_{Ng+2}|} & \cdots & \frac{\partial Q_N}{\partial |V_N|} \end{bmatrix} \tag{2.2.20}$$

$$[\mathbf{J_{22}}] = \begin{bmatrix} \frac{\partial Q_{Ng+2}}{\partial \delta_2} & \cdots & \frac{\partial Q_{Ng+2}}{\partial \delta_N} \\ \vdots & \ddots & \vdots \\ \frac{\partial Q_N}{\partial \delta_2} & \cdots & \frac{\partial Q_N}{\partial \delta_N} \end{bmatrix} \tag{2.2.21}$$

So that:

$$[\mathbf{J}] = \begin{bmatrix} \mathbf{J_{11}} & \mathbf{J_{12}} \\ \mathbf{J_{21}} & \mathbf{J_{22}} \end{bmatrix} \tag{2.2.22}$$

The flowchart showing the Newton-Raphson computation is given in figure 2.3 below.

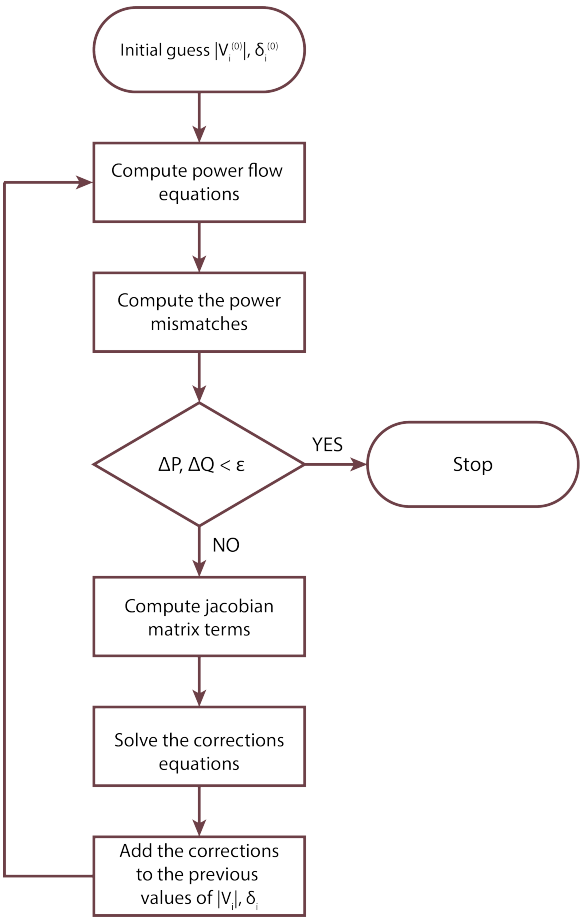


Figure 2.3: Flowchart of the Newton-Raphson computation method [20]

Determining partial derivatives at every iteration step represents a higher computational burden if compared to a simple method such as the Gauss-Seidel. Nevertheless, the convergence of the NR method is quadratic, hence it generally requires less iterations and less time [16, 17]. In order to reduce the iteration effort, many variations and simplifications have been proposed in literature.

### 2.2.3 Decoupled power flow method

The decoupled power flow method is based on the assumption that, for transmission systems, the reactance of overhead lines is much bigger than the resistance. In addition, it is assumed that the differences between voltage angles are small [20]. This makes possible to 'decouple' active power and voltage angles, on one hand, and reactive power and voltage magnitudes on the other. The formulation is as follows:

$$P = \frac{|V_i||V_j|}{X}\sin(\delta_i - \delta_j) \approx \frac{|V_i||V_j|}{X}(\delta_i - \delta_j) \tag{2.2.23}$$

$$Q = \frac{|V_i||V_j|}{X}\cos(\delta_i - \delta_j) - \frac{|V_j|^2}{X} \approx \frac{|V_j|}{X}(|V_i| - |V_j|)\frac{|V_i||V_j|}{X}(\delta_i - \delta_j) \tag{2.2.24}$$

This process of decoupling turns the off-diagonal submatrices $\mathbf{J_{12}}$ and $\mathbf{J_{21}}$ into *null* matrices, simplifying the calculations linked to the jacobian. In one equations are evaluated the active power mismatches, while in the other one the mismatches in reactive power are found.

$$\begin{bmatrix} \frac{\partial P_2}{\partial \delta_2} & \cdots & \frac{\partial P_2}{\partial \delta_N} \\ \vdots & \mathbf{J_{11}} & \vdots \\ \frac{\partial P_N}{\partial \delta_2} & \cdots & \frac{\partial P_N}{\partial \delta_N} \end{bmatrix} \begin{bmatrix} \Delta\delta_2 \\ \vdots \\ \Delta\delta_N \end{bmatrix} = \begin{bmatrix} \Delta P_2 \\ \vdots \\ \Delta P_N \end{bmatrix} \tag{2.2.25}$$

$$\begin{bmatrix} \frac{\partial Q_{Ng+2}}{\partial \delta_2} & \cdots & \frac{\partial Q_{Ng+2}}{\partial \delta_N} \\ \vdots & \mathbf{J_{22}} & \vdots \\ \frac{\partial Q_N}{\partial \delta_2} & \cdots & \frac{\partial Q_N}{\partial \delta_N} \end{bmatrix} \begin{bmatrix} \Delta|V_{Ng+2}| \\ \vdots \\ \Delta|V_N| \end{bmatrix} = \begin{bmatrix} \Delta Q_{Ng+2} \\ \vdots \\ \Delta Q_N \end{bmatrix} \tag{2.2.26}$$

The clear advantage of this method is that two smaller jacobian matrices need to be computed, since the off-diagonal terms are not taken into account.

### 2.2.4 Fast decoupled power flow method

One further approximation can be taken into account in order to separate the jacobian into two different constant matricial equations [20, 23]. This is the case of the fast decoupled power flow. If it is assumed that the reactive power injected into a node is much smaller than the reactive power that would flow if all lines linked to the bus $i$ were short-circuited ($Q_i \ll |V_i|^2 B_{ii}$):

$$\begin{bmatrix} -B_{22} & \cdots & -B_{2N} \\ \vdots & \ddots & \vdots \\ -B_{N2} & \cdots & -B_{NN} \end{bmatrix} \begin{bmatrix} \Delta\delta_2 \\ \vdots \\ \Delta\delta_N \end{bmatrix} = \begin{bmatrix} \frac{\Delta P_2}{|V_2|} \\ \vdots \\ \frac{\Delta P_N}{|V_N|} \end{bmatrix} \tag{2.2.27}$$

$$\begin{bmatrix} -B_{Ng+2,Ng+2} & \cdots & -B_{Ng+2,N} \\ \vdots & \ddots & \vdots \\ -B_{N,Ng+2} & \cdots & -B_{NN} \end{bmatrix} \begin{bmatrix} \Delta|V_{Ng+2}| \\ \vdots \\ \Delta|V_N| \end{bmatrix} = \begin{bmatrix} \frac{\Delta Q_{Ng+2}}{|V_{Ng+2}|} \\ \vdots \\ \frac{\Delta Q_N}{|V_{Ng+2}|} \end{bmatrix} \tag{2.2.28}$$

The advantage of this method is that both matrices are constant and depend exclusively on the susceptance of the grid. Even if the convergence in this case is slower - because of more iterations needed - each iteration is much faster than in the basic Newton-Raphson algorithm. The flowchart showing the FDPF method computation is given in figure 2.4 below.

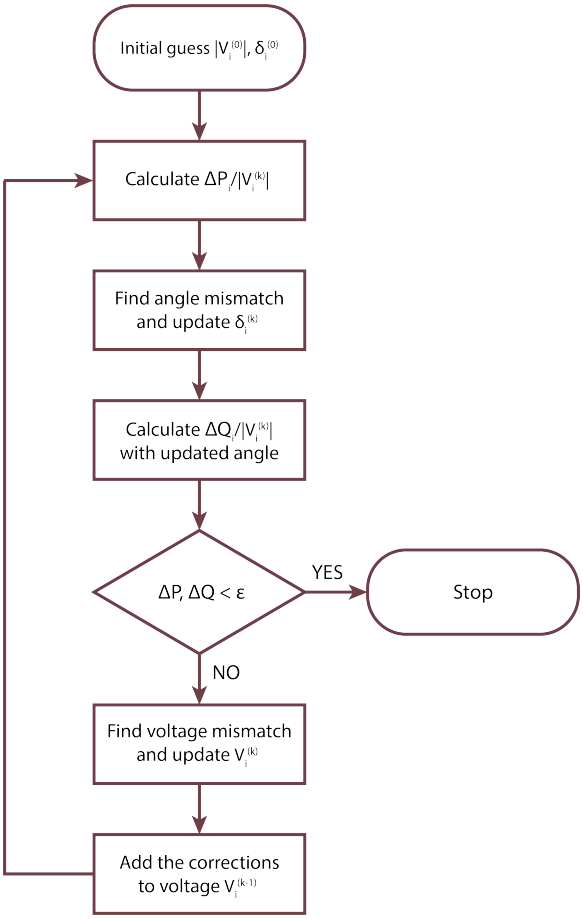


Figure 2.4: Flowchart of the fast decoupled power flow computation method [20]

### 2.2.5 DC power flow method

The DC, or direct current, power flow method is used to have very fast computations, even though the result accuracy is rather low [20]. Even though this method is used for AC system, it is called "DC" because of the analogy in the linear representation. This method can be also used as a first step to determine the starting values of V and $\delta$ before performing calculations with more accurate methods.

In this type of computation the power equation is linearized: this means that the simplifications made are not only present at the jacobian side (which increases the number of iterations only) but also the actual model of the power system is altered, affecting in this way the accuracy of the final solution [20]. The DC power flow is based on three approximations:

- the line resistances are neglected (loss-less), so that $Y_{ij} = B_{ij}$ and $\theta_{in} = \frac{\pi}{2}$;
- the node voltage magnitudes are 1 pu;
- the differences between voltage angles $\delta$ are small.

In this way the non-linear active power equation 2.2.4 can be linearized into:

$$P_i = \sum_{n=1}^{N} |V_i V_n Y_{in}| \cos(\theta_{in} + \delta_n - \delta_i) = \sum_{n=1}^{N} |Y_{in}| \sin(-\delta_n + \delta_i) = -\sum_{n=1}^{N} |Y_{in}|(-\delta_n + \delta_i) \qquad (2.2.29)$$

As mentioned above, in analogy with the DC computation of power, which is given by the formula:

$$P_i = I_{in}(V_n - V_i) \tag{2.2.30}$$

where $n$ and $i$ are two neighbouring nodes. In the AC model, the power is given by the difference in voltage angle $\delta$ and line admittance Y.

## 2.3 Computational methods in distribution networks

Some methods found in literature are for distribution networks in specific and not for big transmission power networks. Even though the methods described in the previous section can be applied successfully also in distribution networks [24], specialized algorithms have been developed in order to cope with some major challenges that arise when a power flow analysis is performed in distribution network-specific environment.

Distribution networks are believed to be key to the infrastructural changes that are occurring in power systems. Integration of renewable sources, new power quality requirements and electric vehicles growing presence are expected to be handled by distribution systems [25]. Three main differences are generally pointed out when comparing distribution and transmission networks [23, 26]:

- distribution networks are three-phase unbalanced oriented;
- the topology is generally radial or weakly-meshed;
- the resistance to reactance ratio $R/X$ in the distribution lines is high.

Unbalances increase the complexity of the network model, since phase quantities have to be considered, including mutual couplings. The radial or weakly meshed nature of these systems, as well as the high $R/X$ ratios are also cause of failure for power flow algorithms usually applied for transmission networks.

### 2.3.1 Forward/Backward sweep method

The forward/backward sweep method has been successfully implemented several times in literature for studies on radial or weakly meshed distribution networks [24, 27, 28]. This is utilized because of its simplicity, robustness and high efficiency [26].

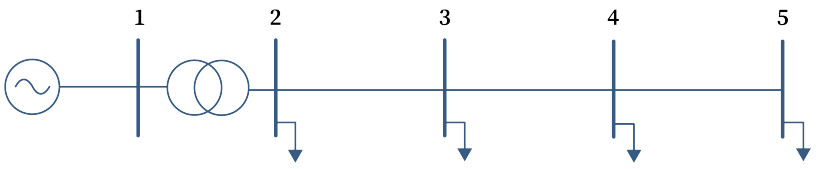


Figure 2.5: Radial network with one in-feed bus [27]

In AC distribution systems it is very common to have a simple situation as depicted in figure 2.5: one bus is connected to the generator - or infinite transmission grid - and works as an in-feed for the system. This bus is chosen as the slack bus because of its known characteristics and voltage.

The next step is to assume an initial voltage at all the nodes, in both magnitude and angle. Here nominal voltage is often used [27] and it corresponds generally to 1 pu. Then, starting from the root and moving forward, towards the feeder and lateral ends, the currents between *i-th* and *j-th* nodes are calculated:

$$I_{ij}^{(k)} = \left[ \frac{S_i}{V_i^{(k-1)}} \right]^* \tag{2.3.1}$$

On the other direction, starting from the feeder bus towards the root, the node voltages are computed:

$$V_i^{(k-1)} = V_j^{(k)} + Z_{ij} I_{ij}^{(k)} \tag{2.3.2}$$

The last stage is the termination criterion, and it is performed by evaluating the power mismatch:

$$\Delta S_i^{(k)} = S_i - V_i^{(k)} \cdot \left[ I_i^{(k)} \right]^* \leq \varepsilon \tag{2.3.3}$$

In order to perform the forward/backward method in a weakly meshed network, it is possible to act a conversion to a radial network by breaking the loops at a point of low current flow. To do so, it is necessary to substitute an equivalent injection current in the points where the loops are broken [27].

### 2.3.2 Direct methods

Some simple iterative methods, also referred to as *direct methods* have been developed to solve distribution network power flow problems. These methods take advantage of the topology of distribution systems in order to produce direct solutions [29, 30].

One type of direct method uses two matrices: the bus-injection to branch-current (**BIBC**) matrix and the branch-current to bus-voltage matrix (**BCBV**). Then, a simple matrix multiplication is used to obtain load flow solution [29]. The **BIBC** matrix is built by considering currents in all buses as current injections. This gives the relationship:

$$\mathbf{B} = [\mathbf{BIBC}] \cdot \mathbf{I} \tag{2.3.4}$$

where the constant **BIBC** matrix is an upper triangular matrix and contains values of 0 and 1 only.

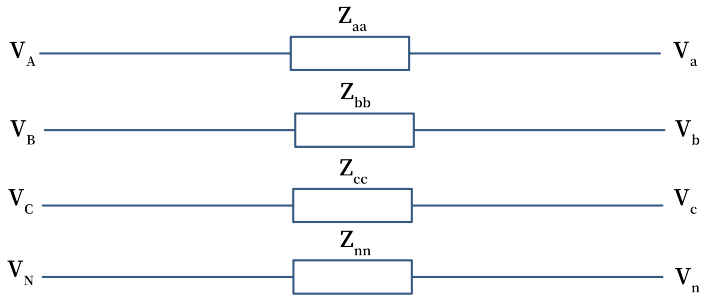


Figure 2.6: Three-phase distribution line [29]

Since three-phase distribution networks are generally unbalanced, the mutual coupling effects on lines can be described by:

$$\mathbf{Z}_{abcn} = \begin{bmatrix} Z_{aa} & Z_{ab} & Z_{ac} & Z_{an} \\ Z_{ba} & Z_{bb} & Z_{bc} & Z_{bn} \\ Z_{ca} & Z_{cb} & Z_{cc} & Z_{cn} \\ Z_{na} & Z_{nb} & Z_{nc} & Z_{nn} \end{bmatrix} \tag{2.3.5}$$

Applying Kron's reduction in the Z matrix, the voltage relation shown in figure 2.6 can be expressed by:

$$\begin{bmatrix} V_a \\ V_b \\ V_c \end{bmatrix} = \begin{bmatrix} V_A \\ V_B \\ V_C \end{bmatrix} - \begin{bmatrix} Z_{aa-n} & Z_{ab-n} & Z_{ac-n} \\ Z_{ba-n} & Z_{bb-n} & Z_{bc-n} \\ Z_{ca-n} & Z_{cb-n} & Z_{cc-n} \end{bmatrix} \begin{bmatrix} I_{Aa} \\ I_{Bb} \\ I_{Cc} \end{bmatrix} \tag{2.3.6}$$

Through this equation it is possible to find the relationship between branch currents and bus voltages as:

$$V_j = V_i - B_i Z_{ij} \tag{2.3.7}$$

Since the feeder is radial, the voltage drops can be summed up and related to the root voltage $V_1$. This makes possible to write the matricial form:

$$\mathbf{\Delta V} = [\mathbf{BCBV}] \cdot \mathbf{B} \tag{2.3.8}$$

where **BCBV** is the branch-current to bus-voltage matrix and it is always a lower triangular matrix with line impedances as elements.

By combining the two equations it is possible to find the relationship between bus voltages changes and currents:

$$\mathbf{\Delta V} = [\mathbf{BCBV}] \cdot [\mathbf{BIBC}] \cdot \mathbf{I} = [\mathbf{DLF}] \cdot \mathbf{I} \tag{2.3.9}$$

where **DLF** is defined as direct load flow matrix.

The solution is found by solving iteratively the following equations:

$$I_i^{(k)} = \left( \frac{P_i + jQ_i}{V_i^{(k)}} \right)^* \tag{2.3.10}$$

$$\mathbf{\Delta V}^{(k+1)} = [\mathbf{DLF}] \cdot \mathbf{I}^{(k)} \tag{2.3.11}$$

$$\mathbf{V}^{(k+1)} = \mathbf{V}^{(k)} \cdot \mathbf{\Delta V}^{(k+1)} \tag{2.3.12}$$

The main advantage of this and similar methods is that only the **DLF** matrix is needed and it is kept constant all along the iteration process since it contains only information over grid characteristics (**BCBV**) and current injections (**BIBC**) [29].

## 2.4 Computational methods for DC systems

Since many renewable sources, especially solar photovoltaic, generate DC voltage and many emerging loads such as LED lighting and electric vehicles consume power in DC, the interest for low voltage DC systems (LVDC) is growing [11, 24]. Given the renewed attention of industry and academia over this topic, some power flow methods found in literature are designed specifically for the DC framework.

Here, first of all, the lack of reactive power and angles allows some simplifications of the mathematical formulation, since the state variable vector as defined in section 2.2 is halved [31]. The power flow analysis in LVDC grids can be presented as a sub-problem within the AC grids methodologies encountered before, such as Newton Raphson or GaussSeidel. Other simple iterative methods, such as the forward/backward sweeps, are also often used [24].

It has also been shown in literature that, even though non-linear problems often give more than one solution, there exists a unique solution in LVDC grids. Moreover, this result has been found to be independent of the numerical method adopted, independent of the network size and load condition and valid for any topology [31].

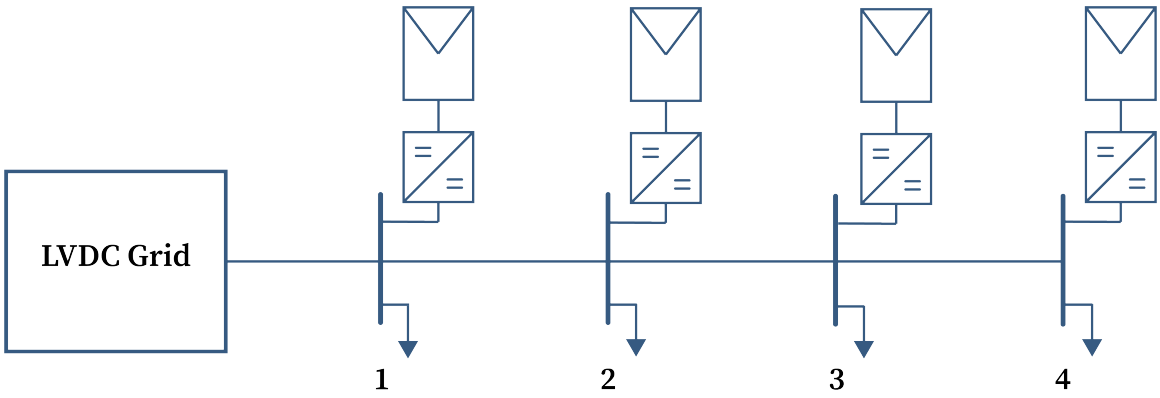


Figure 2.7: DC distribution network feeder with multiple DGs, power converters and loads [24]

Compared to the traditional power flow models, for DC networks it is sometimes impractical to take any of the source buses as slack bus. This is due to the fact that only few controllable generating units are connected to the LVDC system [32]. In figure 2.7 an example of DC distribution network, as a single feeder, is shown. The feeder has 4 nodes, all of them connected to PV panels via DC-DC converters and loads. As it will be explained more extensively in section 3.2, another important difference with AC grids is that the node behaviours other than constant power (PV and PQ) or slack (basically a constant voltage) are not taken into account. Instead, control in DC grids, including constant power, voltage and droop, has a decisive effects on the steady state characteristic of the system [32, 33].

### 2.4.1 Gauss-Seidel method for DC systems

The Gauss-Seidel method is based on Ohm's law relating currents and voltages through the line conductances and it can therefore be used also in a DC framework [24]. The equation in matrix form is:

$$\mathbf{I} = \begin{bmatrix} G_{11} & \dots & G_{1N} \\ \vdots & \ddots & \vdots \\ G_{N1} & \dots & G_{NN} \end{bmatrix} \cdot \mathbf{V} \tag{2.4.1}$$

where the diagonal terms $G_i i$ are the sum of the line conductances in contact with the node $i$, and the off-diagonal terms $G_i j$ are the negative of the conductance between nodes $i$ and $j$. As seen for the AC case, the Gauss-Seidel is based on a simple fixed-point iteration process. In order to solve the equation in this way, the above equation needs to be re-arranged so that the voltages appear on

both sides of the equation: on the left side, the current value (k) needs to be found by using the old values (k-1) of voltage on the right side. This is shown in the following equation:

$$V_i^{(k)} = \frac{1}{G_{ii}} \left[ -\frac{P_i}{V_i^{(k-1)}} - \sum_{j \neq i} G_{ij} V_j^{(k-1)} \right] \tag{2.4.2}$$

The voltage values are updated for all node (except the slack one) at every iteration step, and the iterations are stopped when the voltage mismatch between the current and old values are below a given threshold.

### 2.4.2 Newton-Raphson method for DC systems

Given the interest in off-shore wind farms projects, multi-terminal DC grids connecting wind turbines in clusters has become an important topic [34]. The need for a power flow analysis method that takes into account the characteristics of these DC systems has led to research in this direction [18, 35].

Methods adapted from Newton-Raphson are very common in this multi-terminal DC networks, because of the behaviour of the nodes in the system [18, 24, 34, 36]. One of the methods found in literature is described in this section.

In DC networks, reactive power and phase angles are physical quantities not present in the problem formulation. The unknown vector, as depicted in section 2.2 can be therefore described as:

$$\mathbf{x} = \mathbf{V_{DC}} = \begin{bmatrix} V_{\mathrm{DC},i} \\ \vdots \\ V_{\mathrm{DC,N-1}} \end{bmatrix} \tag{2.4.3}$$

The mismatch vector $\mathbf{h}(\mathbf{x})$ contains only active power mismatches, and it is therefore given by the equation:

$$\mathbf{h}(\mathbf{V_{DC}}) = \begin{bmatrix} h_1 \\ \vdots \\ h_{\mathrm{N-1}} \end{bmatrix} \tag{2.4.4}$$

The load flow equation becomes:

$$h_i = P_{Gi} - P_{Li} - \sum_{j \neq i}^{N} V_{\mathrm{DC},i} V_{\mathrm{DC},j} Y_{ij} - Y_{ii} V_{\mathrm{DC},i}^2 \tag{2.4.5}$$

The jacobian matrix will be:

$$\mathbf{J}(\mathbf{V_{DC}}) = \frac{\partial \mathbf{h}}{\partial \mathbf{V_{DC}}} = \begin{bmatrix} \frac{\partial h_1}{\partial V_{\mathrm{DC},1}} & \cdots & \frac{\partial h_1}{\partial V_{\mathrm{DC,N-1}}} \\ \vdots & \ddots & \vdots \\ \frac{\partial h_{\mathrm{N-1}}}{\partial V_{\mathrm{DC},1}} & \cdots & \frac{\partial h_{\mathrm{N-1}}}{\partial V_{\mathrm{DC,N-1}}} \end{bmatrix} \tag{2.4.6}$$

Since power generation and power demand are constant at the node $i$, the mismatch function $h(x)$ is only function of the voltage and the network admittance matrix $\mathbf{Y}$. The partial derivatives in the jacobian matrix are thus:

$$-Y_{ib} V_{\mathrm{DC},i} \text{ for } k \neq i \tag{2.4.7}$$

$$-\sum_{j\neq i} V_{\mathrm{DC},j} Y_{ij} - 2Y_{ii} V_{\mathrm{DC},i} \text{ for } k = i \tag{2.4.8}$$

Once the DC jacobian is updated, the voltage mismatch between two iterations k and k+1 is found:

$$\mathbf{\Delta V_{DC}}^{(k)} = -\mathbf{J}(\mathbf{V_{DC}}^{(k)})^{-1} \cdot \mathbf{h}(\mathbf{V_{DC}}^{(k)}) \tag{2.4.9}$$

and the values can be updated:

$$\mathbf{V_{DC}}^{(k+1)} = \mathbf{V_{DC}}^{(k)} + \mathbf{\Delta V_{DC}}^{(k)} \tag{2.4.10}$$

The flowchart of the DC power flow algorithm based on Newton-Raphson is shown in figure 2.8 below.

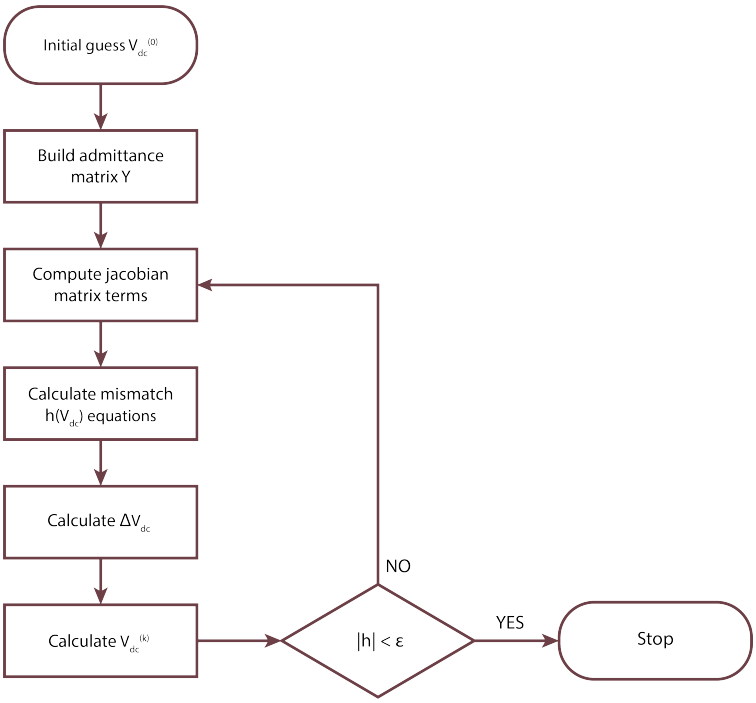


Figure 2.8: Flowchart of the adapted Newton-Raphson DC method for MTDC networks [18]

### 2.4.3 Forward/Backward sweep method for DC systems

The forward/backward sweep method used for AC radial and weakly meshed distribution systems, and shown in section 2.3.1, can be easily adapted to DC systems [24].

The in-feed bus is used again as slack bus, whose voltage is known and kept constant as reference. Starting from the last bus and moving backward towards the root, the currents injections are calculated by using the equation:

$$I_{ij}^{(k)} = \frac{P_i}{V_i^{(k-1)}} \tag{2.4.11}$$

where $i$ and $j$ are two adjacent buses connected by a line characterized by resistance $R_{ij}$. Then, starting from the root and forward towards the load branches, voltages can be calculated with:

$$V_j^{(k+1)} = V_i^{(k)} - R_{ij} I_{ij}^{(k)} \tag{2.4.12}$$

As for the AC version, the iteration stops when a given mismatch criterion is met either for all node voltages or for all node powers.

# 2.5 Conclusion

Many computational methods have been found in literature, generally with slightly different approaches or input variables taken into account. It is of interest to mention *sparse matrix techniques* that have been developed in order to accelerate the computation. These techniques rely on the fact that big network matrices have relatively few non-zero elements. They involve algorithms that can detect the presence of non-zero elements at every iteration, so that the actual computation involves a lower number of elements of the matrix [16, 17].

Table 2.2: Comparison of the different computational methods found in literature

| **Method** | **System suitability** | **Working principle** | **Network adaptability** | **Types of nodes considered** |
|---|---|---|---|---|
| *Gauss-Seidel* | AC and DC | Re-arranges the polynomial equation f(x) into x = F(x) and updates x at each iteration | Works in radial, loop and meshed networks | Works with slack, PV and PQ buses |
| *Newton-Raphson* | AC and DC | Reduces the mismatch in the gradient (linearization as Taylor series) | Works in radial, loop and meshed networks | Works with slack, PV and PQ buses |
| *Decoupled power flow* | AC | Reduces the elements in the Jacobian matrix decoupling P(V) and Q($\theta$). Then it is a Newton-Raphson | Used mainly for complex meshed networks | Works with slack, PV and PQ buses |
| *Fast decoupled power flow* | AC | Constant Jacobian matrix to minimize the number of function evaluations and LU factorizations | Used mainly for complex meshed networks | Works with slack, PV and PQ buses |
| *DC power flow* | AC | Based on simplifications, it takes P as linear function of theta (small angles) | Used mainly for complex meshed networks | Works with slack, PV and PQ buses |
| *Direct methods* | AC | Compute voltages from bus injection currents and three-phase impedance to account for single-phase loads | Radial or weakly meshed networks | Slack and constant power buses |
| *Forward/Backward sweep* | AC and DC | Backward and forward sweeps with Kirchhoff's laws. Then find mismatch in P or V | Radial or weakly meshed networks | Slack and constant power buses |

Table 2.2 shows the main results of the literature study conducted and compares the main methods found. It is important to define whether a method can be used - or adapted - for AC or DC systems. Then, the working principle is reported along with network adaptability and the types of nodes that can be implemented in the algorithm. The node aspect is of particular interest since, as it will be analyzed in the next chapter, in future (DC) power systems nodes behaviours are expected to differ from the current power systems. In particular, the importance of control of the sources and loads linked to the distribution system determines the behaviour of that specific node [31].

In order to show how the different methods that can be adapted from DC in literature are compared, the Gauss-Seidel, the Newton-Raphson and the Forward/Backward sweep methods for DC are applied to the simple three-nodes and two-lines network depicted in figure 2.9.

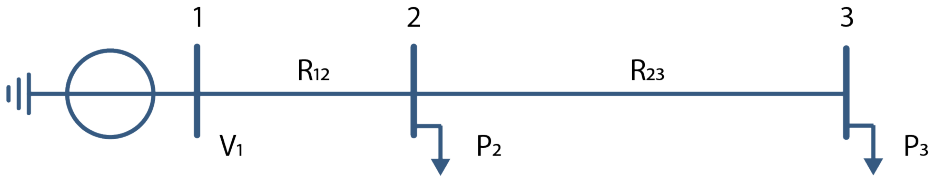


Figure 2.9: Three-nodes/two-lines network with constant voltage node (slack) and constant power nodes

The following data are known for the network: the first node has constant voltage level set at 350 V, thus it behaves as a slack bus. Nodes 2 and 3 are constant power loads set at 800 W and 750 W, respectively. The two lines have resistances $R_{12}$ = 0.642 Ω and $R_{23}$ = 1.284 Ω. In the following tables 2.3, 2.4 and 2.5 the required iterations to achieve a solution - with termination criterion of 0.01 V on the voltage mismatch - are shown for the three DC methods.

Table 2.3: Gauss-Seidel method iteration results for three-nodes/two-lines network

| | *#1* | *#2* | *#3* | *#4* | *#5* | *#6* | *#7* |
|---|---|---|---|---|---|---|---|
| $V_2$ (V) | 350.000 | 349.022 | 348.102 | 347.180 | 347.449 | 347.115 | 347.123 |
| $V_3$ (V) | 350.000 | 347.249 | 344.489 | 345.306 | 344.391 | 344.349 | 344.333 |

Table 2.4: Backward/Forward method iteration results for three-nodes/two-lines network

| | *#1* | *#2* | *#3* | *#4* |
|---|---|---|---|---|
| $V_2$ (V) | 350.000 | 347.157 | 347.134 | 347.133 |
| $V_3$ (V) | 350.000 | 344.222 | 344.265 | 344.149 |

Table 2.5: Newton-Raphson method iteration results for three-nodes/two-lines network

| | *#1* | *#2* | *#3* |
|---|---|---|---|
| $V_2$ (V) | 350.000 | 347.157 | 347.122 |
| $V_3$ (V) | 350.000 | 344.405 | 344.325 |

Figure 2.10 depicts a visual representation of the three tables. Even for the small network taken into account, it is possible to evaluate that the Gauss-Seidel method requires many more iterations to achieve the same result as the backward/forward and Newton-Raphson method.

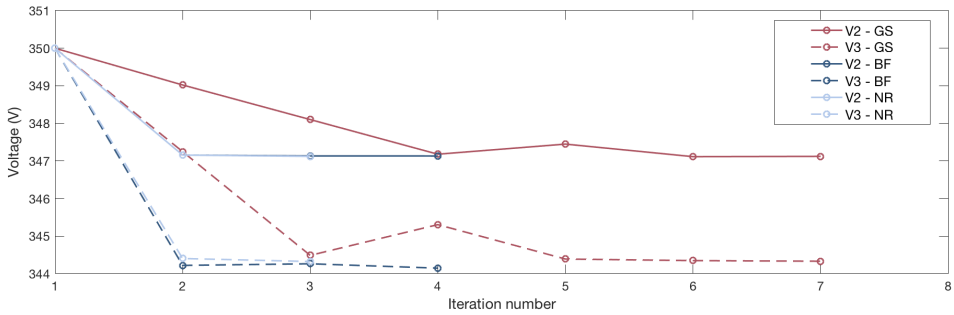


Figure 2.10: Voltage convergence comparison for DC computational methods found in literature

# Chapter 3

# Modeling of DC Distribution Grids

## Table of Contents



This chapter introduces the elements of grid modeling for a DC distribution system. It is divided into two parts: first, section 3.1 discusses the line models and physical assumptions taken into account; second, section 3.2 provides an overview of the different node behaviours that are expected to play a role in future DC distribution systems.

## 3.1 Line modeling

A model of the distribution lines is needed in order to define and characterize the system behaviour. In future DC distribution systems, many different architectures have been suggested to replace the current infrastructure [10, 11, 37, 38]. Three main architectures are of particular interest:

1. Monopolar: this architecture shows only one single DC line. It is clearly the cheapest option, but ground, or sea, return of the current is needed. Ground return is often prohibited because of the corrosion-related damage that high current would cause on the underground structures, such as pipelines, etc. Mono-polar links are generally operated with negative polarity, because of the reduced corona effect when compared to positive polarity.

2. Bipolar: in this case one line will have positive polarity, a second one negative polarity, while the third one, placed in-between, will be the neutral wire. As shown in figure 3.1, the bi-polar solution is much flexible and allows the connection of smaller or bigger loads to the same infrastructure. Each link can also be independently operated when needed.

3. Homopolar: this option features a neutral cable or grounding that separates two DC cables, both with same polarity. Negative polarity is often preferred because of lower corona effect.

This architecture has the advantage of reduced insulation costs. In any case, the disadvantage of the earth return generally outweighs the advantages.

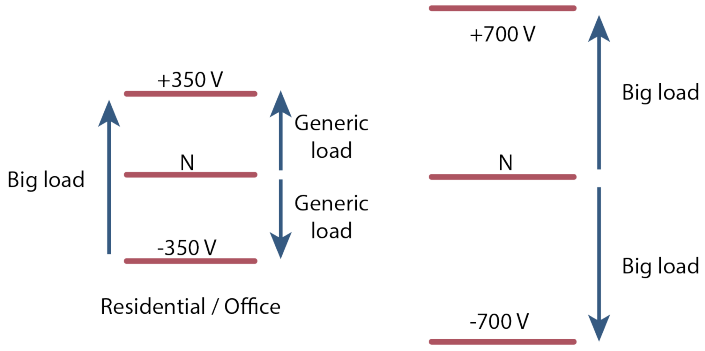


Figure 3.1: Bipolar architecture for distribution system [4]

In the following sections the lumped element theory for line modeling and the concept of topology analysis will be described.

### 3.1.1 Lumped element line models

Transmission and distribution lines can be described and modeled to take into account the electromagnetic phenomena involved [20]. In figure 3.2, below, three of the most used models for single distribution lines are shown. Models with multiple lines need to take into account additional effects given by wire coupling. Among these effects it is possible to leakage resistance and mutual inductance. The effects given by R, L and C are spread all along the line. The lumped element theory, instead, concentrates the properties of each of these characteristic into one component.

It should be noted that the line conductance G is not included because distribution lines typically have a very high R/G ratio, so that G is effectively negligible.

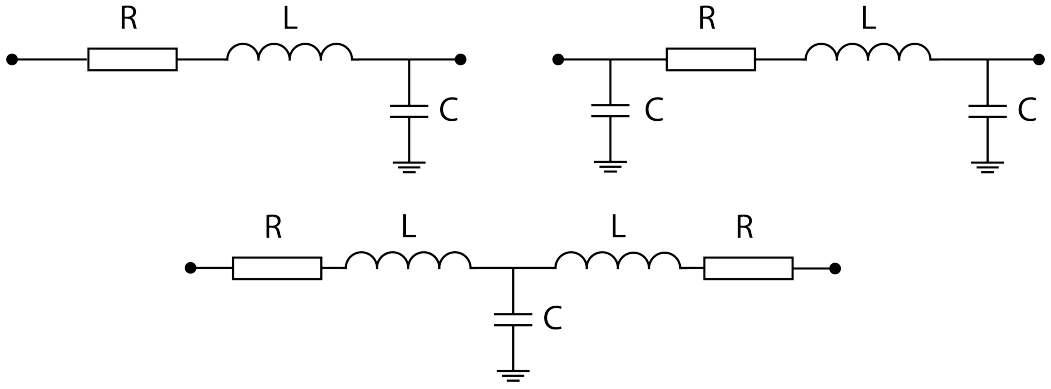


Figure 3.2: Γ (top left), $\pi$ (top right) and T (bottom) lumped element model for distribution grid [13]

The *gamma* (Γ) model includes a resistor, an inductance in series and a conductance in parallel. The *pi* ($\pi$) model, on the other hand, features capacitance to ground at both end nodes of the distribution line. Finally, the T model includes two symmetrical pairs of resistor and inductor in series, with one single capacitance in parallel in-between the two pairs.

All the above mentioned lumped element model, shown in figure 3.2, for example, can be solved with differential equations in order to describe the dynamic effects of currents [13]. Since the power flow problem is a steady state analysis of the network behaviour, it is possible to consider all the time variant behaviours as constant. Therefore, in the steady state model the line can be considered as a simple resistor, as depicted in figure 3.3 below.

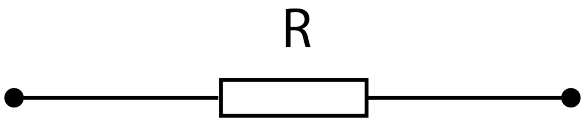


Figure 3.3: Simple resistive line model

### 3.1.2 Line topology analysis simplification technique

Topology analysis technique can be implemented in order to simplify the components that form a node or bus in the system [27]. As shown in figure 3.4, the node A, idealized on the right hand side as a connection bus with a load, is composed in reality by many more components. Among these, breakers, switches and fuses that connect to a bus-bar.

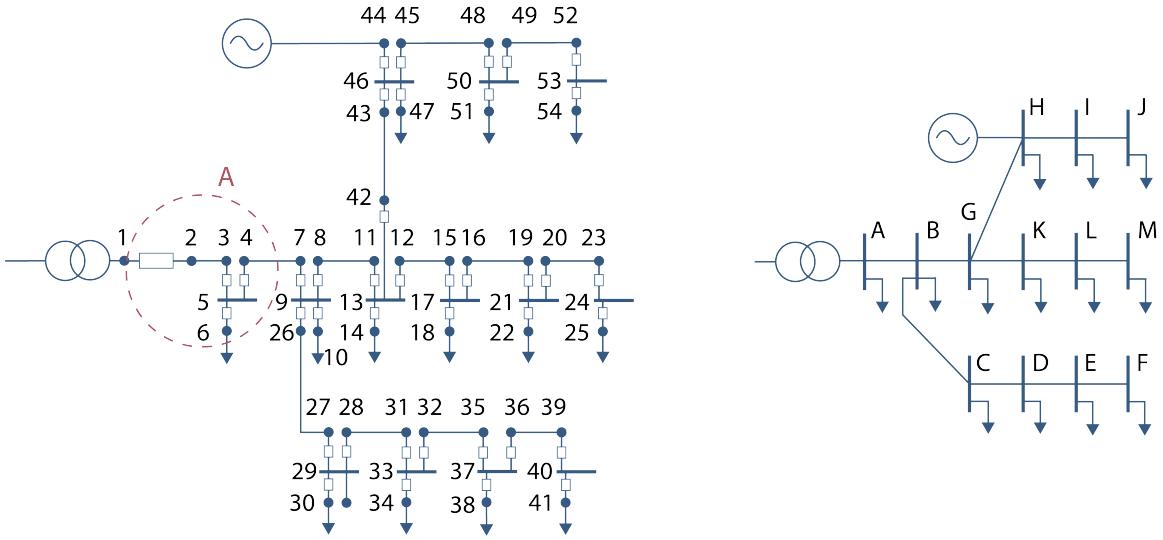


Figure 3.4: Distribution network scheme (on the left) simplified via topology analysis (on the right) [27]

It is possible to assume that all the network nodes under the subsystem A have the same potential and therefore same currents. In this way the number of nodes reduces significantly, from 54 of the left figure to 13 in the right figure. This simplification does not affect the outcome of steady state analysis, such as power flow computation. The voltage difference between the nodal points under same group, in fact, is very low and can be thus neglected. Reducing the number of nodes reduces the dimension of the incidence matrix used in the power flow computation. In this way it is then possible to have faster convergence for the same system analyzed.

## 3.2 Nodes modeling

In the power systems of the future, and more specifically in the distribution systems, there will be a diverse behaviour in the different nodes. This differs radically from traditional power systems, where nodes are almost exclusively treated as in constant power, resulting in a solution limited to power exchange within the grid and voltage in the nodes. Among the different possible types of classification, it is useful to define power converter nodes according to the control strategy locally applied to them. Once the behaviours are described, a more general categorization performed according to the type of node (source, load or hybrid bi-directional) can be given.

Nodes in a distribution network that are not power converter-based can also behave as constant impedance terminals or passive (or step) nodes. The former type is given by loads with a linear behaviour in their I-V characteristic. The latter type, instead, is represented by hub-nodes without generation or load.

### 3.2.1 Node classification by converter control strategy

It is possible to classify nodes according to the type of control: constant voltage, constant current, constant power and constant impedance (or resistance) [31]. A combination of these behaviours is also possible: for example, if in a node more power converters are linked in parallel. Additionally, droop control can be considered as a linear combination of a constant power or current and a constant resistance node [31, 33]. As long as the voltage level is set to an operating point below the power limit of the converter, the droop node behaves as a constant resistance. After the current or power limit is met, the node behaves at constant flow, thus current or power, respectively. Constant voltage terminals can include the main substation converter and converters in the grid which can set the voltage level, and maintain it throughout internal control loops. Nonetheless, most of the power converters in the low voltage grid are likely represented as constant power nodes. These include renewable energy resources, energy storage devices and controlled loads.

Control in power converters is based on voltage as a physical reference for grid stability [10, 37, 33]. It is possible to consider voltage as the analogue of frequency in traditional power system. Nonetheless, voltage is a local property, and therefore it gives limited indication about the overall status of the grid. In any case, the voltage in DC networks is influenced by both power balance and by current flows in the lines, and it is therefore the best indicator for DC grid stability.

One of the most used control strategies is voltage droop control [33]. The proportional relation that regulates the voltage can be established with either current or power. Defining variations as $\Delta V = V - V_{\text{ref}}$ , $\Delta I = I - I_{\text{ref}}$ and $\Delta P = P - P_{\text{ref}}$, it is possible to draw the droop characteristic in current (I) base, in both current (I-V) and power (P-V) characteristics:

$$\Delta I_{\text{I}} = \frac{1}{k_{\text{I}}} \Delta V \tag{3.2.1}$$

Knowing that $P_{\text{ref}} = V_{\text{ref}} \cdot I_{\text{ref}}$, the droop relation can be described in power variations terms:

$$\Delta P_{\text{I}} = \left( \frac{V_{\text{ref}}}{k_{\text{I}}} + \frac{P_{\text{ref}}}{V_{\text{ref}}} \right) \Delta V + \frac{1}{k_{\text{I}}} \Delta V^2 \tag{3.2.2}$$

Similarly, the expression for the power (P) based droop in both characteristics is:

$$\Delta P_{\text{P}} = \frac{1}{k_{\text{P}}} \Delta V \tag{3.2.3}$$

$$\Delta I_P = \left(\frac{1}{k_P} - I_{ref}\right) \frac{\Delta V}{\Delta V + V_{ref}} \tag{3.2.4}$$

The factor $k$ is the droop constant and it is defined according to the chosen base. Figure 3.5 shows the I-V and P-V characteristics of power droop control. On the left, the I-base is linear, while the P-base has hyperbolic behaviour, until the power limit of the converter is reached. On the right, the P-V characteristic shows a linear behaviour of the P-base and a parabolic behaviour of the I-base.

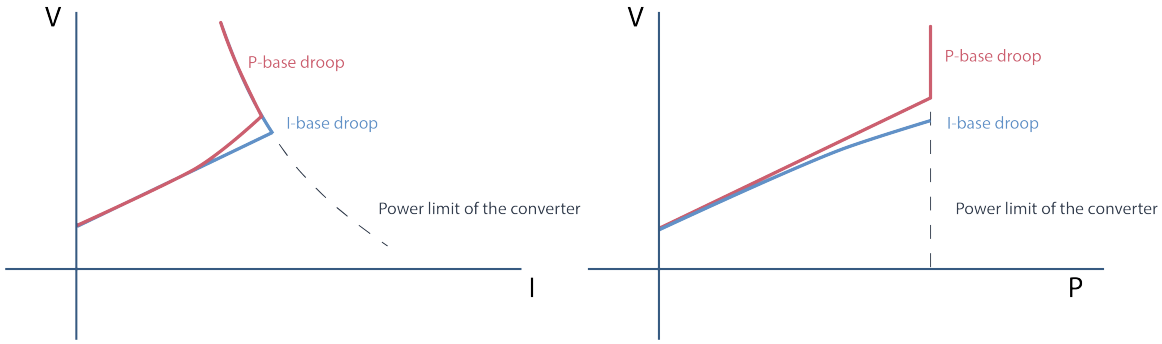


Figure 3.5: I-V curve and P-V curve for voltage droop control in power converters [33]

A second type of control often implemented can be generally defined as constant flow control. It includes both constant current and constant power behaviours. Mathematically speaking, this type of control can be expressed as the limiting case of the voltage droop, for which the droop constant k equals infinity. This suggests that for any value of the voltage, the same amount of power or current will be delivered or absorbed by the power converter.

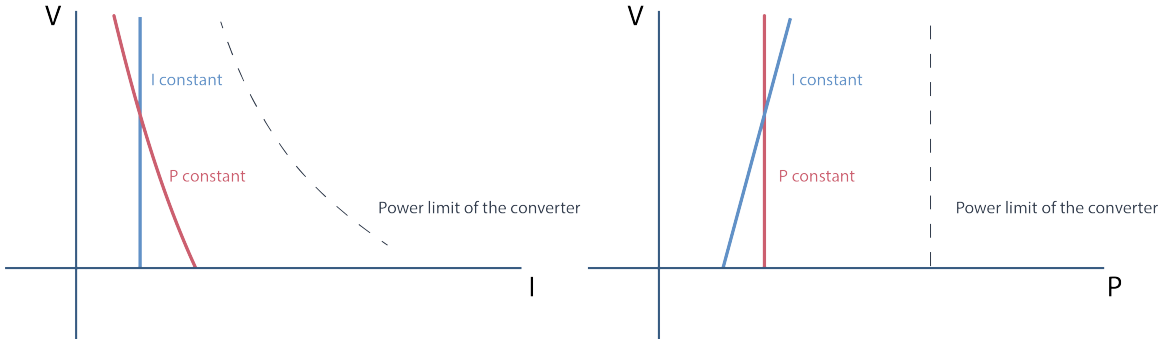


Figure 3.6: I-V curve and P-V curve for constant flow control in power converters [33]

Constant flow control I-V and P-V characteristics are depicted in figure 3.6. On the left side, the I-V curves show that constant current is, obviously, a vertical line. The constant power behaviour has instead an hyperbolic fashion. The graph on the right has a vertical constant behaviour for power nodes, and a linear behaviour for constant current.

Even though in steady state analysis it is not relevant how a certain behaviour is maintained through control, it is important to state that an infinite gain k implemented in the control loop would likely lead to instability. In reality, a PI (proportional-integral) control is implemented [33].

The last type of node control is constant voltage. Here the voltage is maintained constant regardless the amount of current and power delivered or absorbed by the converter. In both the

characteristics, as shown in figure 3.7, the power and current behaviours are overlapping. A horizontal constant voltage behaviour is depicted, as long as the converter operates within its power limit. After that threshold is met, the power converter delivers constant power at nominal value.

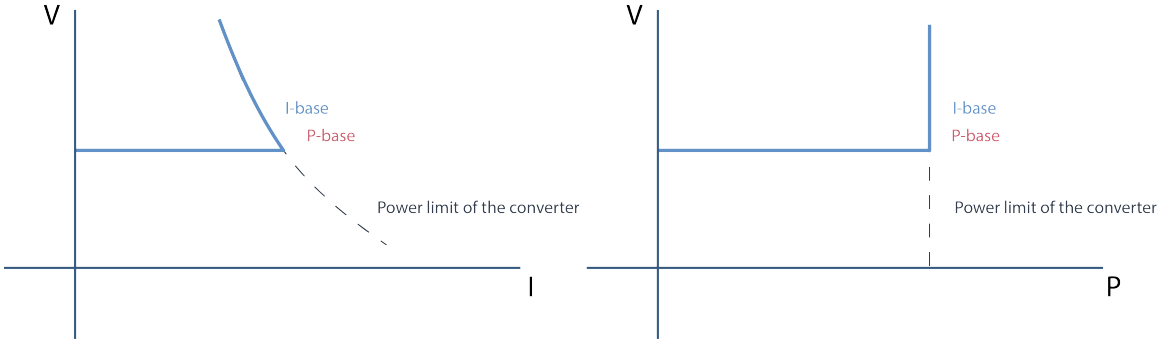


Figure 3.7: I-V curve and P-V curve for constant voltage control in power converters [33]

Constant voltage control can be seen as the limiting case in which the droop coefficients $k_I$ and $k_P$ go to zero. Once again, this result is obtained dynamically with the implementation of a PI controller, for stability reasons.

### 3.2.2 Node classification by type

Once the different possible nodes behaviours have been defined, it is possible to catalogue them depending on their effective use in DC networks. Figure 3.8 shows one of the possible groups in which these behaviours for DC distribution grids can be sorted. Here the node types are arranged depending on their main scope and use. The distinction is based on whether power is injected into the grid (source), retrieved from the grid (load) or a non-simultaneous combination of the two (hybrid).

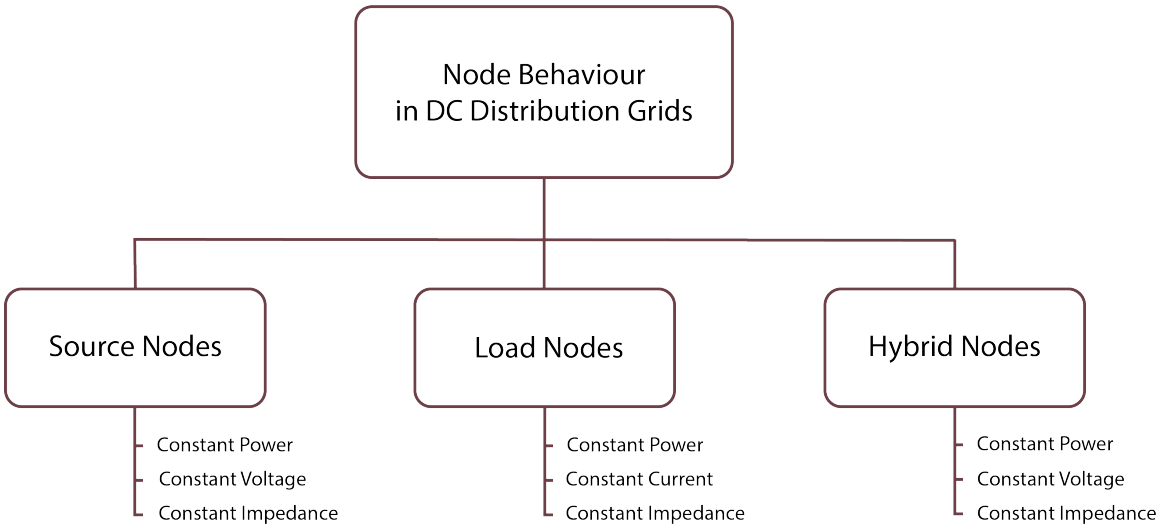


Figure 3.8: Node behaviour scheme in future power systems

The first group is represented by source nodes. These nodes inject power into the grid, and are characterized by three types of elementary behaviours, depending on the nature of the source:

constant power, constant voltage or constant impedance. For example, photovoltaic technologies are expected to play an important role in future DC grids, because of their low installation costs and modularity [4]. These nodes feature a DC to DC converter in order to set the optimal voltage level according to maximum power point tracking algorithms [24]. As for PV, electromagnetic based generators (wind turbines and any type of rotating generator) are characterized by constant power, since again coupled to power converters.

The second group, the load nodes, can be divided into constant impedance, power and current, or a linear combination of these [39]. Constant power and current are characteristic of power converters, according to their control strategy. Constant impedance node, on the other hand, are generally simple loads, such as resistive lighting and heating, which behave with a linear I-V characteristic.

The last group, represented by the hybrid nodes, gathers those network nodes that can either inject or retrieve power from the grid. Examples are batteries and grid connection with AC transmission systems. These nodes are generally modeled as constant power, but constant voltage and impedance and droop behaviours can be also found in literature. An example of constant voltage behaviour is given by batteries directly connected to the network [10]. As for their working principle, batteries have constant voltage characteristic. In any case, the choice of linking batteries directly to the grid is often not considered, because of stability reasons. Additionally, a direct connection would compromise the life-time of the battery system. For these reasons, batteries are expected to be generally interfaced via DC-DC converters to the DC distribution networks.

## 3.3 Conclusion

In this chapter two main model parameters were described: first, the single-line grid model and, second, the node behaviour model. The fact that different generators, loads and hybrid behaviours can be found is expected to play a main role in the power grid of the future. Therefore a power flow method that is able to take into account the different converter control strategies and the different node behaviours is needed in order to describe the steady state of the power network.

In the next chapter the power flow method proposed in this thesis is described and applied. Among the different assumptions, it must be mentioned that the topology architecture chosen is monopolar (single DC line) and that the losses related to the power converters are neglected.

# Chapter 4

# Low Voltage Direct Current Power Flow

## Table of Contents



This chapter introduces the mathematical modeling of the different distribution network elements previously introduced in chapter 3 and the power flow tool built in order to perform steady state analysis at network level. In section 4.2 the objective of the tool is explained, together with the modeling of different nodes behaviours. Important focus is put into section 4.3 where two different linearization methods are introduced and applied to the power flow model. In section 4.4 the complete model is shown and the power flow tool is applied for two network topologies in order to show its working principles. Finally, in section 4.5 a solvability analysis of the system is shown. In this section the aim is to investigate what are the network configurations that give a solution - in mathematical terms - and that are thus stable configurations in experimental context.

# 4.1 Introduction

Because of the recent interest of academia and industry for direct current (DC) distribution systems, a number of research papers have been written in order to determine different power flow methods that could be used in this new context. The shift from AC to DC simplifies - in mathematical terms - the power flow problem because voltage angle and reactive power are not anymore taken into account. Nonetheless, a number of other issues need to be faced, especially when it comes to power converter control. In AC transmission and distribution systems all loads and generators are considered as delivering or absorbing constant power (namely, PQ and PV nodes), with the only exception of the slack bus, which is modeled as a reference in voltage magnitude and angle. It is instead expected that the power systems of the future will include also different node behaviours, as previously shown in section 3.2.2. This aspect will be taken into account in the model developed in this chapter.

Moreover, it has been found in literature that effort has been put into solving LVDC (low voltage DC) power flow problems only for radial or weakly meshed networks. Even though these kind of topologies are nowadays the most used at distribution level, it is believed that also a highly meshed or looped network topology should be considered, especially in a scenario in which distributed generation will have a high impact on distribution systems.

It has been found in literature that another characteristic of LVDC networks is that, unlike AC systems, under certain light assumptions it is always possible to have convergence and a unique solution of the power flow problem, regardless of the computational method used [31]. This aspect is investigated more thoroughly in section 4.5 of this chapter.

# 4.2 Objective of the tool and modeling

The objective of the power flow solver modeled is to provide a steady state solution as a *snapshot* of the system under certain distributed load and generation conditions. This is possible once given a proper number of inputs such as node information (node type and parameters) and network information (topology, directed graph and line parameters). The solution found is a vector of state variables (unknown node voltages) and flow variables (line currents). The solver of the power flow is matrix based and it is therefore based on linear equations. Since the power flow problem is typically non-linear, linearization methods are needed. Two types of linearization are showed and compared in section 4.3.

## 4.2.1 Line network modeling

The network can be completely described when in the model are taken into account both physical characteristics and topological characteristics. The former element, as described previously in section 3.1.1, is modeled as a simple resistive line that connects two nodes to each other. The latter element, on the other hand, can be simply imported in form of oriented (or directed) incidence matrix. The incidence matrix **F** is a matrix with dimensions *LxN*, where *L* is the number of lines and *N* the number of nodes in the network. The incidence matrix is defined as a sparse matrix with the following elements:

$$\mathbf{F}(n,m) = \begin{cases} 1, & \text{if current in line } n \text{ leaves node } m \\ -1, & \text{if current in line } n \text{ enters node } m \\ 0, & \text{if line } n \text{ is not connected to node } m \end{cases}$$

### 4.2.2 Simple nodes modeling

Three types of nodes are first considered and modeled as *elemental* node behaviours. Constant voltage gives nodes are nodes in which the voltage level is known and therefore the number of unknown variables is reduced. These nodes can be compared to the slack buses in AC systems, since they both are meant to bring stability to the system and guarantee the power balance of the system. In AC systems the node chosen as slack is generally corresponding to the biggest generator in the system, so that there is a higher chance that the feasibility of dispatch is ensured. For distribution systems in general, an example of constant voltage is usually the connection to the medium voltage grid.

Constant current nodes are generally loads such as universal motors or DC motors. The current injected into the node is constant, but both voltage and line currents are still unknown (unless only one line is connected to the node: then that line current will be equal to the node current).

Last, constant impedance nodes are modeled. These nodes show a linear behaviour in the I-V characteristic and thus the higher the current absorbed by the load, the higher the voltage level at the node. A representation of the three elemental nodes can be found in figure 4.1.

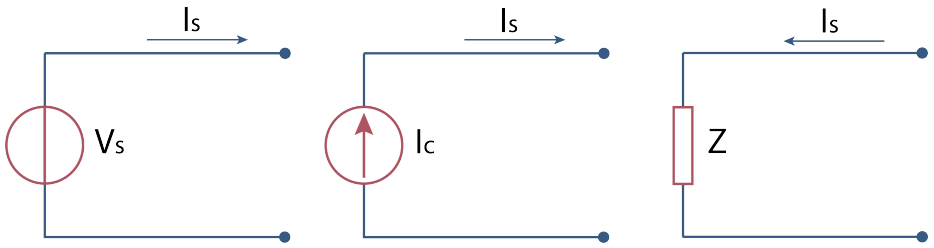


Figure 4.1: Constant voltage node (on the left), constant current node (in the centre) and constant impedance node (on the right)

Droop controlled power converters, as shown before in section 3.2.1, are mainly used in DC distribution grids and microgrids in the current-base variant [40]. The characteristic of droop is given by the following equation:

$$V - V_{\text{ref}} = k_{\text{I}} \cdot I_{\text{s}} \tag{4.2.1}$$

This relation shows that a droop node can be modeled as a constant voltage source set at $V_{\text{ref}}$ in series with an impedance of value $k_{\text{I}}$. In order to keep the node parameters separated from the line parameters, it is advantageous to represent the droop source as a Norton equivalent instead. In this way, as shown in figure 4.2, the source is simply described as a current source in parallel with an impedance.

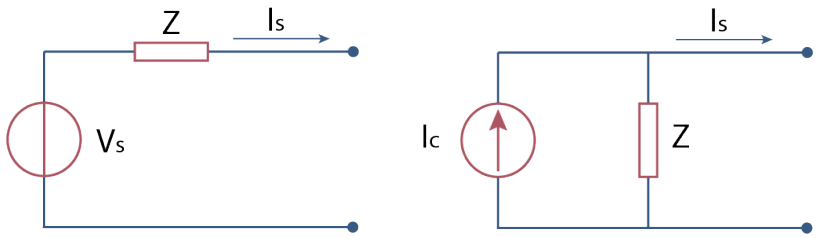


Figure 4.2: Droop source as Thevenin equivalent (on the left) and as Norton equivalent (on the right)

The value of the impedance is again equal to the droop coefficient, whereas the current source is defined as:

$$I_c = \frac{V_{ref}}{Z} \tag{4.2.2}$$

Lastly, it is possible to consider combinations of some of the nodes previously shown. Considered that a constant voltage node would be unpractical in combination with others, we can take into account multiple current sources and impedances in parallel. As it will be shown in the next section, also constant power nodes can fall under this group. In figure 4.3 an example of two current and two impedances nodes is shown.

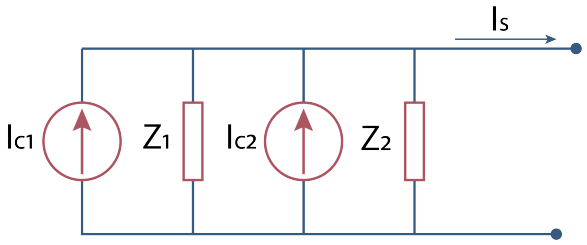


Figure 4.3: Node with a combination of two elemental node behaviours

Since all nodes are placed in parallel, it is possible to compute an equivalent node with one current source and one impedance load. The currents can be found summing up the values of the single elements:

$$I_{c,eq} = \sum_{i=1}^{N} I_{c,i} \tag{4.2.3}$$

while in order to find the equivalent of multiple impedances in parallel the following elementary equation should be used:

$$Z_{eq} = \left( \sum_{i=1}^{N} Z_i^{-1} \right)^{-1} \tag{4.2.4}$$

## 4.3 Linearization methods

Linearization is a crucial aspect in any power flow method, as previously described chapter 2. Both Gauss-Seidel and Newton-Raphson based computational methods fall under the fixed-point iteration problem, through which it is possible to rewrite a complex function $f(x)$ in the form $x = F(x)$ and solve $f(x)$ with successive attempts [41]. All nodes so far presented behave according to

linear equations. The non-linear nature of power systems rises when the constant power behaviour is taken into account.

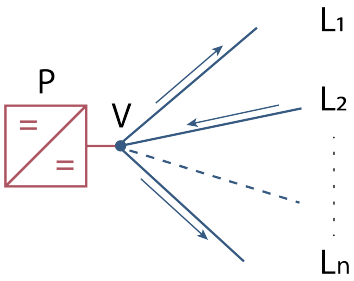


Figure 4.4: Constant power node connected to an arbitrary number of lines

In figure 4.4 it is depicted a generic constant power node, connected to $n$ lines. The equation describing the behaviour of a generic node $i$ connected to a number $n$ of lines is:

$$V_i \cdot \left( \sum_{j=1}^{n} I_j \right) + P_i = 0 \tag{4.3.1}$$

In order to include constant power nodes into the tool framework as described in the previous sections, the constant power node behaviour needs to be linearized and solved in an iterative way. Two methods have been investigated and applied in order to find a solution to the problem, taking into account the nature of DC systems. In the following sections both methods will be applied and compared in order to seek the most efficient, both in computational time and number of iterations needed to get an acceptable result.

### 4.3.1 Linearization as current source

The first method is found rewriting equation 4.3.1 as follows:

$$\sum_{j=1}^{n} I_j + \frac{P_i}{V_i} = 0 \tag{4.3.2}$$

This is acceptable since $V_i$ cannot be zero. In this way the nodal information is stored in one single variable, which can be conceptualized as a current source as shown in figure 4.5.

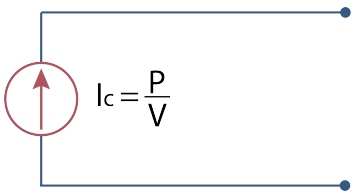


Figure 4.5: Scheme of power node linearized as current source

A guess value $V_i^{(0)}$ is used to start the iteration process, so that:

$$I_{c_i}^{(0)} = \frac{P_i}{V_i^{(0)}} \tag{4.3.3}$$

The so defined current source can be included in the linear equations for the current node balance and, once the system is solved, a new value $V_i^{(1)}$ is found. Convergence is checked for all node voltages, considering the voltage mismatch vector $\mathbf{\Delta V}$ against an arbitrary tolerance $\varepsilon$, as expressed in:

$$|\mathbf{\Delta V}| = |\mathbf{V}^{(k)} - \mathbf{V}^{(k-1)}| \leq \varepsilon \tag{4.3.4}$$

In figure 4.6 it is drawn the flowchart of the above described iteration method.

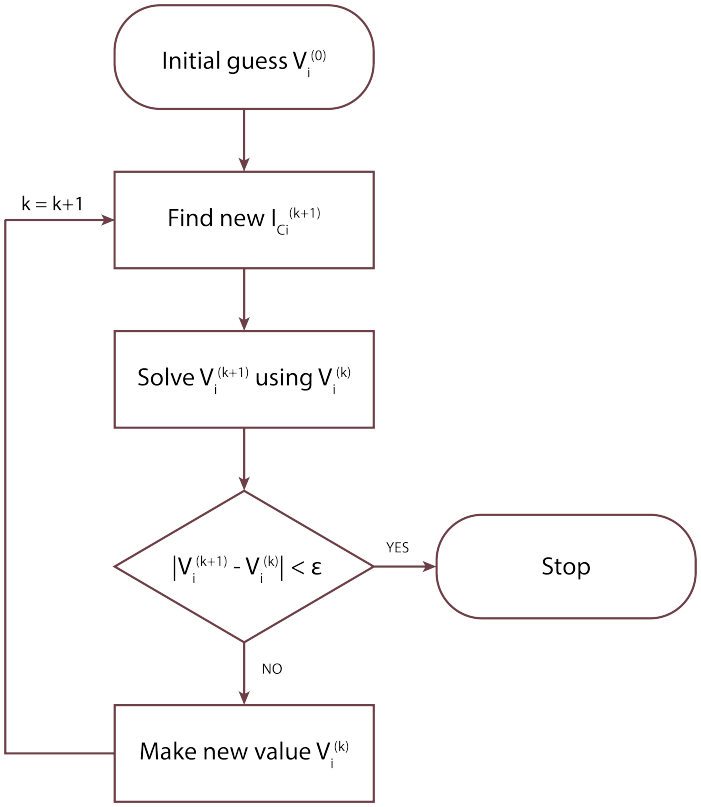


Figure 4.6: Flowchart of equivalent current source linearization method

This type of linearization, even though very fast and computationally not expensive, does not ensure convergence for some particular cases. It is possible to take the small circuit in figure 4.7 below as an example of how this first method can fail in convergence also for very simple problems.

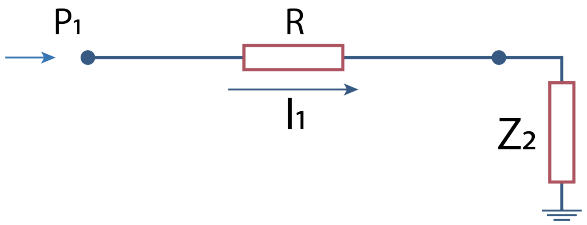


Figure 4.7: Simple two-node circuit with constant power source and constant impedance load

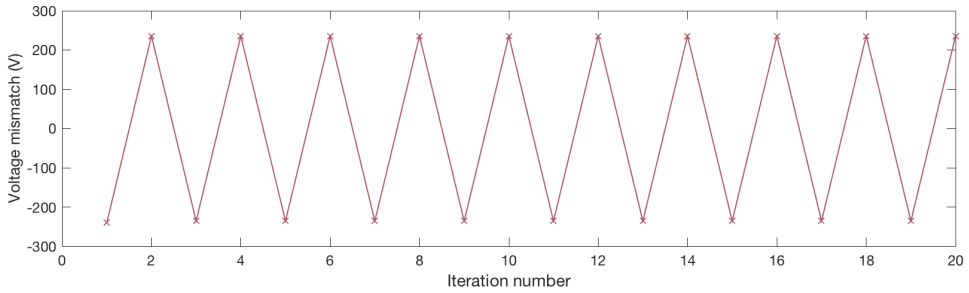


Figure 4.8: Voltage mismatch for results of two-node circuit with P and Z nodes

As shown in figure 4.8, a result cannot be found since the solver will continue iterating between the same two values of voltage for both nodes 1 and 2 (overlapping in the figure). Here the voltage mismatch is defined for both nodes as previously stated in equation 4.3.4. An alternative way to linearize the power behaviour of the LVDC network is therefore needed in order to solve as many cases as possible. The second method is discussed in the next section.

### 4.3.2 Linearization as current source and impedance in parallel

The second linearization method tested is based on the concept of negative incremental impedance, as illustrated in figure 4.9 for a constant power behaviour in the I-V framework [21]. This type of linearization guarantees convergence for a higher number of cases when compared to the previous linearization method.

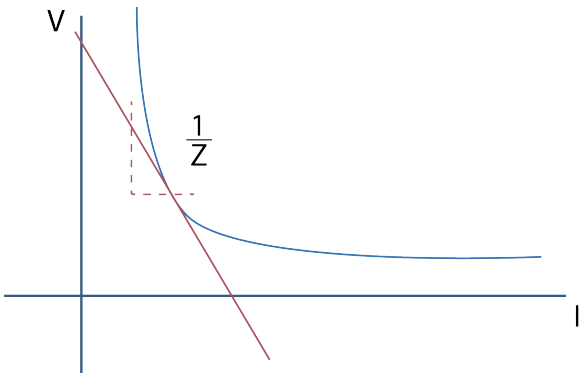


Figure 4.9: I-V characteristic of a constant power converter and linearization as negative incremental impedance

In this case the constant power node is simplified into a node with constant current source and impedance placed in parallel, as shown in figure 4.10.

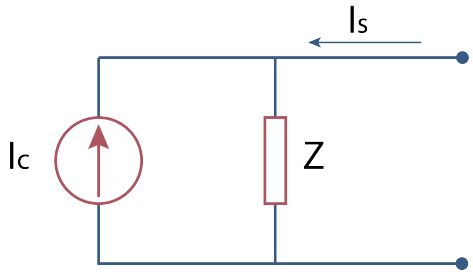


Figure 4.10: Scheme of a constant power source node linearized as current source and impedance in parallel

Considering figure 4.10 we know that the following equation holds true for the current:

$$I_s = -I_c + \frac{V_s}{Z} \tag{4.3.5}$$

while from figure 4.9 we know that:

$$\frac{1}{Z} = \frac{dI_s}{dV_s} = \frac{d}{dV}\left(-\frac{P}{V_s}\right) = \frac{P}{V_s^2} \tag{4.3.6}$$

If a correct solution value of the voltage $V_s$, which we will call $V_0$, is guessed, it is possible to find that:

$$I_s = -\frac{P}{V_0} = -I_c + \frac{V_0}{Z} \tag{4.3.7}$$

Substituting equation 4.3.6 into 4.3.7, we obtain the following equation for the current injected by the current source:

$$I_c = \frac{P}{V_0} + \frac{V_0}{Z} = \frac{P}{V_0} + \frac{P}{V_0^2} \cdot V_0 = 2\frac{P}{V_0} \tag{4.3.8}$$

From this equation we can finally find the value of the current injected by the constant power node, substituting 4.3.6 and 4.3.8 into 4.3.7:

$$I_s = -2\frac{P}{V_0} + \frac{P}{V_0^2} \cdot V_s = -I_c + \frac{1}{Z} \cdot V_s \tag{4.3.9}$$

With this equation we are back at the behaviour described in equation 4.3.5, but in this case we have defined values for both $I_c$ and $Z$, which depend on P (known node information) and $V_s$, that needs to be found by guess and iteration. In order to do so, $I_c$ and $Z$ are then used in the computation, as later described in section 4.4. Figure 4.11 shows the flowchart of the above described linearization method. As explicitly mentioned, the matrix A used to solve the linear system, unlike the current source based linearization before described, needs to be updated at every iteration step. This, as it will be analyzed also later, has an effect on the computational time required by the solver.

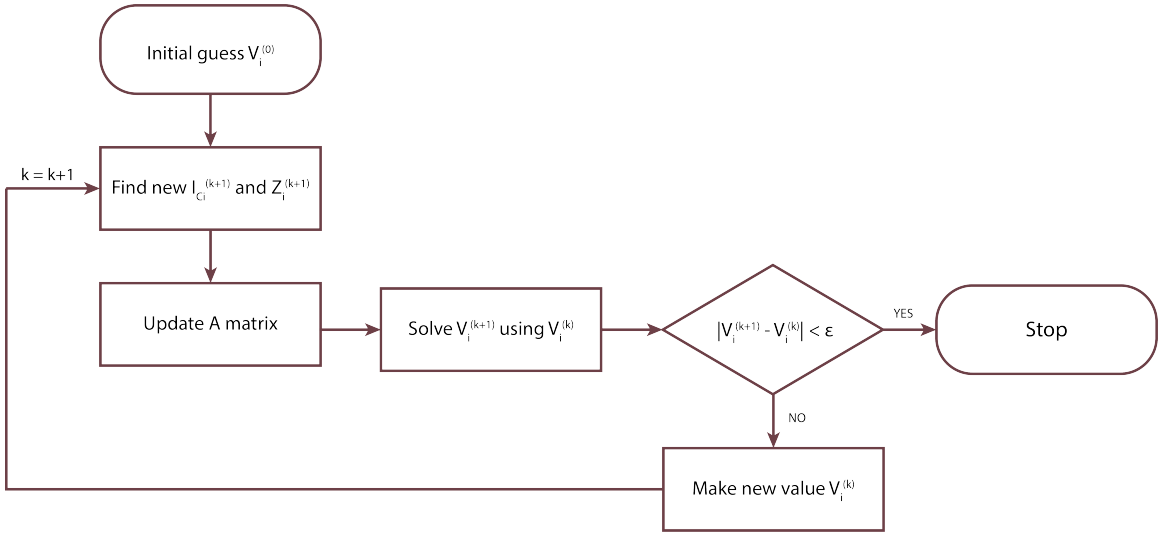


Figure 4.11: Flowchart of current source-impedance linearization method

It is therefore possible to check how the convergence behaves for the simple two-node circuit with constant power source and constant impedance load as depicted in figure 4.7 in the previous section. As shown in figure 4.12, the convergence is assured in 4 iterations.

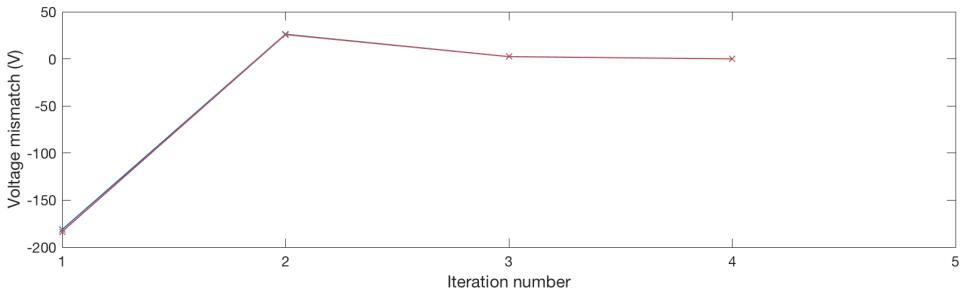


Figure 4.12: Voltage mismatch for convergence shown through voltage mismatch for two-node (I-Z) network

## 4.4 Full model and applications

Once all lines and nodes are represented as linear equations, it is possible to solve the linear system in matrix form. The solution is based on Kirchhoff's laws that allow to find both state variables (voltages) and flow variables (currents). The number of unknown in the system is $N - N_V + L$, where $N$ and $L$ are the number of nodes and lines, and $N_V$ is the number of constant voltage nodes.

The model is based upon three sets of linear equations which relate voltages and currents with the known variables of the system. A number $L$ of equations are used to express Ohm's law on the distribution line, according to the following equation, valid for every line connecting a node $i$ to a different node $j$ :

$$V_i - V_j - I_{ij} \cdot R_{ij} = 0 \tag{4.4.1}$$

where $V_i$ and $V_j$ are the voltages in nodes $i$ and $j$ and $I_{ij}$ and $R_{ij}$ current and resistance between those two nodes, respectively. The second set of equations is applied for every node $i$ with a

constant current behaviour $I_{ci}$ and it is a node balance as represented by the equation:

$$\sum_j I_j + I_{ci} = 0 \tag{4.4.2}$$

Lastly, the third set of equations represents the node balance at every node $i$ with a constant impedance behaviour expressed by $Z_i$. This set of equations is given by:

$$\sum_j I_j - \frac{V_i}{Z_i} = 0 \tag{4.4.3}$$

Constant power nodes, droop nodes and combination nodes all fall under these three equation sets, since, as explained previously, they all can be seen as linear combinations of current source and impedance behaviour. The coefficients found in the Kirchhoff's equations above described can be stored in a matrix, here called **A**, defined as:

$$\mathbf{A} = \begin{bmatrix} \mathbf{\Gamma} & -\mathbf{R} \\ -\mathbf{Z} & -\mathbf{\Gamma}^T \end{bmatrix} \tag{4.4.4}$$

Matrix **A** is a square matrix, divided into four sub-matrices as shown in equation 4.4.4. Matrix $\mathbf{\Gamma}$ is a reduced version of the oriented incidence matrix **F** of dimensions $L$ by $(N - N_V)$, as defined in section 4.2.1. In matrix $\mathbf{\Gamma}$ the columns corresponding to nodes with constant voltage behaviour are taken out.

Submatrix **R** is a diagonal matrix, where the diagonal elements are the line resistances so that:

$$\mathbf{R} = \begin{bmatrix} R_1 & 0 & \dots & 0 \\ 0 & R_2 & 0 & \vdots \\ \vdots & 0 & \ddots & 0 \\ 0 & \dots & 0 & R_{\mathrm{L}} \end{bmatrix} \tag{4.4.5}$$

Submatrix **Z** is a diagonal matrix, where the diagonal elements are the inverse of the node impedances, zero if the node does not have any impedance load. As for the matrix $\mathbf{\Gamma}$, also **Z** is reduced, as the columns corresponding to the constant node voltages are taken out. It should be noted that the **Z** matrix is always squared and with dimensions $(\mathrm{N} - \mathrm{N_V})$ by $(\mathrm{N} - \mathrm{N_V})$. The impedance matrix can be therefore described as follows:

$$\mathbf{Z} = \begin{bmatrix} \frac{1}{Z_1} & 0 & \dots & 0 \\ 0 & \frac{1}{Z_2} & 0 & \vdots \\ \vdots & 0 & \ddots & 0 \\ 0 & \dots & 0 & \frac{1}{Z_{\mathrm{N-N_V}}} \end{bmatrix} \tag{4.4.6}$$

where $\frac{1}{Z_n}$ equals zero if $n$ corresponds to a node with no impedance behaviour.

The last elements to take into account are the constant voltages set at node level and the constant current loads in the system. A vector column **K** of dimensions 1 by $(\mathrm{N} - \mathrm{N_V} + \mathrm{L})$ is defined. The vector **K** contains a column of L zeros and a column of constant current elements $(\mathrm{N} - \mathrm{N_V})$ so that $\mathbf{I}_{\mathrm{c}}(n)$ is taken away if $n \in \mathrm{N_V}$, as specified in the following equation:

$$\mathbf{K} = \begin{bmatrix} 0 \\ \vdots \\ 0 \\ \mathbf{I_c} \end{bmatrix} \tag{4.4.7}$$

The constant voltages are included in a vector $\mathbf{V_c}$ of dimensions $N_V$ by 1, which is in turn multiplied by a matrix $\mathbf{C}$, of dimensions L by $N_V$. The matrix $\mathbf{C}$ contains the columns taken away from the incidence matrix $\mathbf{F}$ that refer to the nodes with constant voltage and are therefore taken away from the incidence matrix $\mathbf{F}$ when matrix $\mathbf{\Gamma}$ is found. It is therefore possible to say that $\mathbf{F}$ is found combining matrices $\mathbf{\Gamma}$ and $\mathbf{C}$. The two constant vectors have the same dimensions and can be therefore summed up into a single vector $\mathbf{B}$ of known constant values:

$$\mathbf{B} = \mathbf{K} + \mathbf{C} \cdot \mathbf{V_c} \tag{4.4.8}$$

Finally, the power flow problem can be represented as a linear problem in standard notation as shown in the following equation:

$$\mathbf{A} \cdot \mathbf{X} + \mathbf{B} = \mathbf{0} \tag{4.4.9}$$

Matrix $\mathbf{A}$ is therefore squared and of dimensions $(N - N_V + L)$ by $(N - N_V + L)$. The solution vector $\mathbf{X}$ is found as shown in equation 4.4.10 below:

$$\mathbf{X} = \begin{bmatrix} V_1 \\ \vdots \\ V_{N-N_V} \\ I_1 \\ \vdots \\ I_L \end{bmatrix} = - \begin{bmatrix} \mathbf{\Gamma} & -\mathbf{R} \\ -\mathbf{Z} & -\mathbf{\Gamma}^T \end{bmatrix}^{-1} \cdot \mathbf{B} \tag{4.4.10}$$

Clearly, the possibility of finding a solution of the problem is limited to the case in which matrix $\mathbf{A}$ is non-singular, therefore invertible. In section 4.5 the different cases in which the solution cannot be found for the power flow problem will be addressed in more detail.

A direct comparison between the two linearization methods described in section 4.3 can be now carried out. In fact, the linearization as simple constant current source will require the vector $\mathbf{K}$ to be updated at every iteration, since the value of the linearized current varies. On the other hand, the linearization method as constant current and impedance in parallel will require that both matrix $\mathbf{A}$ and vector $\mathbf{K}$ are updated at every iteration step. Moreover, in this latter case, the inverse of matrix $\mathbf{A}$ needs to be computed as well at every iteration step. This fact makes the first iteration method less computationally intensive, for each iteration, compared to the second one. Nonetheless, linearizing as current source and impedance is expected to give an acceptable result in a lower number of iteration compared to the linearization as only current source.

### 4.4.1 Application to a simple network topology

In order to answer the research questions, it is relevant to apply the methods previously described to networks with different nodes behaviours to check if the solution found is correct. Different checks can be performed to control whether the solution found is correct or not:

- Check the current balance in the nodes, so that the net current in the network is equal to the sum of the currents injected to and retrieved from the distribution system;
- Check the power balance of the system, so that the power injected in the grid minus the power absorbed by the loads is equal to the sum of the ohmic power losses in the lines.

The power flow tool is tested first for the network shown in figure 4.13 below. The network is a meshed topology with 5 nodes and 6 lines. The network parameters are given in table 4.1 and table 4.2.

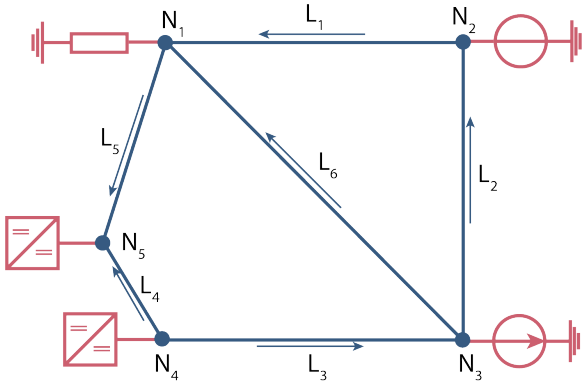


Figure 4.13: 5 nodes and 6 lines meshed network

Table 4.1: Simple network topology node parameters

| Node # | Node type | Node parameter |
|---|---|---|
| 1 | Z constant | 68 Ω |
| 2 | V constant | 350 V |
| 3 | I constant | 4 A |
| 4 | P constant | 1500 W |
| 5 | P constant | -800 W |

Table 4.2: Simple network topology line parameters

| **Line #** | 1 | 2 | 3 | 4 | 5 | 6 |
|---|---|---|---|---|---|---|
| **Resistance** (Ω) | 0.642 | 0.642 | 0.642 | 0.214 | 0.428 | 0.908 |

In order to solve the power flow problem, matrices **A** and **B** needs to be composed according to what previously explained in the chapter. Depending on the linearization method used, matrix **A** does or does not need to be actualized at every iteration step. The oriented incidence matrix, as defined in section 4.2.1, for this topology is given by:

$$\mathbf{F} = \begin{bmatrix} -1 & 1 & 0 & 0 & 0 \\ 0 & -1 & 1 & 0 & 0 \\ 0 & 0 & -1 & 1 & 0 \\ 0 & 0 & 0 & 1 & -1 \\ 1 & 0 & 0 & 0 & -1 \\ -1 & 0 & 1 & 0 & 0 \end{bmatrix} \tag{4.4.11}$$

Knowing that node 3 has constant voltage, it is now possible to find the solution of the problem with both linearization methods proposed. In figure 4.14 the main results of the power flow analysis on the simple network are shown: from top left, node voltages, line currents, voltage mismatch at every iteration step and ohmic losses in the lines.

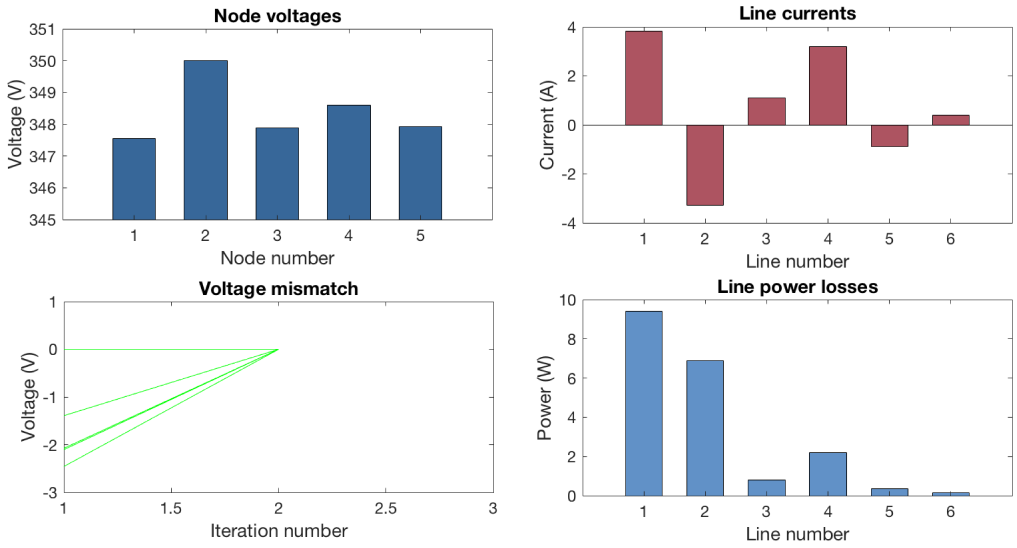


Figure 4.14: Simple network topology power flow results

The method used to run this simulation is the linearization of power nodes into current source and impedance in parallel. In this case only two iterations are needed to find a very close approximation of the result, since the tolerance is set to 0.01 V. For a comparison of the methods, using linearization as constant current source, 3 iterations are instead needed to find the same result. The power flow results are also summarized in table 4.3 below.

Table 4.3: Simple network topology power flow results

| **Line #** | **1** | **2** | **3** | **4** | **5** | **6** |
|---|---|---|---|---|---|---|
| **Line current** (A) | 3.8286 | -3.2788 | 1.1100 | 3.1928 | -0.8934 | 0.3888 |
| **Power losses** (W) | 9.4108 | 6.9018 | 0.7911 | 2.1815 | 0.3417 | 0.1373 |
| **Node #** | **1** | **2** | **3** | **4** | **5** | |
| **Node voltage** (V) | 347.5420 | 350 | 347.8950 | 348.6077 | 347.9244 | |

### 4.4.2 Validation of simple network topology LVDC power flow

In order to validate the results of the model previously described in this chapter, the power system can be tested against other models already accepted in literature. The dynamic model shown in [21] has been chosen because of the similarity in how the nodes are modeled. With the same parameters as in section 4.4.1, the results of the dynamic model can be found in figure 4.15.

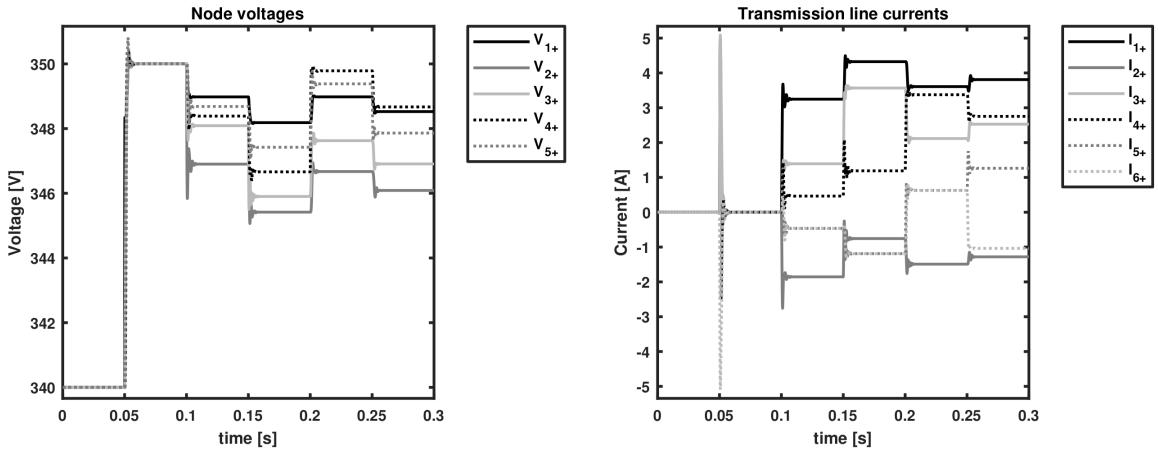


Figure 4.15: Dynamic results for simple network topology for validation

The final results for both node voltages and line currents represent the steady state of the network. As it is possible to see at 0.3 seconds the steady state is reached and the values of voltages and currents are identical to the results obtained with the power flow tool developed in this chapter. It is therefore possible to consider the results correct for a simple network. It should be noted that only the simple network was tested because of the computational burden required by the dynamic analysis. In any case, the validity of the results can be extended also for more complex topologies, such as the ones shown in the next section 4.4.3 and later in the thesis in chapter 5.

### 4.4.3 Application to a complex network topology

The next research question to address is on how to apply the chosen computational method for LVDC power flow to a complex network topology. In this case we consider a loop neighbourhood distribution network. The connection to the medium voltage (MV) grid is placed in node one, which works as a constant voltage. In the rest of the network, loads are represented in red and can be found as constant power, constant current and constant impedance. On the other hand, distributed generation is taken into account so that generators in nodes 3 and 17 work in constant power, while generator in node 7 is set as a droop source with voltage reference set at 350 V and droop constant at 0.1. This will help stabilize the voltage. On the other hand, because of the high power requested, the capacity of the source needs to be previously assessed in order to determine the feasibility of the power dispatch.

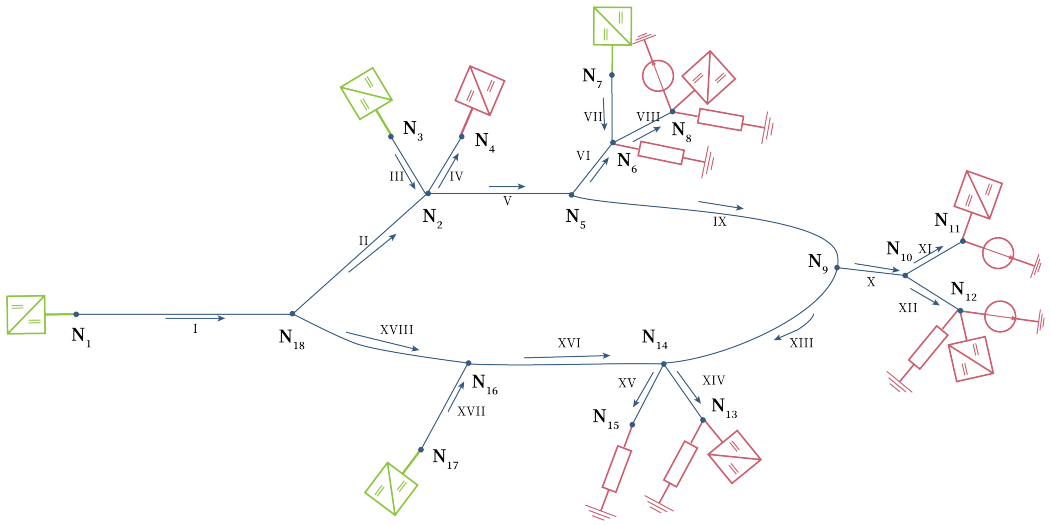


Figure 4.16: Complex network topology with droop and combination nodes

The complete list of parameters used to run the simulation, containing the node types and parameters, is shown in table 4.4.

Table 4.4: Complex network topology node parameters

| Node # | Node type | Node parameter |
|---|---|---|
| 1 | V constant | 350 V |
| 2 | Passive | [-] |
| 3 | P constant | 3 kW |
| 4 | P constant | -2.5 kW |
| 5 | Passive | [-] |
| 6 | Z constant | 68 Ω |
| 7 | Droop | $V_{ref}$=350 V, k=0.1 |
| 8 | Constant P, I and Z | -1.4 kW, -4 A, 60 Ω |
| 9 | Passive | [-] |
| 10 | Passive | [-] |
| 11 | Constant P and I | -5 kW, -6 A |
| 12 | Constant P, I and Z | -3.5 kW, -5 A, 68 Ω |
| 13 | Constant P and Z | -2 kW, 40 Ω |
| 14 | Passive | [-] |
| 15 | Z constant | 120 Ω |
| 16 | Passive | [-] |
| 17 | Constant P | 7 kW |
| 18 | Passive | [-] |

In figure 4.17 the results of the power flow analysis can be found.

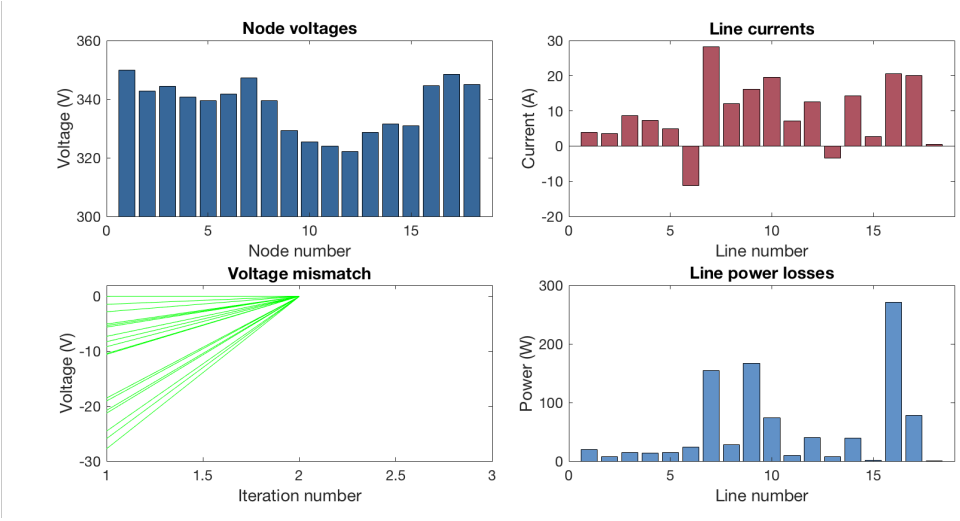


Figure 4.17: Simulation results for a complex network with droop and combination nodes

From the results in figure 4.17 it is possible to see the voltage levels in the network, that are clearly influenced by the distributed generation present in the network. The presence of a generator with droop control in node 7 helps to stabilize the voltage level around the nominal value. In fact, the voltage levels remain in the range $\pm$ 10% of the nominal value. The highest current is found in proximity of the droop source because of the quantity of power directly injected in the next nodes (9.82 kW, as shown in table 4.5). Taking into account the losses, these are only the 4.55% of the total power generated or injected by the medium voltage grid into the system.

Table 4.5: Complex network topology power flow results

| Node # | Voltage (V) | Power (kW) |
|---|---|---|
| 1 | 350 | 1.38 |
| 2 | 342.68 | 0 |
| 3 | 344.36 | 3 |
| 4 | 340.80 | -2.5 |
| 5 | 339.55 | 0 |
| 6 | 341.72 | -1.72 |
| 7 | 347.17 | 9.82 |
| 8 | 339.41 | -4.08 |
| 9 | 329.20 | 0 |
| 10 | 325.42 | 0 |
| 11 | 324.06 | -2.29 |
| 12 | 322.21 | -4.04 |
| 13 | 328.68 | -4.70 |
| 14 | 331.44 | 0 |
| 15 | 330.91 | -0.91 |
| 16 | 344.63 | 0 |
| 17 | 348.50 | 7 |
| 18 | 344.92 | 0 |

| Line # | Current (A) | Power loss (W) |
|---|---|---|
| 1 | 3.95 | 20.07 |
| 2 | 3.49 | 7.84 |
| 3 | 8.71 | 14.62 |
| 4 | 7.34 | 13.82 |
| 5 | 4.87 | 15.23 |
| 6 | -11.26 | 24.40 |
| 7 | 28.29 | 154.19 |
| 8 | 12.01 | 27.80 |
| 9 | 16.13 | 166.94 |
| 10 | 19.61 | 74.08 |
| 11 | 7.08 | 9.66 |
| 12 | 12.53 | 40.33 |
| 13 | -3.49 | 7.80 |
| 14 | 14.30 | 39.40 |
| 15 | 2.76 | 1.46 |
| 16 | 20.54 | 271 |
| 17 | 20.09 | 77.71 |
| 18 | 0.46 | 0.14 |

## 4.5 System solvability analysis

In order to assess the general validity of the computational method previously showed and tested for simple networks in the previous sections, a series of cases can be considered and simulated to see how the power flow solver behaves and if the solution is correct. As expressed before, a higher number of node types are considered in the low voltage DC distribution system of the future. Thus, network nodes combinations will be evaluated in the next section.

Furthermore, convergence criteria are tested for the two linearization methods previously shown in order to evaluate for which conditions those computational methods are expected to give the physically correct solution.

### 4.5.1 Network nodes combinations

Clearly, different node combinations can lead to a solution or not, depending on how the node parameters contribute in filling up matrices **A** and **B** as described previously in the chapter. We take now into account four types of nodes: constant voltage (V), constant current (I), constant impedance (Z) and constant power (P). Even though P nodes are linearized into current or a combination of current and impedance, it is still relevant to keep this behaviour separated from the other three. Droop and combination nodes are instead combination of the first three and can be included in the cases shown.

Networks with all V nodes give a solution, since only the currents need to be computed. On the other hand, when only I nodes are present, a system with infinite number of solution is found since the determinant of matrix **A** is equal to zero, therefore the matrix is not invertible. All Z nodes represent a network with only (resistive) loads, which thus cannot obviously have a feasible solution. From a mathematical point of view, the system has only the trivial solution (all voltages and currents are zero).

Other multi-node combinations are found to give always a solution, except in the case in which only constant power and constant current nodes are present. In this case, as for the case with only constant power or with only constant currents, a solution cannot be found since the matrix A is not invertible. It is possible in fact to see that for both linearization methods previously shown, a circuit with only constant power sources will not lead to convergence in the power flow analysis. This result is expected, since it is not possible to account for ohmic losses without knowing *a priori* all current levels in the lines. However, an example is here drawn to simulate the case in which only constant power nodes are present into the system. To do that, we take into account the simple two-nodes network as represented in figure 4.18.

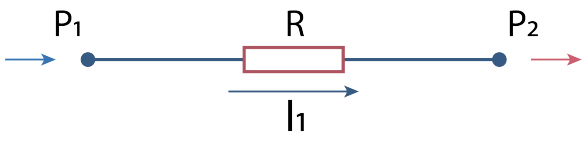


Figure 4.18: Simple two-nodes network with all nodes behaving in constant power

It is clear that if the constant power sources and loads are modeled as equivalent current nodes, the system would be over-determined and therefore a solution of the linear equations cannot be found, just like the case with only constant current sources or loads. A more interesting situation

occurs when the power nodes are linearized as a parallel of current source and impedance. This type of linearization, as shown in section 4.3, leads to the following equation:

$$\begin{bmatrix} 1 & -1 & -R_1 \\ -\frac{1}{Z_1} & 0 & -1 \\ 0 & -\frac{1}{Z_2} & 1 \end{bmatrix} \cdot \begin{bmatrix} V_1 \\ V_2 \\ I_1 \end{bmatrix} + \begin{bmatrix} 0 \\ I_{c1} \\ I_{c2} \end{bmatrix} = \begin{bmatrix} 0 \\ 0 \\ 0 \end{bmatrix} \tag{4.5.1}$$

The matrix-form equation 4.5.1 can be in theory solved, since matrix **A** is non-singular and therefore invertible. Nonetheless, due to the type of linearization, the generic solution will give the following iteration for voltages and currents:

$$V_n^{(k)} = \quad 2 \cdot V_i^{(k-1)} \quad \forall i, k \tag{4.5.2}$$

$$I_i^{(k)} = \quad 0 \quad \forall i, k \tag{4.5.3}$$

This result is found to be general and it applies for every topology combination. A simulation result for a network composed of 5 nodes and 6 lines with all power converters in constant power is shown in figure 4.19. In the figure it is possible to see how voltage mismatches diverge with a quadratic fashion up to the 30th iteration, when the simulation is interrupted.

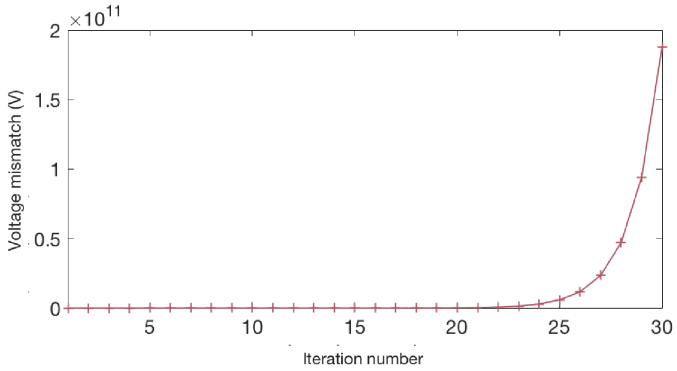


Figure 4.19: Divergence in voltage mismatch (V) for a network with all constant power nodes

The option in which only droop nodes are applied, even with different droop constant $k_1$ will give a solution where all the voltages are equal to the voltage reference chosen. Table 4.6 below shows a summary of the solvable node combinations in a network.

Table 4.6: Summary of solvability analysis for different node combinations

| Node combination | Solvability |
|---|---|
| All V | Solution exists |
| All I | Not solvable (det(**A**) = 0) |
| All Z | Only trivial solution (**A** · **X** = 0) |
| All P | Not solvable |
| V and Z | Solution exists |
| V and I | Solution exists |
| I and Z | Solution exists |
| P and Z | Solution exists |
| P and I | Not solvable |
| P and V | Solution exists |
| U, P and Z | Solution exists |
| U, I and Z | Solution exists |
| U, P and I | Solution exists |
| P, I and Z | Solution exists |
| U, P, I and Z | Solution exists |

### 4.5.2 Convergence analysis

As stated previously, it was found in literature that convergence for LVDC power flow should be guaranteed for any initial guess and for every network regardless of the numerical method used to solve the problem with fixed-point iterations [31]. Additionally, a unique solution is found, even though the non-linear nature of the power flow problem leads naturally to more mathematical solutions. In this section a convergence analysis will be carried out for the two linearization methods proposed.

Among the assumptions for the theorem of uniqueness of the solution, based on the notion of Banach spaces, there is that the LVDC network needs at least one constant voltage node and at least one constant power node. Thus, the simple network shown in figure 4.20, which features one constant power and one constant voltage node, will be used to test the two methods.

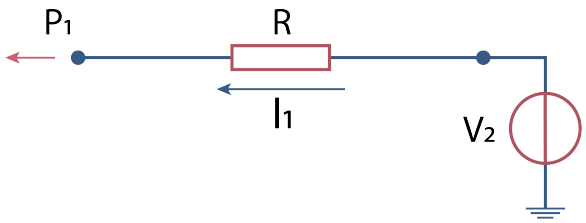


Figure 4.20: Simple two-node circuit with constant power load and constant voltage source

Firstly, the linearization of the power node into constant current is tested. Sampling 1000 initial points, it has been found that in every case the method was leading to convergence towards the correct solution. In general, the closer the initial point to the actual solution, the less iterations are needed.

Secondly, the linearization as constant current and impedance in parallel is tested for convergence. In this case the solution found is not unique for every initial guess, even though convergence

is always obtained. The incorrect solution is generally found when an initial guess is very far from the condition of "flat start" (i.e. 1 p.u.) for the node voltages. For the case shown in figure 4.20, this incorrect solution corresponds to the case in which the voltage source $V_1$ is positive and small enough to still be a mathematically correct although physically an unstable solution.

In any case, one of the results obtained is obviously incorrect and it does not comply with another of the assumptions for uniqueness of solutions, since it is demanded that voltage levels are between reasonable minimum and maximum values [31].

## 4.6 Conclusion

In this chapter an innovative power flow method for the universal direct current distribution grid was presented and applied first to a simple network, then to a more complex distribution network including also combination nodes and droop nodes. Furthermore, the solutions of the power flow were compared to the steady state results obtained from a dynamic model found in literature.

In the last section of this chapter, an analysis of the requirements to obtain a solvable system was performed. It was found that systems with only current nodes, only impedance nodes or only power nodes is either not solvable or gives only the trivial solution $\mathbf{A}\cdot\mathbf{X}=0$. The only other combination which do not provide a solution to the system is the one with only constant power nodes and constant current nodes. Finally, it was found that - as soon as the nodes combination gives a solvable network - the linearization with constant current gives always a unique solution, regardless the start point of the voltage iteration. In the case of the constant current and impedance linearization, this is true only if the start point is not excessively close to zero. It was found, in fact, that if the initial guess is very low, it is possible that the system will converge to the wrong result. It is thus recommended to choose a "flat start" of 1 p.u., or a "hot start" derived from a previous steady state of the system.

In the next chapter, the power flow tool will be applied to the IEEE Low-Voltage Test Feeder in order to have further testing and insight into the possible applications of the tool.

# Chapter 5

# Testing Via IEEE European Low-Voltage Test Feeder

## Table of Contents



This chapter focuses on the study of the IEEE European Low-Voltage Test Feeder and the implementation of the power flow analysis using the tool developed and presented in the previous chapter. In section 5.2 the test feeder is described together with the steps required to implement it into the power flow tool environment. In section 5.3 the low voltage DC power flow analysis is performed and results are interpreted to assess both the network status and the algorithm performance over a whole day of simulation. Finally, in section 5.4 conclusions are drawn.

## 5.1 Introduction

The implementation of the power flow computational method presented in chapter 4 on the IEEE European Low-Voltage test feeder gives the opportunity to test the analytic tool for a realistic network topology, with realistic cable data and load shapes over one full day. Furthermore, one of the research questions is how the analytic tool developed would behave when applied to a standardized neighbourhood. A more complete study will be performed in the next chapter, where different case scenarios for distributed generation and consumption will be presented.

## 5.2 Description of the test feeder

The IEEE Test Feeders Working Group provides a number of different topology and the related data, such as cable parameters and load patterns, in order to benchmark new mathematical methods for different types of analyses such as power flow, dynamic analysis, etc [42]. It is common in Europe to find low-voltage systems with a loop or meshed topology, in addition to the classic radial feeder type. This is different with respect to the case of North America, on which the majority of test feeders provided by the IEEE are currently based.

The European Low-Voltage Test Feeder is a 416 line-to-line voltage radial system, based on a topology found in the United Kingdom. The aim of feeder, in an AC system context, is to provide a system with high load imbalance between the three phases [43], as commonly found in Europe at distribution level.

### 5.2.1 Topology analysis simplification

The test network is provided by the IEEE Test Feeders Working Group as a set of *.csv* files containing information about bus coordinates, line codes, loads, load shapes, source and transformer at the MV-LV interface [42]. In particular, about the topology, the network is provided with 906 nodes (buses) and 905 lines (branches). The number of loads is 55. It is clear that the topology can be simplified in order to have faster computation, without affecting the results.

The simplification approach is the following: if one node is connected to only other two nodes (one preceding and one successive), then that node can be deleted and the resistance of the two lines, now connected into one, can be summed up. On the other hand, if one node is connected to three or more other nodes, then that node is maintained and it will behave as a passive node (not generating nor absorbing active power). Figure 5.1 shows a comparison of the IEEE standard version, in the background, and its simplification in the foreground.

Additionally, it is also shown in literature that such simplification does not affect sensibly the results outcome [44].

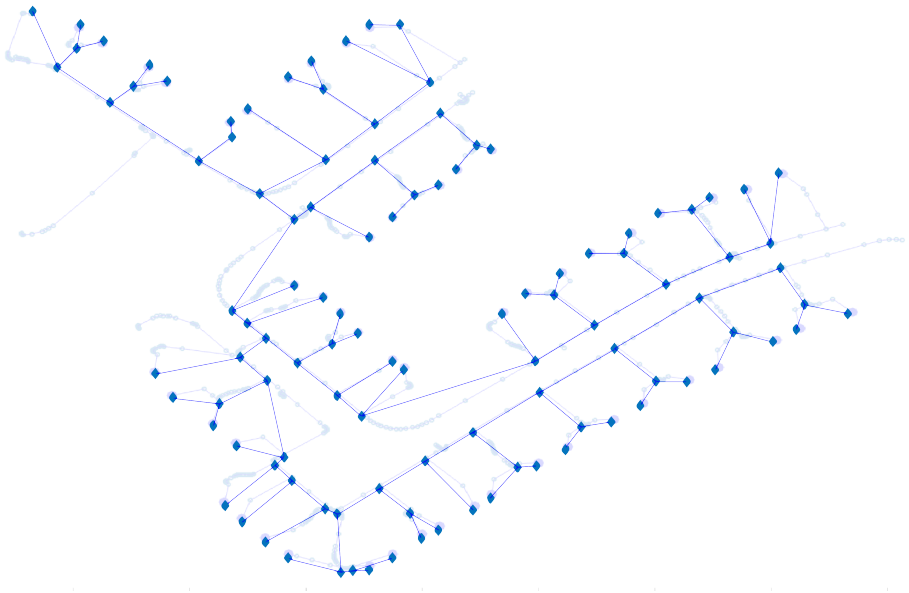

Figure 5.1: Comparison between IEEE standard version (in the background) and simplified network (in the foreground) [42]

After the simplification is performed, the feeder presents 55 loads, one MV/LV connection, 112 total nodes and 111 total lines.

### 5.2.2 Network parameters

The data is provided by IEEE for topology, cables and loadshapes. In particular, cable data presents resistance R, reactance X and capacitance C, both in the positive and in the zero sequence. Ten types of cables, with different parameters, are given. As shown in chapter 3 section 3.1.1, only the resistance is taken into account in the direct current power flow analysis. Table 5.1 below shows the different types of cables and their resistance value per kilometer of length.

Table 5.1: Cable types and resistance values provided in the IEEE Test Feeder

| **Cable** | Type 1 | Type 2 | Type 3 | Type 4 | Type 5 | Type 6 | Type 7 | Type 8 | Type 9 | Type 10 |
|---|---|---|---|---|---|---|---|---|---|---|
| **R (Ω/km)** | 3.97 | 1.257 | 1.15 | 0.868 | 0.469 | 0.274 | 0.089 | 0.116 | 0.446 | 0.332 |

In figure 5.2 below the simplified version of the test feeder is shown, with numbered nodes and two different colours for different types of nodes. Node 1, in green, represents the MV-LV connection with the transmission system. This type of connection is generally implemented with a power converter (AC to DC or DC to DC) with a constant voltage setting [31], but a droop strategy can be implemented, as an alternative. Different options for the voltage level to be chosen are available in literature and have been implemented in experimental setups [45]. For instance, 400 V has been used for DC data-centers projects. Another example of voltage level is 325 V, which equals the peak of a 230 V AC system once rectified, and it is therefore a ready solution with available devices in the market. Finally, 230 V is often chosen because it is the rated phase voltage for household applications, and it can thus be directly implemented for resistive heating devices. Other lower voltage levels, such as 48 V, are found in telecommunication systems projects. Nonetheless, for

the purpose of this test with a Low-Voltage test feeder, a level of 350 V has been implemented as suggested in recent literature studies [4]. This voltage level is close enough to 325 V but also high enough to be implemented for distribution systems. Furthermore, 350 V line-to-ground DC voltage can be adopted in bipolar architectures to achieve higher voltage levels in a modular way. For example, industrial loads might require higher power and be therefore supplied with 700 V or 1400 V. This possibility of multiplying the voltage level is important because the standard definition of low voltage is set at 1500 V, and it cannot be exceeded in a distribution network environment [4].

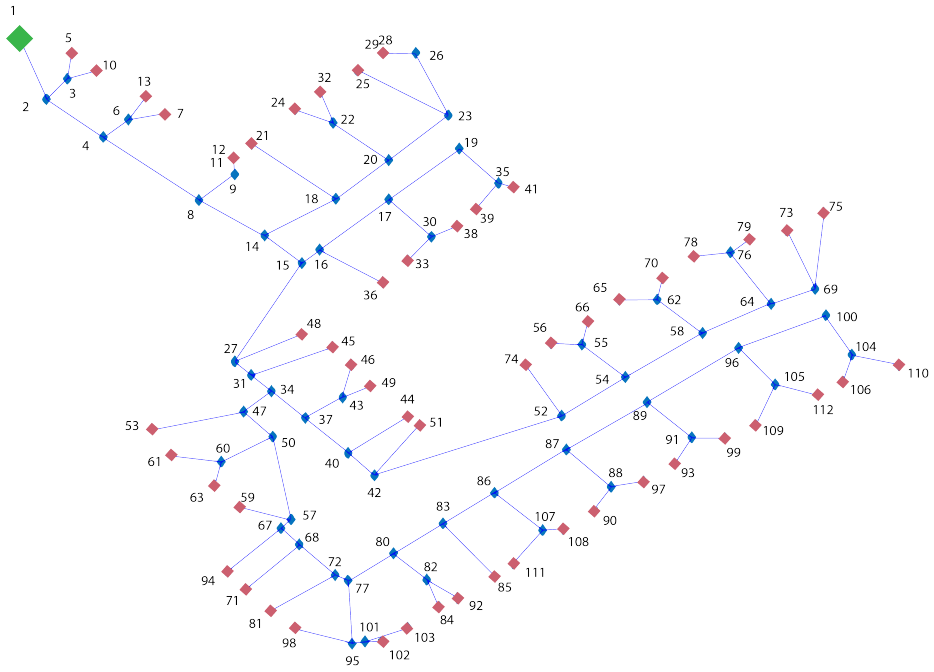


Figure 5.2: Simplified version of the test feeder with MV-LV connection (in green) and loads (in red)

The nodes shown in red in figure 5.2 are constant power household loads, as provided together with the IEEE test feeder. The data is provided as a time-series of one minute accuracy. In figure 5.3 below a 3-D graph showing load number and time of the day is provided. This type of data visualization is useful to determine at a glance how the loads are distributed along the network both geographically and during the day. It is found that the daily average load per household is 366 W, with a peak of 14.66 kW, registered in node 7 at 22:47.

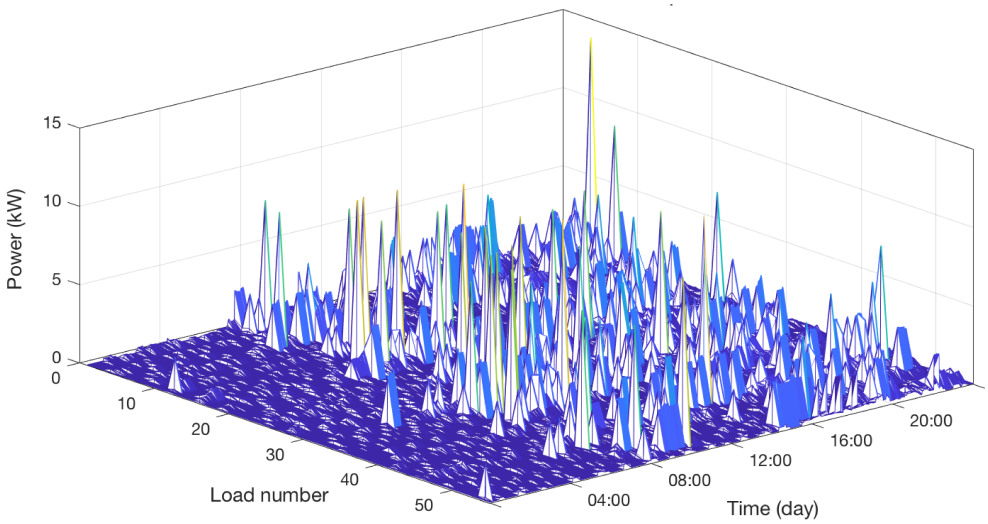


Figure 5.3: IEEE Distribution network loadshapes (one day time)

## 5.3 LVDC power flow analysis

In this section the power flow analysis is performed on the IEEE European Test Feeder during one day of simulation. The load data is provided every minute, therefore the number of power flow computations in one day is 1440. In section 5.3.1 the results of the power flow are shown, so that different aspects of the grid working conditions can be tested. Namely, voltage levels for power quality testing, current levels for congestion analysis and power losses in the lines are computed.

In section 5.3.3 the algorithm performance is analysed and a comparison between the two linearization methods implemented in the power flow tool is carried out.

### 5.3.1 Voltage level analysis and grid response

One of the major concerns in resistive DC distribution grids is whether the voltage levels will remain within safe limits all along the feeder. In absence of distributed generation and battery systems, it is expected that, in any load condition, the voltage will show a decreasing fashion moving from the root towards the end of the feeder. Figure 5.4 below shows the node voltage shapes for one day simulation.

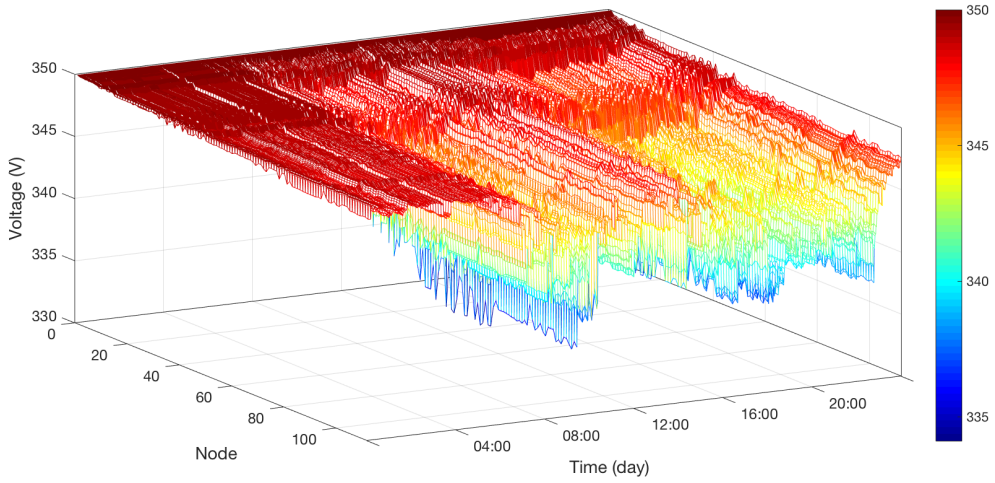


Figure 5.4: Node voltage shapes for IEEE test feeder (one day simulation)

The 3-D representation shows the node number on the x-axis, the time of the day in the y-axis and the voltage level on the z-axis. It is clear that the higher the load levels, the lower will be the voltage in the nodes. A voltage fluctuation of $\pm$ 5% is generally accepted by international standards for power quality, and it is expected the same will be applied for DC systems. The steady-state analysis shows that indeed the minimum value of 332.5 V is not reached. The node which is affected the most by the voltage dips is node 75, one of the furthest from the MV-LV connection.

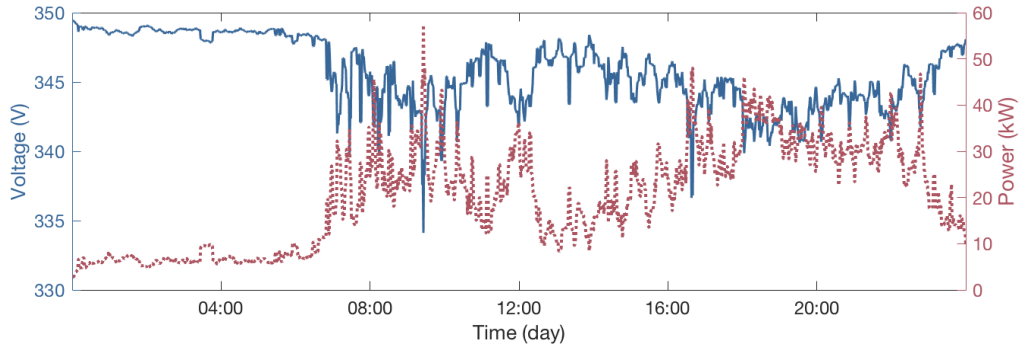


Figure 5.5: Voltage at most critical node (75) vs total power load (one day simulation)

As it is possible to see from figure 5.5 above, the minimum voltage value for node 75 is expected to be 334 V, so above the recommended threshold. In the same figure it is also depicted the cumulative load consumption during the whole day of simulation. It is clear that the voltage shape is directly influenced by the power level in the whole grid.

Another important power flow result is represented by the line currents along all the lines of the distribution network. For grid planning and congestion analysis purposes it is in fact interesting to evaluate the current levels and what are the most stressed line in the grid. The current shapes for the one-day simulation are shown in figure 5.6.

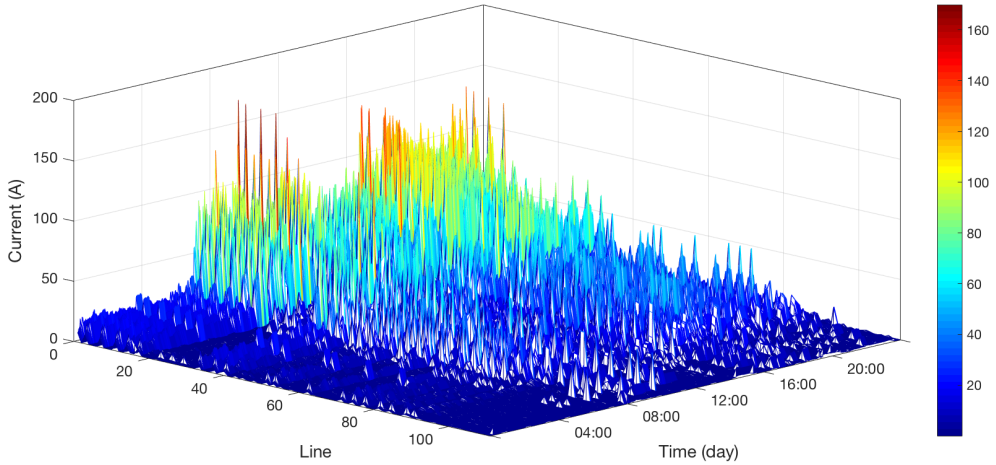


Figure 5.6: Line currents for IEEE test feeder (one day simulation)

As expected, the highest current levels are found when the load demand is higher and towards the root of the low voltage feeder, since all the power is retrieved from the medium voltage grid. The highest current level found in the simulation is 169.97 A through the line connecting nodes 1 and 2, i.e. the one connecting to the medium voltage converter. The time at which this current is registered is 9:26 AM, which, as it is possible to see from the graph in figure 5.5, corresponds to the time of highest cumulative power demand. One last direct output of the power flow calculation are the power losses along the distribution lines. The cumulative losses for one day of simulation are depicted in figure 5.7 below.

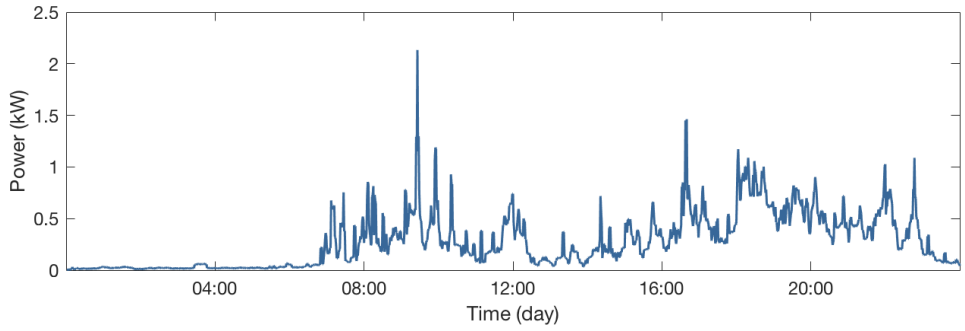


Figure 5.7: Cumulative power losses in the distribution lines on one day of simulation

Clearly, the higher the power demand in the system, the higher the line losses will be. This is also shown by comparing the losses shape with the behaviour represented in figure 5.5. The total losses in one day are 6.75 kWh, which amount for 1.40% of the total power load in one day for the test system (483.91 kWh). This low value can be explained by taking into account the low resistance values, reported in table 5.1 and the short distances covered by the cables at distribution level. Moreover, other types of losses, such as power converters losses and grounding losses are not taken into account in this analysis.

The description of distribution line losses is a relevant outcome of the power flow analysis since it can be used to assess the grid impact of distributed loads and generators such as electric vehicles

(EVs), photovoltaic panels and small wind turbines. The just described ohmic loss profile will be used in the next chapter as reference case in the scenario study with implementation of some of the above mentioned technologies.

### 5.3.2 Power flow result accuracy

In order to assess whether the result obtained for the power flow, namely voltage at the nodes and currents in the lines, is correct, some evaluations based on physical laws can be made. A first evaluation can be implemented by applying Kirchhoff's current law in every passive node present in the IEEE distribution network. As previously stated, of the total 112 nodes 55 are constant power loads and one is a constant voltage MV to LV connection point. It comes that 56 nodes are passive and these can therefore be tested to make sure that for every passive node, the sum of the N currents $i$ flowing to or from it respect the equation:

$$\sum_{i=1}^{N} I_i = 0 \tag{5.3.1}$$

Since the results obtained are approximated by the linearization, it is expected that the result will not be exactly zero. Moreover, computational precision must be taken into account since MATLAB has a floating-point relative accuracy of 2.2204e-16 (found by using the command *eps* for a 'double' type). Figure 5.8 shows the accuracy of equation 5.3.1 obtained through the power flow method.

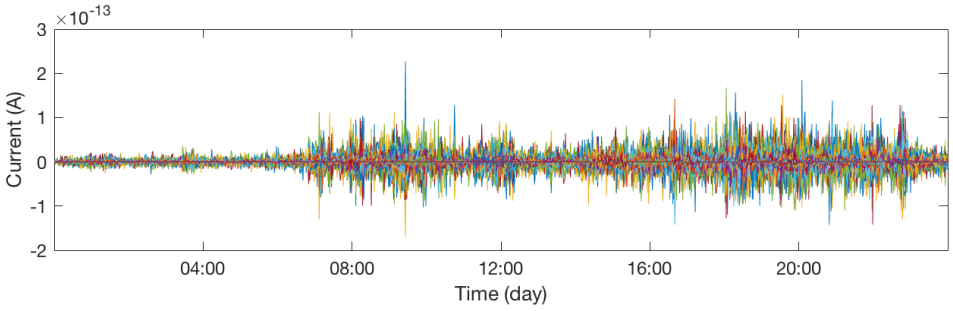


Figure 5.8: Current balance in 55 passive nodes of the IEEE network (one day simulation)

From the figure it is immediately clear that an high accuracy of the node balance, of around $10^{-13}$ A, is obtained in all passive nodes and along all day of simulation. Considering that passive nodes are 50% of the total nodes in the network, the fact that the node balance is guaranteed with very high precision means that the linearizations methods used to solve the non-linear power flow problem give very accurate solutions.

A second way to assess the quality of the result is to check that the conservation of power in the system is guaranteed, according to the following equation:

$$\sum P_{\text{loss}} + \sum P_{\text{loads}} - P_{\text{input}} = 0 \tag{5.3.2}$$

The $P_{\text{loss}}$ is here related exclusively to the ohmic losses along the distribution lines, since losses given by the power converters or any other types of losses are neglected in the power flow analysis. The term $P_{\text{input}}$ is the amount of power delivered by the medium voltage network through node 1. The results of equation 5.3.2 are shown in figure 5.9 for the whole day of simulation.

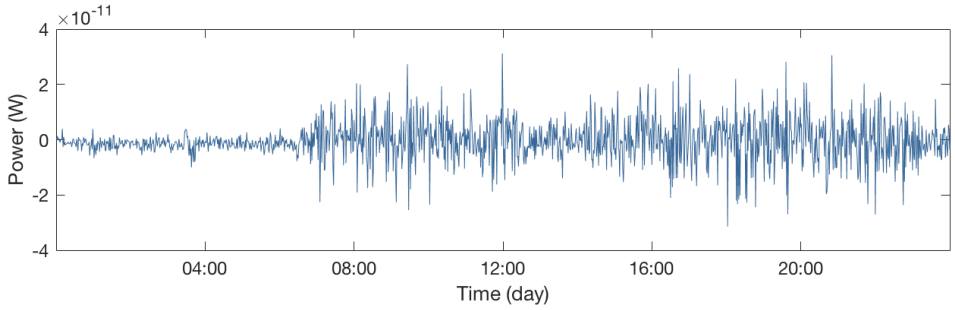


Figure 5.9: Conservation of power within the distribution system (one day simulation)

Once again, the results are very close to zero, around the order of magnitude $10^{-11}$ W, compared to the power magnitude in the system which is of the order $10^3$ W. The results in figure 5.8 and in figure 5.9 appear to be related, since a higher accuracy in node balance represent a higher accuracy in conservation of power and vice-versa. Both patterns follow the increase in cumulative load power as shown in figure 5.5. This can be explained considering that a higher amount of loads in the system means a higher amount of power nodes that need to be linearized.

In fact, it is also possible to evaluate the accuracy of the linearization for the constant power nodes. This is made considering that the threshold chosen for the voltage mismatch vector, as defined in section 4.3.1, has been set to 0.01 V. In figure 5.10 the different between constant power (as input value) and the value obtained through linearization over one day of simulation are shown. Three load nodes have been chosen in order to show three examples with different distances from the MV to LV connection of the network.

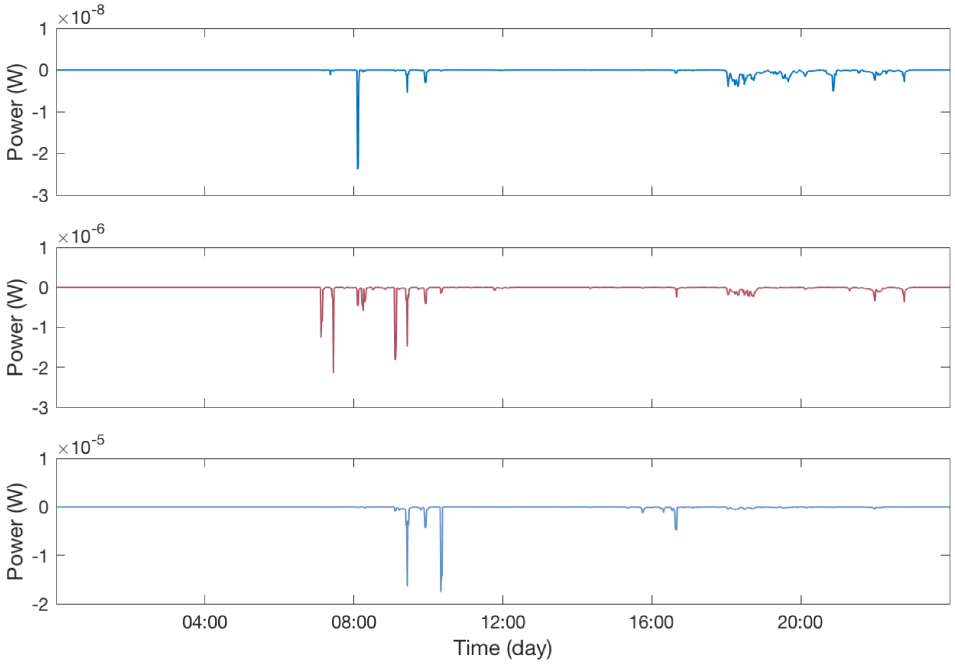


Figure 5.10: Difference between constant power and linearized value over one day simulation for node 10 (top), node 44 (centre) and node 110 (bottom)

As expected from the previous patterns, a lower linearization accuracy is found when the load start increasing (around 08:00) and when the load is higher around 18:00. It should be noted that

a higher distance from the constant voltage reference - in node 1 - translates into a lower accuracy of the linearization. In the figure the highest relative error is of around $2 \cdot 10^{-5}$ W, an incredibly low percentage of the power exchanged in the system. This can be explained considering that the voltage in node 110, for example, is affected by the error present in all preceding feeders and nodes. A node closer to the voltage reference, e.g. node 10, is less affected by calculation errors.

### 5.3.3 Algorithm performance analysis

In this section the performance of the power flow tool will be briefly analyzed in order to give an insight of how the two linearization methods behave and how these can be compared, in order to address one of the research questions of this thesis. The computer used is a **MacBook Pro** with processor **2.6 GHz Intel Core i5**. The software used to run the power flow tool is **MATLAB 2017b**.

First, it is interesting to analyze the simulation time, for one day of simulation, considering both linearization methods. As previously mentioned, one day of simulation with a 1-minute time span corresponds to 1440 time points. In order to measure time, the commands *tic* and *toc* embedded in Matlab have been used, as it is suggested to be the best available solution nowadays [46]. Nonetheless, the measure is still CPU-dependent and therefore an evaluation of the resolution of the used hardware is needed. In this case, the average resolution has been found to be 0.000014 seconds.

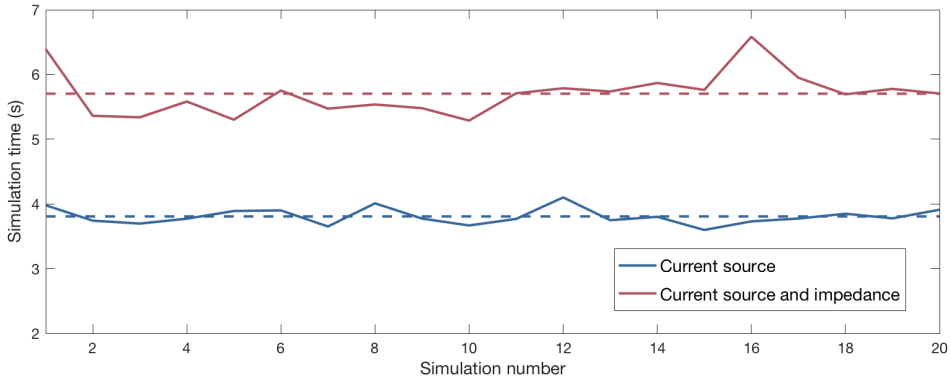


Figure 5.11: Simulation time for the two linearization methods analyzed (20 samples) and average values (dashed lines)

Figure 5.11 shows the simulation time using 20 samples, corresponding to 20 full-day simulations. In chapter 4 the two linearization methods implemented in the LVDC were modeled and explained. It is clear from how the two methods work that linearizing with a current source in parallel with an impedance will require more time, as opposed to the case with constant power simplified as a simple current source. The average elapsed time for the two computational methods are 3.8068 seconds and 5.7037 seconds for the current source and the current source and impedance linearizations, respectively. The results are also illustrated in table 5.2 below.

Table 5.2: Average computational time for one day simulation

| **Type of linearization** | **Average computational time** |
|---|---|
| Current source | 3.8068 s |
| Current source and impedance | 5.7037 s |

As previously stated, this is mainly due to the fact that the former method requires the inversion of the coefficients matrix **A** at every iteration step, since its submatrix **Z** receives an updated value. It is thus interesting to see what is the weight of the inverse calculation over the total power flow computation time for the linerization with current source and impedance. To do so it is necessary to make use of nested elapsed time measurements implemented in Matlab.

The simulation was run for an entire day in order to evaluate the percentage of time required for the inversion operation only. It was found that an average of 59% of the computational time is indeed required for the inverse calculation. This fact partially explains why, as seen in table 5.2, adding an impedance to the current source increases the computational time by around 50%.

Another interesting analysis can be performed over the number of iterations needed for the two different methods to reach convergence. To do so the IEEE European Low-Voltage test system was run for the whole day, thus 1440 times. The results are shown in figure 5.12 for the two types of linearization so far described. The linearization with current source, even though faster, as seen previously in this chapter, requires on average more iterations compared to the current source and impedance type. The histogram shows that the highest occurrence is 4 for the former type, and 3 for the latter.

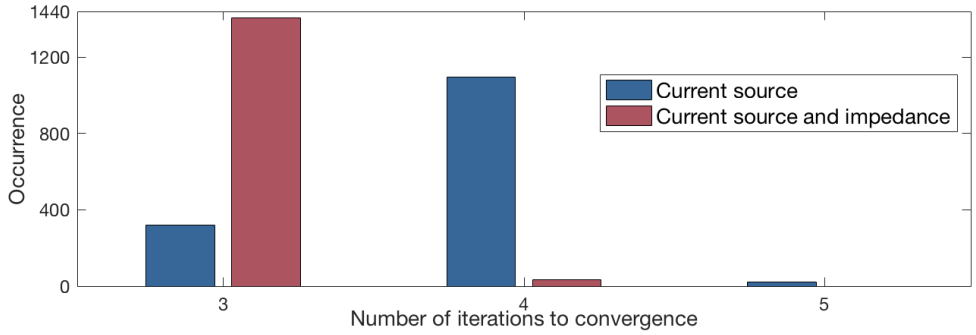


Figure 5.12: Comparison of iteration number for the two linearization methods analyzed (one day simulation)

Finally, the analysis will focus on a comparison in computational time and number of iterations between three types of networks, with increasing number of lines and nodes.

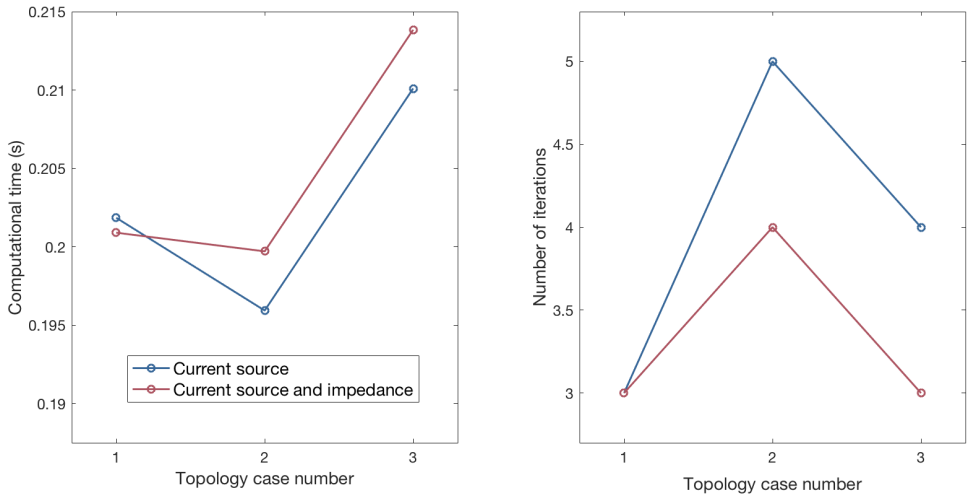


Figure 5.13: Comparison of average power flow computational time and iteration number for the two linearization methods analyzed between three topology cases (20 samples)

Figure 5.13 features both the computational time and the number of iterations for the three topology cases and for the two linearization methods. Case 1 refers to the 5-nodes and 6-lines case as presented in figure 4.13, while case 2 refers to the 18-nodes and 18-lines case given in figure 4.16, both in chapter 4. Case 3 refers instead to the IEEE European Low-Voltage test system, which features 111 nodes and 112 lines.

The results depicted in figure show that the number of iterations required for convergence do not necessarily impact the time needed to perform the computation. The time needed for a single power flow computation to be solved is in each case between 0.195 and 0.215 seconds. The difference is in fact not really evident between case 1 and 2, with actually case 2 slightly faster in computation. Considering that the number of nodes is not so different between the two cases, it is possible to affirm that the computational times are almost identical, taken into account a measurement error tolerance. For both linearization types, the third case requires a higher time, even though the difference is not so emphasized.

It is worth mentioning that these time measurements are done on one single time moment. For the third case, which as explained before has 1440 time points for a full-day simulation, one cannot multiply 0.215 seconds times 1440, which would give 309.6 seconds. This result is clearly different from the results shown in section 5.3.2, which is between 3.8 and 5.7 seconds. This discrepancy can be explained by the fact that, when the time-series analysis is performed, the input data and the variables do not need to be re-initialized at every time step, thus reducing the elapsed computational time.

The second aspect shown in figure 5.13 is the number of iterations. For the most simple case 1, the two iteration methods require the same amount of iterations, while a higher number is needed for case 2. Additionally, the convergence for the most complex case 3 is achieved with less iterations with both iterations. This counter-intuitive result can be explained considering that case 3 is a radial feeder, while case 2 is - even though weakly - meshed. This fact influences the problem solution because in the meshed case the state variables are present in more equations, thus increasing the difficulty in finding the solution by iteration.

## 5.4 Conclusion

In this chapter the low voltage DC computational method presented in the previous chapter has been applied to a standardized neighbourhood provided by the IEEE. Even though the test feeder is intended for AC systems, it has been possible to run a DC steady state analysis since the data on the resistance of the cables and the power of the loads were given. Since the test feeder is mainly a radial topology, it has been possible to have a very fast solution of a one-day simulation with a one-minute time step. It seems therefore that there is good potential for the DC power flow tool to be implemented also for other types of analysis, such as market-oriented analyses useful for distribution system operators (DSOs). In particular, new types of Power Transfer Distribution Factors (PTDF), nowadays used to indicate the changes in real power in transmission lines given by power transfers between two regions, can be modeled in order to include grid-code related billing models for prosumers [47]. This aspect would take into account new factors such as the amount of current injected and the quantity of line losses introduced in the grid.

Moreover, the power flow tool can be useful in order to help grid planning under different in different scenarios. The next chapter will focus on this aspects, with the implementation of DC-native technologies such as PV, battery and EVs in the IEEE standardized distribution grid.

# Chapter 6

# Case Study: Implementation of PV and EVs

## Table of Contents



In this chapter a case study is performed in order to evaluate the impact of different DC-native technologies in the IEEE test feeder previously analysed during chapter 5. In section 6.2 it is reported how EV load and PV generation are modeled. In section 6.3 the case study scenarios are shown and simulation results are presented and analysed. Finally, conclusions are drawn for the different scenarios of the case study.

## 6.1 Introduction

The IEEE European Low-Voltage test feeder is used in order to conduct a case study that implements photovoltaic (PV) and electric vehicles (EVs) in the distribution network. The aim of the case study is to assess the utility of the LVDC power flow tool developed for forecasting, operation and maintenance of future low voltage direct current grids.

## 6.2 EV load and PV generation modeling

For the case study, two DC-native technologies such as PV and EVs have been chosen to be implemented in the grid in order to asses their impact on voltage profile, line currents and distribution power losses. PV is already a well established technology which is able to provide a good amount of power also for residential systems [48]. Electric vehicles, on the other hand, are expected to play a more important role in the near future due to big investments that car manufacturers are making

in this years in order to deliver a product with higher battery autonomy in order to relieve any range anxiety on the drivers [49]. Moreover, the implementation of fast chargers based on DC technology is already happening and it is believed to have a significant impact on grid stability in the near future.

Since both technologies - but also batteries and other loads such as resistive heating - are DC-native, it is possible to imagine that a DC distribution grid would be beneficial in order to implement these element, reducing the number of conversion steps given by DC to AC converters.

### 6.2.1 EV load modeling

Electric vehicles introduce high uncertainty in the power grid because of the high number of cars that can be plugged to the charging station at the same time. Different standards have been introduced in order to accelerate the deployment of electric vehicle technology. The Society of Automotive Engineers (SAE) standards are U.S. based standards based on six levels: three for AC charging (with on-board charger) and three for DC charging (with off-board charger). Table 6.1 shows different charging levels for both PHEV (plug-in hybrid) and BEV (battery) technologies.

Another important standard is CHAdeMO, which is designed for modern electric vehicles and set norms for very fast DC charging (around 50 kW) that are able to recharge up to 80% of the SoC of the vehicle in around 30 minutes [49].

Table 6.1: SAE Standardized EV charging levels [49]

| **Charging level** | **Charging rating** | **Charging time** |
|---|---|---|
| AC level 1 | 120 V, 1.4 kW, 1.9 kW | PHEV: 7 h (SOC-0% to full)<br>BEV: 17 h (SOC-20% to full) |
| AC level 2 | 240 V, up to 19.2 kW | **For 3.3 kW charger:**<br>PHEV: 7 h (SOC-0% to full)<br>BEV: 17h (SOC-20% to full)<br>**For 7 kW charger:**<br>PHEV: 1.5 h (SOC-0% to full)<br>BEV: 3.5 h (SOC-20% to full)<br>**For 20 kW charger:**<br>PHEV: 22 min (SOC-0% to full)<br>BEV: 1.2 h (SOC-20% to full) |
| AC level 3 | >20 kW, single and three phase | To be determined |
| DC level 1 | 200-450 $V_{DC}$, up to 36 kW | **For 20 kW charger:**<br>PHEV: 22 min (SOC-0 to 80%)<br>BEV: 1.2 h (SOC-20% to full) |
| DC level 2 | 200-450 $V_{DC}$, up to 90 kW | **For 45 kW charger:**<br>PHEV: 10 min (SOC-0 to 80%)<br>BEV: 20 min (SOC-20 to 80%) |
| DC level 3 | 200-600 $V_{DC}$, up to 240 kW | **For 45 kW charger:**<br>BEV (only): <10 min (SOC-0 to 80%) |

Among the assumptions made for this case study, SAE DC level 1 as reported in the table has been taken as reference. Thirteen nodes which do not correspond to households have been chosen to host the fast DC charging stations that can be used by the car owners in the neighbourhood. Each charging station can host one car per time and delivers 20 kW of power to the outlet, so that BEVs can be fully charged in 72 minutes. The car time presence has been randomly selected between

14:00 and 23:00 in order to simulate car charging when the car owners are back from work. Some nodes host more than one car per day, so that the total amount of vehicles charged in the day of simulation is 20. This type of load shaping approach has been also found in literature [50]. Figure 6.1 shows the fast DC charging load during the day and the cumulative load due to the electric vehicles. The load peaks are found between 19:00 and 22:00 and are equal to 100 kW.

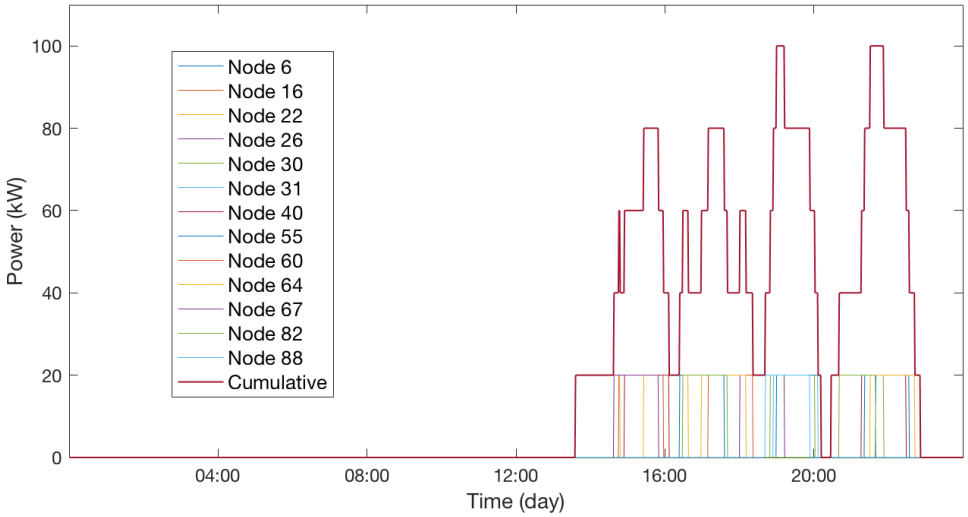


Figure 6.1: Electric Vehicles load with DC charging stations (20 kW) in 13 nodes for one day simulation

### 6.2.2 PV generation modeling

In order to simulate the effect of power generation from renewable energy sources, household PV systems have been collocated in 23 nodes in the network. For sake of simplicity, one type of module was chosen and simulated for all the household systems. The amount of panels per house was randomly chosen between 4 and 8 modules per system. The chosen panel is the Panasonic HIT (330 W) and its main specifications are shown in table 6.2.

Table 6.2: Panasonic HIT VBHN330SJ47 PV module main specifications [51]

| Pmax | Vmp | Imp | Voc | Isc | Efficiency |
|---|---|---|---|---|---|
| 330 W | 58.0 V | 5.70 A | 69.7 V | 6.07 A | 19.7 % |

The power generated by the PV panels has been calculated taking into account both internal (panel specifications) and external (weather data) parameters. Ambient temperature, ground temperature and wind speed have been considered in the so-called *fluid-dynamic model*. This model aims at calculating the module temperature which affects both the efficiency and the open circuit voltage ($V_{OC}$). The other major parameter, the short circuit current ($I_{SC}$), is mainly influenced by the sun irradiance [52]. In figure 6.2 the scheme of the PV model implemented can be found. The climate data used have been retrieved from the Royal Netherlands Meteorological Institute [53] and are referred to the region of South Holland, in the Netherlands, for the 20th of April 2018. The weather data has been retrieved in 10-minute basis and then slightly randomized to be fitted in the per-minute analysis.

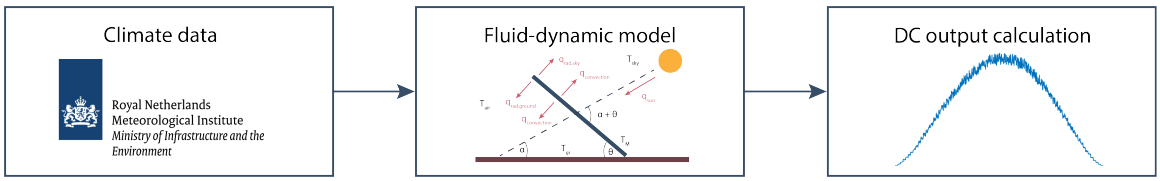


Figure 6.2: Scheme of PV model implemented

The overall installed capacity is 44.55 kW peak and the DC production can be found in figure 6.3. Since the PV systems are interfaced to the distribution network via a DC to DC converter, this source has been modeled as a constant power source. The DC to DC converter has the aim of adapting the PV voltage output to the 350 V level and, at the same time, is responsible for setting the voltage input level of the PV according to the MPPT (maximum power point tracking) algorithms [52]. It is also assumed that the system is connected to the grid via a net metering billing framework, which allows self-consumption of the household load when the energy is produced. In this way, the energy exchanged with the grid is modeled as the difference between load and PV production.

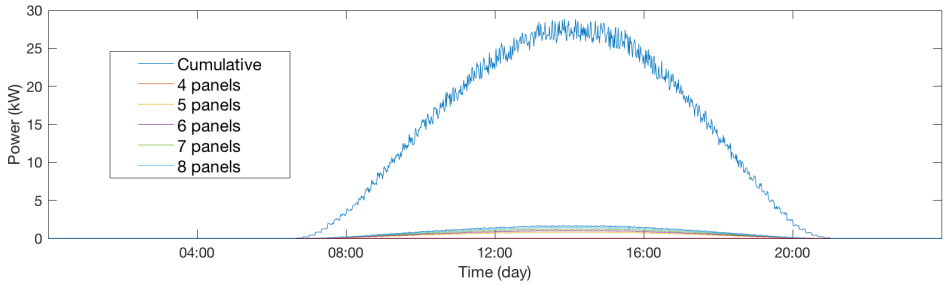


Figure 6.3: PV power production for single systems and cumulative production over one day of simulation

## 6.3 Case study scenarios

For the case study, the IEEE European Low-Voltage test feeder as shown in chapter 5 has been used. The case study aims at implementing the LVDC power flow tool in order to demonstrate that it is possible to evaluate the impact on the grid of some DC-native technologies that are believed to play a fundamental role in the future power systems. Namely, photovoltaic technology, electric vehicles and DC fast charging, electric resistive heating and battery systems. Figure 6.4 shows a scheme of an example of DC household. Electric vehicles, PV modules and DC loads (such as LED lighting) are interfaced via DC to DC converters, while resistive heating is modeled as a constant impedance. The value of the resistance chosen for all the heating systems is 48 Ω, which deliver a power of around 2.5 kW when in use.

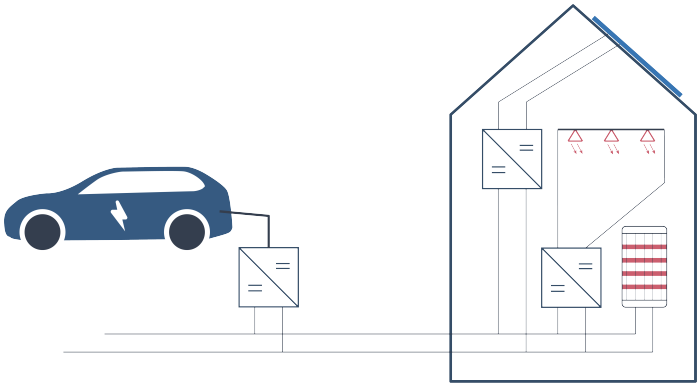

Figure 6.4: Scheme of a DC household node with PV production, constant power consumption (e.g. LED) and resistive electric heating with an EV charging station

Since the process of electrification of heating is expected to be considerable in the next years, 16 households have been randomly selected to have resistive heating as an addition to the electric power load already present. The battery system consists of four grid-storage sized batteries positioned at the root of different feeders. The storage systems are interfaced with the grid via DC to DC converters featuring droop control. Finally, the electric vehicle fast charging stations are distributed along the grid in nodes that are not households and that can therefore be used by car owners of the whole neighbourhood. In figure 6.5 it is depicted the IEEE test feeder with all the components featuring in the different scenarios studied in this chapters.

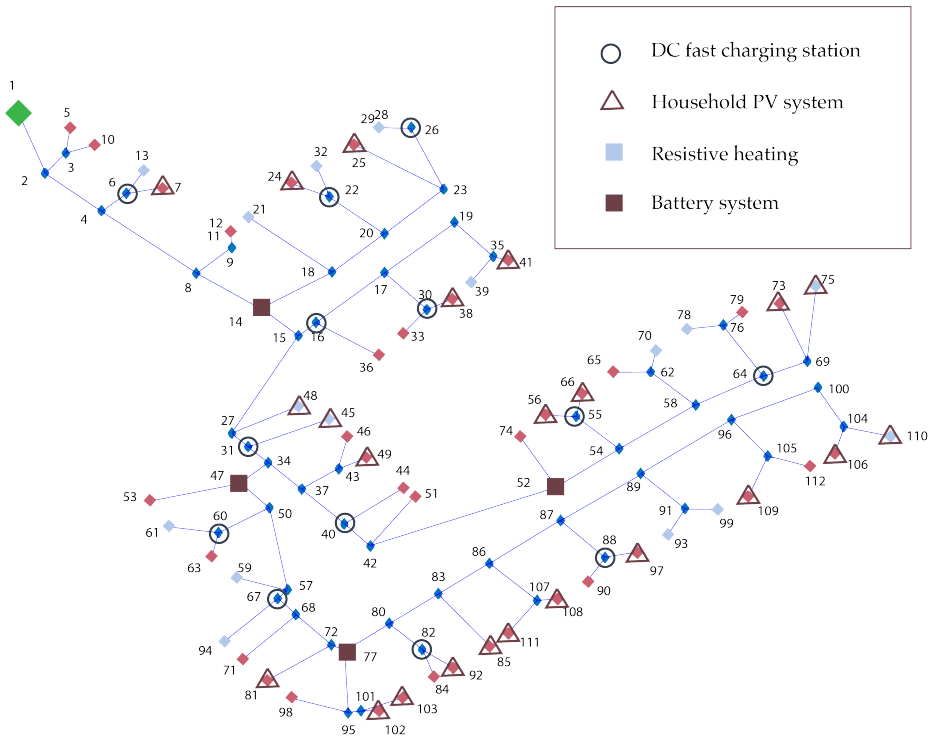


Figure 6.5: Simplified version of the test feeder with random node choice for the implementation of EV fast charging stations, household PV systems, resistive heating and battery systems

The case scenarios are structured as follows: the first case features PV and EVs with the addi-

tion of DC resistive electric heating; while the second and last case features four storage systems distributed in the network, in addition to the previous case. In each of these two cases the effects of the PV and EV components are evaluated by adding one component at a time: first base case, then PV only, EV only and finally both PV and EV. Network voltage shapes are then presented for each case and a comparison is made also for line power losses between the four cases. Congestion analysis for each case and scenario can be found in appendix B.

### 6.3.1 Implementation of PV, EVs and DC resistive heating

The first case examined features the base load-shapes of the IEEE test case seen in chapter 5, with the gradual addition of PV and EV technologies. Since the power flow method developed in chapter 4 can take into account the different node behaviours that are expected to play an important role in the power grid of the future, constant impedance nodes are added to the loads. In particular, 16 nodes were randomly selected in order to simulate a penetration of 30% of electric heating at household level. A resistance value of 48 Ω have been chosen in order to deliver 2.5 kW at the grid voltage of around 350 V. Two short heating times were selected: one in the morning between 6:30 and 7:30, and one in the evening between 18:30 and 19:30.

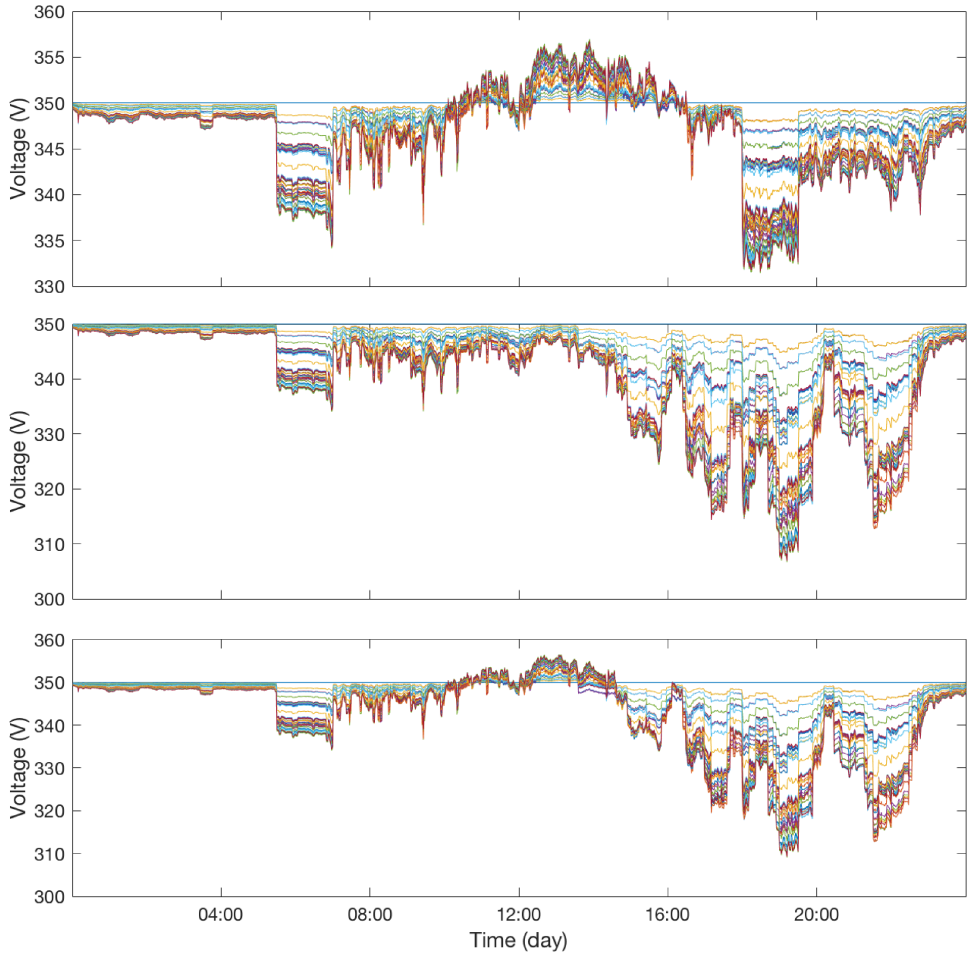


Figure 6.6: Node voltage shapes with resistive heating (one day simulation) for only PV (top), only EV (centre) and PV and EV (bottom)

The power flow was run for one day of simulation in order to evaluate the impact on the system voltage for an only PV, an only EV and an PV and EV case. Figure 6.6 shows the voltage shapes for the three cases.

It is possible to note that the addition of the resistive heating load creates two voltage dips, that affect all the nodes of the grid, during the two hours of load activity. The voltage increases rather linearly with the distance from the MV-LV connection, making the furthest nodes the most affected by the newly added resistive loads. It is possible to see the impact of the photovoltaic system on the grid, which determines an over-voltage up to 355 V between 11:00 and 15:00, but it is not really able to create any relief on the voltage dips. Since the resistive load is on top of the EV load, the result is that in both the graphs in the centre and on the bottom the voltage goes down to around 310 V for an unacceptable amount of time. In order to guarantee better power quality and not to compromise the equipment in the distribution grid, it is necessary, in this case scenario, to provide the grid with other solutions such as smart charging or a storage system in order to provide flexibility in the energy demand. In the next scenario of the case study a grid-sized storage system will be introduced and the effects on the grid will be analysed.

Lastly, it is interesting to analyse what are the effects on the power losses when PV and EV technologies are implemented. Figure 6.7 shows the comparison between the four cases of this scenario. First of all, the presence of EV charging stations determines much higher losses because of high power delivered. Second, the PV implementation has - even though limited - capacity to reduce the losses compared to both the base case and the EV only case. This is possible because the local generation of electricity reduces the household load and thus the need to retrieve power from the MV-LV connection.

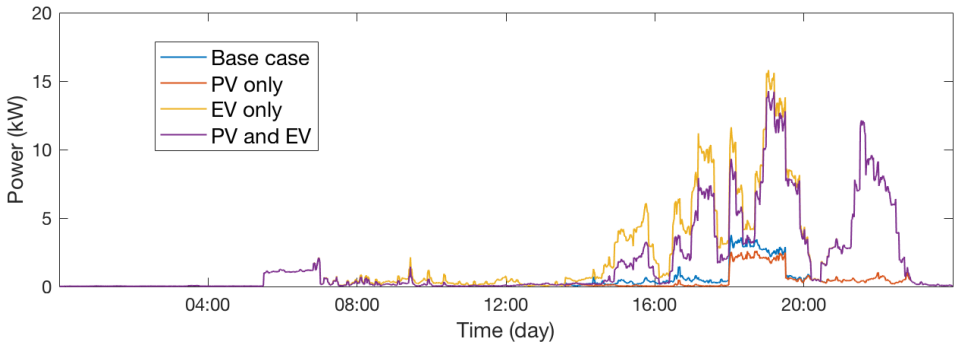


Figure 6.7: Comparison of the distribution network power losses for the four scenario cases with resistive heating

A comparison in energy loss over one day of simulation between the four cases can be found below in table 6.3. It is possible to note that, thanks to the PV local generation, the power loss is reduced to 30% and 12% with respect to the base and EV only cases, respectively.

Table 6.3: Energy loss comparison on one day of simulation for the four case scenarios with resistive heating

| Case | Energy loss (one day) |
|---|---|
| Base | 11.73 kWh |
| PV only | 8.28 kWh |
| EV only | 50.83 kWh |
| PV and EV | 44.74 kWh |

### 6.3.2 Battery implementation in the distribution grid

Battery systems, for example in MTDC (multi-terminal DC) or microgrid contexts, are usually regulated in primary control in a decentralized fashion. Decentralized control is a non-communication control system implemented locally at the power converter level. Batteries normally feature a I-V droop characteristic as reported in this example. More sophisticated control schemes have been utilized in order to take into account the battery capacity and the SoC (State of Charge) [54]. For this case scenario an easier control model has been implemented in order to have a near-zero net energy exchange on the day. For every scenario the reference voltage $V_{ref}$ set for the droop control is slightly lowered from the grid value of 350 V in order to force batteries to charge without taking directly into account their SoC. The values of voltage reference and droop coefficient have been found by tuning and simulating, in order to obtain a value close to zero for the total energy exchanged in the day, while maintaining a good amount of power exchange with the grid. In table 6.4 below the values are reported for the case with both PV and EVs implemented in the distribution grid.

Table 6.4: Batteries reference voltage and droop tuning for PV and EVs case

| Battery node | Voltage reference | Droop |
|---|---|---|
| Node 14 | 346.5 V | 0.2 |
| Node 47 | 344 V | 0.6 |
| Node 52 | 343 V | 0.6 |
| Node 77 | 342.5 V | 0.2 |

In figure 6.8 the voltage shapes are shown for one day of simulation and for different scenarios. It is possible to note that, since the batteries have lower reference levels compared to 350 V, most of the nodes have slightly lower voltage also in the first hours of the day, when the load is very low. Nonetheless, the impact of the resistive heating load is lower on the voltage level: the voltage dip barely reaches the value of 337 V, while it was getting up to 331 V in the case without batteries. The batteries also help reducing the over-voltages due to PV in the central part of the day.

When the effects of EV charging are also taken into account, the voltage is maintained over the 325 V level, thus ensuring a voltage level closer to the 350 V reference and thus better power quality. The battery influence is even more evident when PV is employed, where the central part of the day shows a voltage shape very close to 350 V for the whole network.

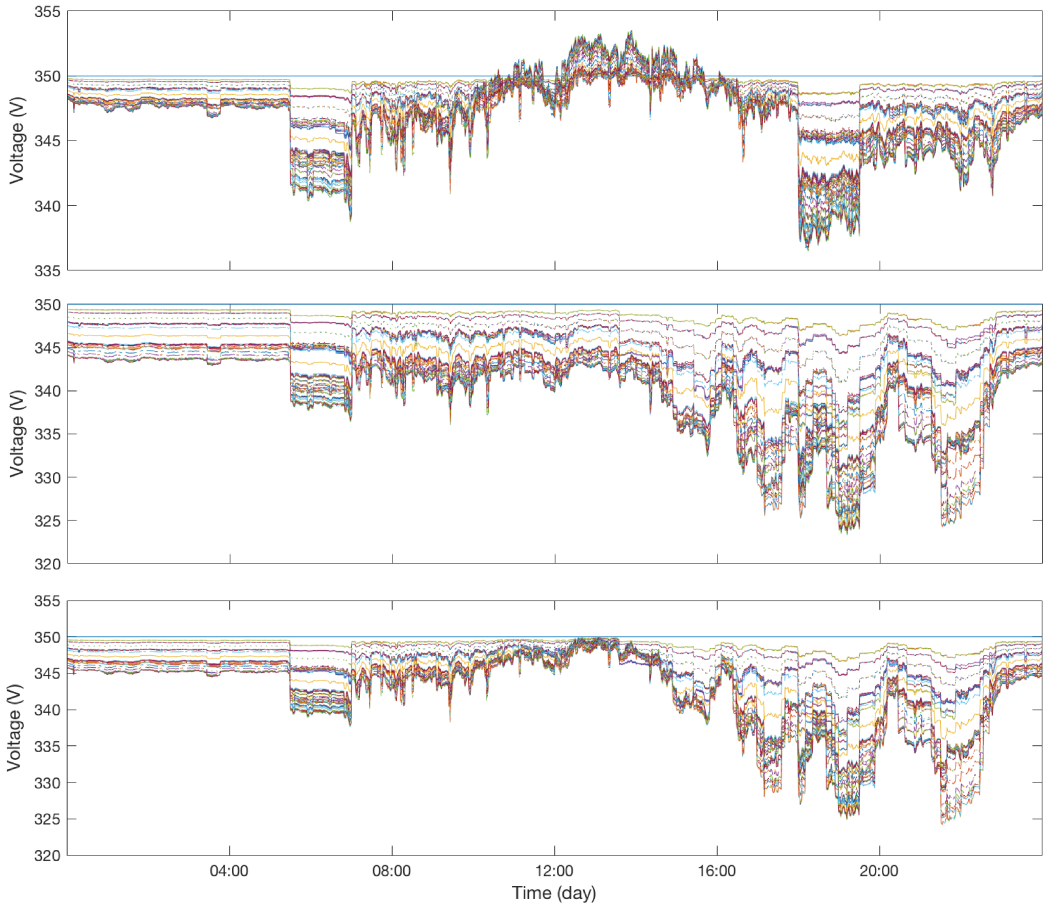


Figure 6.8: Node voltage shapes with resistive heating and batteries (one day simulation) for only PV (top), only EV (centre) and PV and EV (bottom)

When the losses are taken into account, it is possible to see that, similar to the previous scenario, the presence of PV is again of relief when an EV load and batteries are present. In fact the losses are decreased by 27% compared to the case with only EV and batteries. Against the base case with only household and heating loads, PV panels reduce the losses by 46%. Comparing with the results of table 6.3, batteries make possible to reduce the energy losses by 45% when both PV and electric vehicles are present in the system. The result can be found in figure 6.9 and in table 6.5.

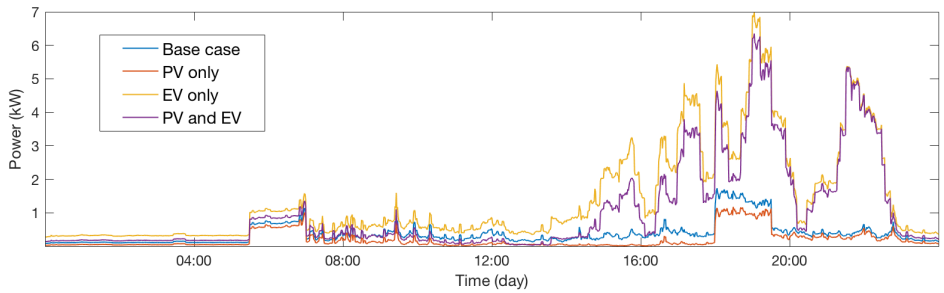


Figure 6.9: Comparison of the distribution network power losses for the four scenario cases with resistive heating and batteries

Table 6.5: Energy loss comparison on one day of simulation for the four case scenarios with batteries implementation

| Case | Energy loss (one day) |
|---|---|
| Base | 8.98 kWh |
| PV only | 4.82 kWh |
| EV only | 33.4 kWh |
| PV and EV | 24.46 kWh |

For the most comprehensive case, the one with both PV and EVs, it is interesting to see a simple and intuitive way of sizing the batteries in the system, depending on their position and control strategy. As mentioned previously in this section, the control is based on the I-V droop primary control. Since the battery is controlled in order to charge and discharge of roughly the same amount over one day of simulation, the simple formula in the following equation has been used:

$$\text{capacity} = \frac{1}{2}\int_T |P_{\text{batt}}(t)|dt \tag{6.3.1}$$

where $T$ is the minutes in the day, $P_{\text{batt}}(t)$ is the power exchanged by the battery during the day. The power exchanged can be found for the four batteries in figure 6.10.

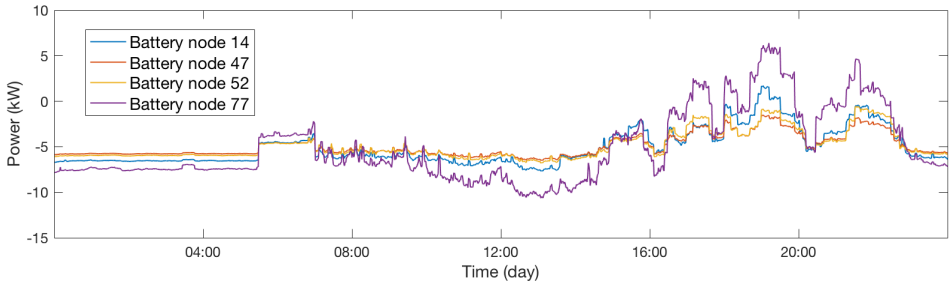


Figure 6.10: Batteries power exchange for the PV and EV case over one day of simulation

Finally, using equation 6.3.1 the values reported in table 6.6 were found. It should be noted that the battery sizing should include also the fact that the depth of discharge (DoD) of the battery cannot be 100% (usually a SoC of less than 15% is not recommended) and the fact that some losses occur for the battery storage, depending on the amount of power exchanged. Any further battery sizing concept is beyond the scope of this thesis.

Table 6.6: Calculated needed capacity according to battery power exchange (PV and EV case)

| Battery node | Capacity |
|---|---|
| Node 14 | 39.5 kWh |
| Node 47 | 23.3 kWh |
| Node 52 | 28.94 kWh |
| Node 77 | 76.93 kWh |

## 6.4 Conclusion

To sum up the content of this chapter, it is possible to take a look at what are the overall effects of the battery system compared to the scenario without battery. In figure 6.11 the distribution power losses between the two cases are shown for the day of simulation.

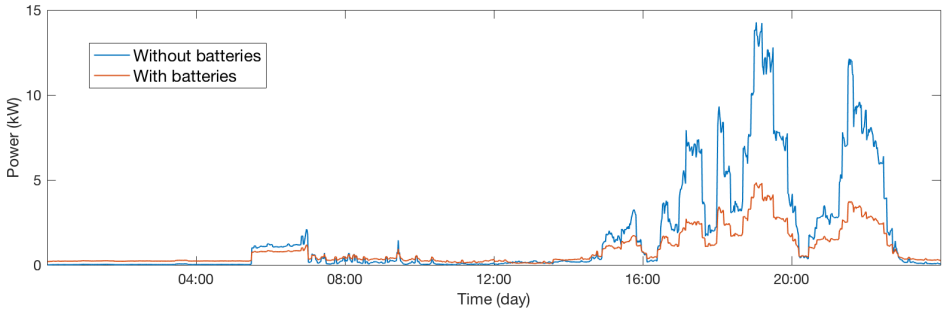


Figure 6.11: Comparison of the distribution network power losses (PV, EVs and resistive heating) with and without batteries

It is interesting to additionally consider the efficiency of the battery system in this comparison. It has been calculated that the cumulative energy exchange for one day, in the scenario involving both PV and EVs, amounts to 337.38 kWh. Commercial grid-size storage systems, such as the ones provided by the Dutch company Alfen, have a charging and discharging efficiency of 98.6% [55]. In this case the losses coming from the battery are 4.72 kWh. If added to the line losses, the total losses in the case with battery will become 29.19 kWh. This value is still lower than the case without battery, which was 40.74 kWh.

Another relevant effect of the storage system is the difference in the amount of power that needs to be retrieved from the medium voltage grid. As shown in figure 6.12 for the case with both PV and EVs, there is a peak shaving effect over the amount of power that needs to be taken from the grid towards the neighbourhood network. Moreover, the presence of the battery results in the absence of power sent back towards the MV grid, because when the power is in surplus in the system because of the PV production, this will be stored in the batteries. Overall, the amount of energy retrieved is 902.44 kWh without the batteries and 886.73 kWh with the batteries. This is not much of a difference in energy terms, but the lower power peaks will result in lower line congestion toward the root of the distribution feeder.

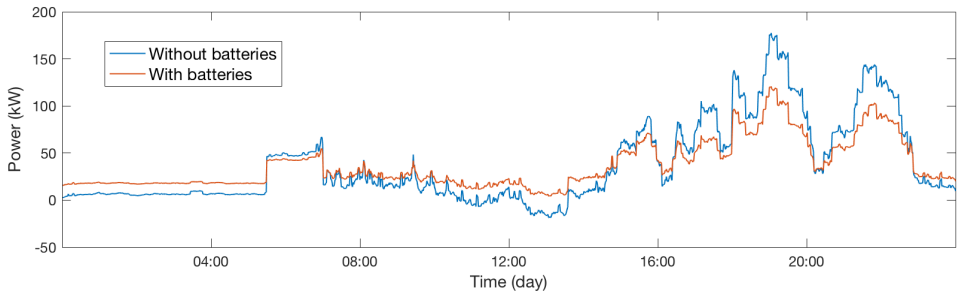


Figure 6.12: Comparison of the MV-LV power exchange (PV, EVs and resistive heating) with and without batteries

The goal of this chapter was to show how the LVDC power flow tool developed in this thesis can be used for grid planning purposes and to evaluate the impact of different new components in the low voltage distribution grids of the future. It was possible to see that, for example, PV implementation reduces losses because less energy transport is needed, resulting in less line congestion. Although, massive implementation of PV and EVs would negatively affect the power dispatch, since higher bi-directional flows are generated [4]. Then, through power flow analysis it has been determined that uncontrolled EV charging might be a problem in the network because of the high power demanded (especially for fast DC charging) and the increasing number of the electric vehicle fleet. Among the possible solutions, ToU (Time of Use) tariffs and smart charging could be implemented [49]. In addition, new market models can be thought in order to manage congestion through nodal pricing and optimal power flow dispatch [4].

Finally, it was also seen that via steady-state analysis it is possible to evaluate how batteries can help managing voltage dips and reduce line losses and that power flow analysis could eventually help in component choice and sizing in order to properly take into account the needs and constraints of the network.

# Chapter 7

# Conclusions and Recommendations

## Table of Contents



The last chapter of this thesis exhibits the main conclusions of the research done. In order to address them in a clearer way, the research questions will be again proposed and answered in detail. Finally, recommendations on further work related to power flow in DC grids are provided.

## 7.1 Conclusions

The conclusions of this thesis are drawn by answering the research questions, previously formulated in chapter 1.

**Why is a power flow calculation tool needed for DC distribution grids?**

As reported in the introduction chapter, the interest in DC for transmission and distribution network has raised in the last years. The power flow is an essential tool to assess the steady state of the grid, and thus its voltage levels, current levels and ohmic losses.

**What are the different methods shown in literature to perform AC and DC power flow calculations?**

Since the power flow is a highly non-linear problem, different mathematical methods have been developed in the years in order to find the solution in an iterative way. It has been found that the methods can be divided into three groups: first, AC methods used in transmission systems; second, AC methods developed for distribution systems; and third, DC methods. The main computational methods for AC transmission systems are the Gauss-Seidel and the Newton-Raphson based methods. Methods specifically developed for distribution networks are mainly based on the backward/forward sweep methods and focus on the radial topology. Last, methods for DC systems are generally adapted from the AC framework by simplifying the number of unknown state variables from two (voltage magnitude and angle) to one only: the voltage. These methods are all generally built in order to comply with systems based on traditional power dispatch.

**What is a suitable method in terms of network adaptability?**

It was found that a method based on Kirchhoff's equations and Ohm's law can be applied and developed in order to solve the DC power flow problem taking into account diverse node behaviours. Three elemental linear behaviours have been identified: constant voltage, constant current and constant impedance. It has been also shown that the non-linear behaviour of the constant power nodes can be linearized as a combination of the elemental behaviours. Two types of linearization of the constant power nodes have been presented in the thesis: the first one linearizes the constant power node as a constant current source by guessing the value of the node voltage; the second type is obtained by linearizing the I-V behaviour of the node with the concept of negative incremental impedance.

**How can this method be applied to simple network topologies?**

In order to apply the method to a simple system topology, it is required to find the oriented incidence matrix of the network and classify the different nodes depending on their behaviour and state. This approach makes it possible to find a solution also for highly meshed or looped topologies. It has been found that for a simple network, the proposed method guarantees a fast convergence towards the correct solution. It has been also found that linearizing as a constant current source guarantees convergence to the correct solution for every starting point, whereas the linearization as constant current and impedance may lead to the incorrect solution - even though only for near-zero initial guess.

**How can this method be generalized for any kind of network?**

During the modelling part of the thesis, the first approach was to find the equations for small systems and then implement a linearization method to obtain a linear system solvable with MATLAB. The next step was to define a general form that allowed to find the solution of any type of network meeting the solvability requirements. In order to test the general validity of the method, a number of different networks has been tested and the results analysed by hand to make sure that the solution was correct. Any network can be solved if the topology and the data on the different nodes is known.

**How can this method be applied to a standardized IEEE European low-voltage test feeder?**

The IEEE European low-voltage test feeder must be adapted to fit the DC framework. In this sense, the topology is simplified in order to reduce the number of nodes and lines without affecting the physical results. The line model is reduced to a simply resistive one-line graph. The data on power consumption of the households is adapted in order to be input into the power flow solver and the MV-LV connection is set at 350 V. The test feeder is provided with a one-minute time-series for the power consumption, thus different steady-state calculations are needed to simulate one day of grid. With the method developed, only around 5 seconds were found sufficient to run one day of simulation. This shows that the computational method developed in the thesis is fast and efficient, and that it can be used for a number of diverse analyses.

**What are the applications of such tool once implemented?**

Through the case study presented in chapter 6, it was possible to assess the utility of the power flow tool for DC systems. It was seen how the presence of distributed generation, the electrification

of household heating and the penetration of electric vehicles will affect the grid causing power quality related issues, such as voltage dips and network congestion. Along with these analyses, N-1 analysis and the development of new market frameworks can be also thought of.

## 7.2 Further work and recommendations

In the following section, recommendations on further research on the topic of power flow analysis for DC systems are concisely presented.

- First, in further work it will be necessary to validate the power flow algorithm also with an experimental setup;
- In further work the overall analysis might be also including the losses in the power converters;
- The line model and, subsequently, the line equations can be updated taking into account the conductance G placed in parallel in order to extend the power flow method with higher precision to high voltage applications;
- As seen in the case study, in the future DSOs might use this type of analysis in order to better assess whose distributed generators and loads are contributing more to network losses and congestion. In this way, targeted billing techniques could be developed in order to give the burden of the system losses to those prosumers that are responsible for them;
- Since DC distribution grids and microgrids allow different types of network architectures (like homopolar and bipolar), this aspect should be taken into account in future developments;
- The results of this thesis and, especially, the power flow tool, can be further used in studies related to the DC microgrid environment for steady-state analysis.

# Appendix A: Fluid-Dynamic Model

The fluid-dynamic model takes into account different meteorological parameters in order to find the steady-state module temperature $T_M$ of the PV panels. The temperature is derived by considering conductive, convective and radiation heat exchange between the surface of the panel and the surrounding area. An overall display of the heat exchange is given in figure A1 below.

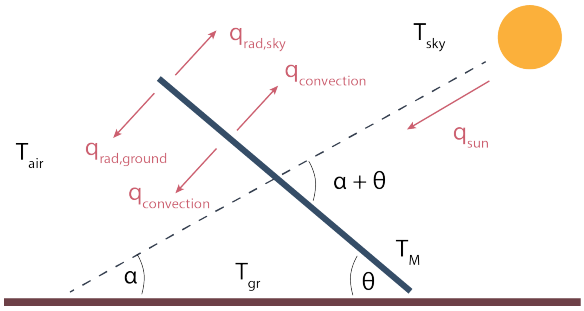


Figure A1: Heat exchange between a tilted module surface and the surroundings [52]

Operating a heat transfer balance over the panel, a first order differential equation is obtained. When a steady-state condition is achieved, the temperature of the module can be expressed by:

$$T_M = \frac{\alpha G + h_c T_a + h_{r,sky} T_{r,sky} + h_{r,gr} T_{r,gr}}{h_c + h_{r,sky} + h_{r,gr}}$$

where $h_c$, $h_{r,sky}$ and $h_{r,gr}$ are all function of $T_M$ and thus the equation needs to be solved by iteration. Once the temperature of the module has been found, the effects of this on the PV module performance can be evaluated. In order to do so, first the effects of irradiance $G_M$ on the external parameters of the PV module must be calculated according to:

$$V_{oc}(25°C, G_M) = V_{oc}(STC) + \frac{n k_B T}{q} \cdot \ln\left(\frac{G_M}{G_{STC}}\right)$$

$$I_{sc}(25°C, G_M) = I_{sc}(STC) \cdot \frac{G_M}{G_{STC}}$$

$$P_{mpp}(25°C, G_M) = FF \cdot V_{oc}(25°C, G_M) \cdot I_{sc}(25°C, G_M)$$

$$\eta_{mpp}(25°C, G_M) = \frac{P_{mpp}(25°C, G_M)}{G_M \cdot A_M}$$

Finally, combining the effects of temperature and irradiance, the module efficiency can be found:

$$\eta(T_M, G_M) = \eta(25°C, G_M)[1 + \kappa \cdot (T_M - 25°C)]$$

where $\kappa$ has a typical value of -0.0035/°C for crystalline silicon [52].

# Appendix B: Congestion Analysis

In this second appendix the congestion analysis from the case scenario is shown, in order to more thoroughly describe how the tool can be used for grid planning and microgrids design purposes. Figure B1 shows current levels over one day of simulation for the case with only PV, case with only EV and case with both PV and EV implementation.

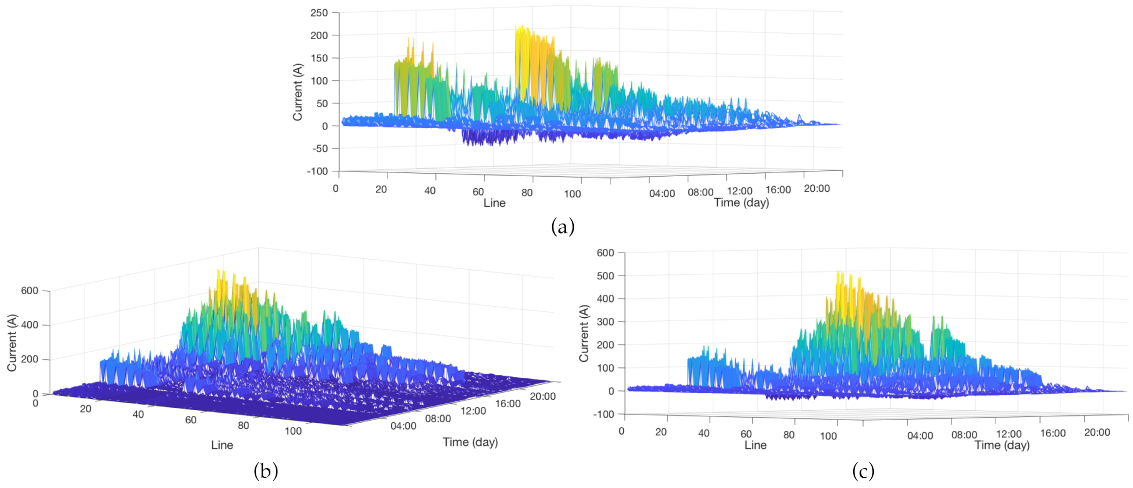


Figure B1: Current levels for one day of simulation: only PV (a), only EV (b) and PV and EV (c)

In figure B1 the simulation results are shown for the current levels in the case scenario exposed in chapter 6. For this first case without battery, it is relevant to note that some bidirectional currents are present when PV panels are integrated in the systems (sub-figure a). These currents go up to 50 A, while the highest current levels in general can be found closer to the MV-LV connection. As opposed to the line current graph shown in figure 5.6 - with the base IEEE case - in the central part of the day the PV panels help relieving line congestion in the upper part of the system. As expected, in this case the highest currents are present when the resistive heating in the households is turned on. In sub-figure (b) the EVs are implemented, showing that a much higher current level - up to 500 A - is required during the charging time. Finally, sub-figure (c) depicts the combined effects of PV and EVs, showing that, given to the different time in which these two technologies are affecting the grid, no particular relief is provided by the PV on the total load and thus total current congestion in the network.

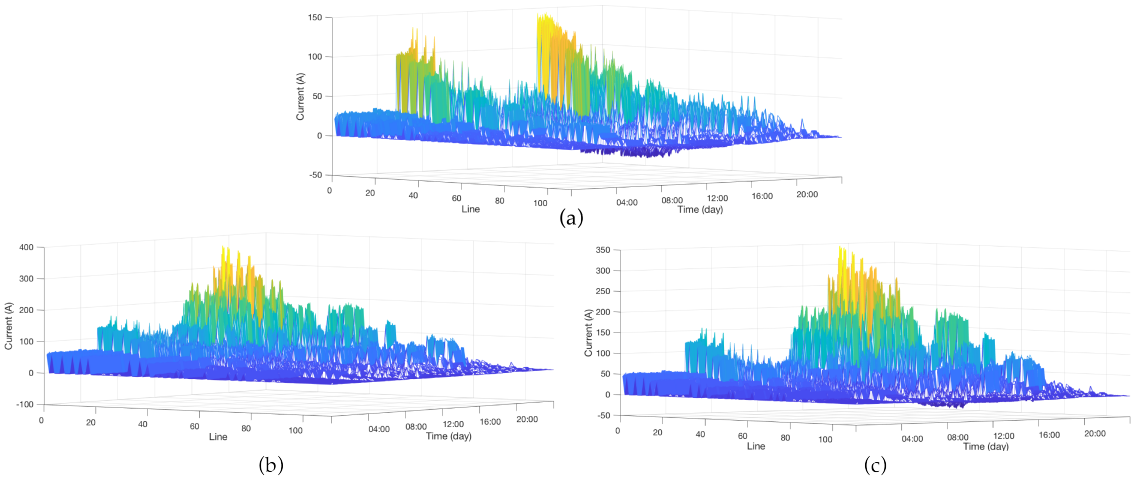


Figure B2: Current levels for one day of simulation with batteries: only PV (a), only EV (b) and PV and EV (c)

The second simulated scenario includes four grid-size batteries as implemented in chapter 6. In figure B2 it is possible to see that the general pattern is the same as in the previous figure. Nevertheless, the current levels are sensibly lower when the batteries are applied. In fact, maximum current levels in the case with only PV drops from 200 A to 150 A; in the case with only EV it drops from 500 A to 370 A; and in the case with both EV and PV the current levels go from 500 A to around 350 A. This shows how battery integration can have positive effects on the distribution network.

Ultimately, this analysis shows how power flow can be implemented in order to assess the current levels and therefore help in grid planning and distribution grids and microgrids operation.

# Appendix C: Conference Paper

# Steady-State Power Flow Analysis of DC Distribution Systems

Dario Chaifouroosh Mamagany, Nils H. van der Blij, Laura Ramirez-Elizondo and Pavol Bauer

***Abstract* -- The steady-state power flow analysis is used in electrical engineering to assess the flows of power in the network. Most algorithms aim to solve the non-linear power flow problem without taking into account characteristics typical of future dc networks, such as highly meshed topologies and the presence of power electronics interfaces. An innovative power flow method has therefore been developed in order to include different node behaviors, such as constant voltage, constant current, constant impedance, constant power and I-V droop control. This paper shows that it is possible to linearize the system equations considering the constant power node either as a current source or as a parallel of current source and impedance. Both methods allow very fast convergence for complex meshed networks and can therefore be adopted for diverse studies such as market analysis and N-1 redundancy analysis, among others. The IEEE European Low-Voltage Test Feeder is analyzed to provide an example of the application of the power flow method.**

***Index Terms* -- dc, distribution, microgrid, power flow, steady-state.**

## I. Introduction

RESEARCH on direct current (dc) systems has earned attention among academics and companies in the last decade. Several reasons can be addressed to explain this renewed interest on the topic. It appears inevitable that an energy transition towards renewable sources will take place, due to environmental concerns on global warming and depletion of traditional energy sources such as coal, oil and gas [1]. Nonetheless, this transition will require efforts on multiple levels, among which the most important are markets, policies and technological advancement [2].

In the last decade renewables have started playing an important role, which is expected to consolidate in the next 20 years [3]. In this framework, PV (photovoltaic), batteries, EVs (electric vehicles) and wind turbines play a vital role. Since three of the four above mentioned technologies produce a dc output [2], the implementation of a dc grid at medium and low voltage level becomes technically and economically viable [4]. Moreover, at consumption level, several loads are becoming more and more dc-based: LEDs for low power lighting, laptops and smartphones that can be charged through USB connection, electric vehicles with re-chargeable batteries, internet servers and data centers, marine and naval shipboard power systems. All these appliances can more efficiently be applied in direct current grids and it is expected that an even more massive *dc-fication* of society will take place in the next decades [4], [5].

The power flow problem consists of finding the steady-state operating point of an electric power system. More specifically, given the load in the buses and the power supplied by generators, the goal is to obtain all bus voltages and power flowing through all network components [6]. The power flow analysis is the most widely used for operating and planning, either as a stand-alone tool or as a sub-problem in complex processes such as stability analysis, optimization problems, flow-based market simulations, N-1 security assessment among others [7].

The contribution of this paper is the development of a power flow method for dc distribution systems that takes into account the behavior of the power grid of the future. In particular, the tool presented here provides the steady-state of the power system with constant voltage, current, impedance and power sources and loads, as well as droop control behavior. Moreover, the power flow calculation is possible for highly meshed networks and it is characterized by high computational speed and accuracy.

This paper is organized as follows: In Section II the lumped element line models used for distribution and transmission grids are shown and the three most common computational methods to solve the dc power flow problem are assessed. Section III introduces the power flow method developed in this paper. Section IV presents two methods for linearizing the power flow equation. Section V contains the application of the method to the IEEE European Low-Voltage Test Feeder. Finally, conclusions are drawn in Section VI.

## II. Review of Power Flow Methods

### A. Line Model

Transmission and distribution lines can be described and modeled to take into account the electromagnetic phenomena involved [8]. In Fig. 1 below, three of the most used models for single distribution lines are shown. Models with multiple lines need to take into account additional effects given by wire coupling. Among these effects, it is possible to mention leakage resistance and mutual inductance.

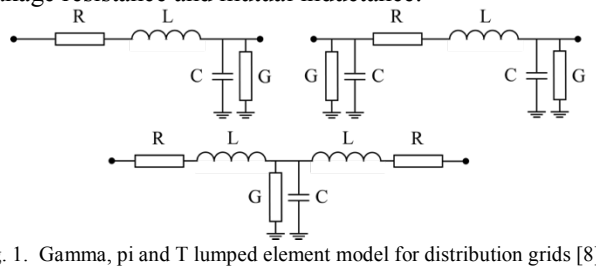


Fig. 1. Gamma, pi and T lumped element model for distribution grids [8].

The authors are with the Electrical Sustainable Energy Department, Technische Universiteit Delft, Netherlands (email: dario.chaifo@gmail.com)

The effects given by R, L, C and G are spread all along the line. The lumped element theory, instead, concentrates the properties of each of these characteristic into one component.

All the lumped element models shown in Fig. 1 can be solved with differential equations in order to describe the dynamic effects [8]. Since the power flow problem is a steady state analysis of the network behavior, it is possible to consider all the time variant behaviors as constant. Furthermore, since the scope of this paper is to provide a power flow method for distribution systems, the conductance G can be neglected. This is possible given that distribution lines exhibit a very high R/G ratio. Therefore, in the steady-state model the line can be considered as a simple resistor.

### *B. Computational Methods*

Three computational methods have mainly been used in literature for dc power flow analysis, namely: the Gauss-Seidel method, the Newton-Raphson method and the Backward/Forward sweep method [6], [7], [9].

The Gauss-Seidel method is based on a simple fixed-point iteration process [6], [9]. In general, a non-linear equation $f(x)$ is re-arranged in order to have the form $x = F(x)$. The variable $x$, representing the voltages, appears on both sides of the equation: on the left side, the updated value (k) needs to be found by using the old value (k-1) of voltage on the right side. The voltage values are updated for all nodes (except the slack node) at every iteration step, and the iterations are stopped when the voltage mismatch between the current and old values are below a given threshold.

The Newton-Raphson method allows to find the solution of the power flow by reducing the power mismatch between the specified and calculated power at the network nodes. To do so, the power mismatch equation is approximated with a Taylor series and, thus, the Jacobian matrix is used to obtain a relation between power and voltage mismatches. The voltages are updated and the Jacobian needs to be calculated and inverted at every iteration step, although some simplifications of the method are commonly used to avoid the computational burden related to the matrix inversion [6], [7].

The Backward/Forward sweep method has been successfully implemented in literature for studies on radial or weakly meshed distribution networks [9]. The in-feed bus, or root, is used as slack bus with known and constant voltage. Starting from the last bus and moving backward towards the root, the current injections are calculated dividing the given power by the voltage. The voltage at the load buses is not known, and thus an initial guess is made. Then, starting from the root and forward towards the load branches, the voltage values can be calculated applying Ohm's law, until the result is opportunely approximated.

Fig. 2 shows a simple distribution system with three nodes and two lines. Node 1 is at constant voltage set at 350 V. Nodes 2 and 3 are connected to constant power loads, consuming respectively 800 W and 750 W. The resistance of the lines are 0.642 Ω and 1.284 Ω, respectively.

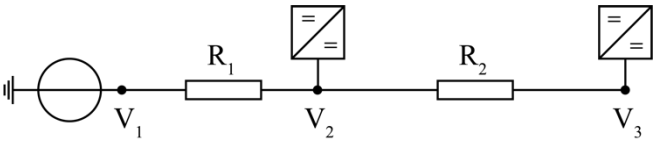


Fig. 2. Radial distribution feeder example with three nodes and two lines.

Fig. 3 shows the comparison of the voltage trajectory and the number of iterations needed to find the solution of the problem in Fig. 2.

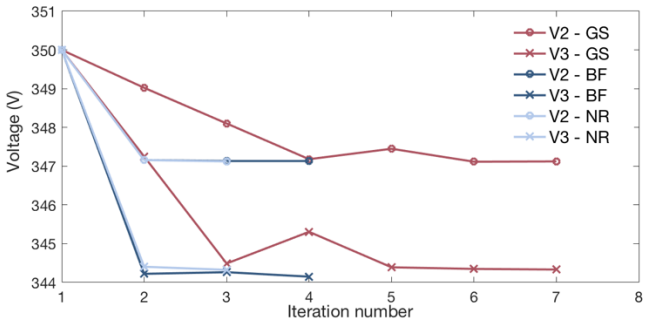


Fig. 3. State variable (voltage) trajectory for the two node voltages with three different power flow methods.

These three methods can only be adopted in network with both constant voltage (slack) and constant power nodes. Nonetheless, it is expected that the power grid of the future will feature also other node behaviors [8], [10], [11]. Thus, a power flow method for dc systems, that can be adopted in such network, is developed in the next sections.

## III. DC Power Flow

### *A. Three Node Behaviors*

Three elementary linear node behaviors can be modeled for dc networks: constant voltage, constant current and constant impedance behavior, depicted in Fig. 4. Note that the term *impedance* is used to differentiate from the line *resistance*, but in dc systems these two are equivalent. It will be shown that all the possible node behaviors can be modeled as combinations of these three elementary behaviors [8], [11].

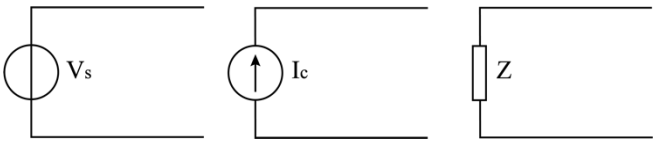


Fig. 4. Three elemental nodes behaviors: constant voltage, constant current and constant impedance.

For each constant voltage node in the network, the number of unknown state variables reduces by one. On the other hand, two sets of equations are used to model the constant current and impedance behaviors. One set of equations represents the current balance at every node $i$ with a constant impedance behavior expressed by $Z_i$ (in Ω):

$$\sum_j I_j - \frac{V_i}{Z_i} = 0\,, \tag{1}$$

where $I_j$ are the currents in the $j$ lines connected to the node $i$ and $V_i$ is the voltage in that node.

The second set of equations is applied for every node $i$ with

a constant current behavior $I_{Ci}$ and it is a node balance as represented by

$$\sum_j I_j + I_{Ci} = 0 . \tag{2}$$

A linear combination of (1) and (2), for instance, allows to model the I-V droop control as in (3). It is in fact possible to model the I-V droop as a Norton-equivalent circuit with a current source $I_{C,ref}$ - found dividing the reference voltage by the droop coefficient $k_I$ - and an impedance with value $k_I$ placed in parallel:

$$I_{C,droop} = \frac{V - V_{ref}}{k_I} = \frac{V}{k_I} - I_{C,ref} , \tag{3}$$

where $V_{ref}$ is the voltage reference set in the droop controller, while $I_{C,droop}$ is the current effectively drawn or delivered by the power converter.

### *B. Proposed Method*

The network can be completely described when in the model are taken into account both physical and topological characteristics. The latter element can be simply imported in form of oriented (or directed) incidence matrix. The incidence matrix **F** is a matrix with dimensions L by N, where L is the number of lines and N the number of nodes in the network. The incidence matrix is defined as a sparse matrix with the elements as:

$$\mathbf{F}(i,j) = \begin{cases} -1, & \text{if current flows from node } i \text{ to } j \\ 1, & \text{if current flows from node } j \text{ to } i \\ 0, & \text{otherwise} . \end{cases} \tag{4}$$

Taking into account the incidence matrix and the resistive line model, it is possible to find that the line balance (Ohm's law) in every line can be expressed in matrix form by

$$\mathbf{F} \cdot \mathbf{U_N} - \mathbf{R} \cdot \mathbf{I_L} = \emptyset , \tag{5}$$

where $\mathbf{U_N}$ is the vector of all the node voltages, $\mathbf{I_L}$ is the vector of all the line currents and **R** the diagonal matrix of the line resistances. Similarly, taking into account (1) and (2), the node balance at every node can be written in matrix form as

$$\mathbf{I_C} - \mathbf{F}^T \cdot \mathbf{I_L} - \mathbf{Z} \cdot \mathbf{U_N} = \emptyset , \tag{6}$$

where $\mathbf{I_C}$ is the vector of all the constant current nodes and **Z** is the vector of node impedances.

Considering (5) and (6) as a linear system of equations, the power flow problem can be represented in standard notation as

$$\mathbf{A} \cdot \mathbf{X} + \mathbf{B} = \emptyset , \tag{7}$$

where the matrix of coefficients **A** is defined as

$$\mathbf{A} = \begin{bmatrix} \mathbf{\Gamma} & -\mathbf{R} \\ -\mathbf{Z} & -\mathbf{\Gamma}^T \end{bmatrix} . \tag{8}$$

**A** is a square matrix with dimensions (N – $N_V$ + L) by (N – $N_V$ + L), divided into four sub-matrices as shown in (8). Matrix **Γ** is a reduced version of the oriented incidence matrix **F** with dimensions L by (N – $N_V$). In matrix **Γ** the columns corresponding to nodes with constant voltage behavior are taken out. Sub-matrix **R**, as shown in (5), is a diagonal matrix where the diagonal elements are the line resistances, so that:

$$\mathbf{R} = \begin{bmatrix} R_1 & 0 & \cdots & 0 \\ 0 & \ddots & \ddots & \vdots \\ \vdots & \ddots & \ddots & 0 \\ 0 & \cdots & 0 & R_L \end{bmatrix} . \tag{9}$$

Submatrix **Z** is a diagonal matrix, where the diagonal elements are the inverse of the node impedances, zero if the node does not have any impedance load. As for the matrix **Γ**, also **Z** is reduced, as the columns corresponding to the constant node voltages are taken out. **Z** is square and has dimensions (N – $N_V$) by (N – $N_V$):

$$\mathbf{Z} = \begin{bmatrix} \frac{1}{Z_1} & 0 & \cdots & 0 \\ 0 & \ddots & \ddots & \vdots \\ \vdots & \ddots & \ddots & 0 \\ 0 & \cdots & 0 & \frac{1}{Z_{N-N_V}} \end{bmatrix} . \tag{10}$$

The last elements to take into account are the constant voltages set at node level and the constant current loads in the system. A vector column **K** of dimensions 1 by (N – $N_V$ + L) is defined. The vector **K** contains L zeros and (N – $N_V$) constant current elements. This reflects the fact that the elements corresponding to constant voltage nodes are taken away. The constant voltages are included in a vector $\mathbf{V_C}$ of dimensions $N_V$ by 1, which is in turn multiplied by a matrix **Ψ**, of dimensions L by $N_V$. The matrix **Ψ** contains the columns of the incidence matrix **F** that refer to the nodes with constant voltage. It is therefore possible to say that **F** is found combining matrices **Γ** and **Ψ**. The two constant vectors have the same dimensions and can be therefore summed up into a single vector named **B** of known constant values defined

$$\mathbf{B} = \mathbf{K} + \mathbf{\Psi} \cdot \mathbf{V_C} . \tag{11}$$

From (7), the solution vector **X** is found as shown in (12):

$$\mathbf{X} = \begin{bmatrix} \mathbf{U_N} \\ \mathbf{I_L} \end{bmatrix} = -\mathbf{A}^{-1} \cdot \mathbf{B} . \tag{12}$$

Clearly, the possibility of finding a solution of the problem is limited to the case in which matrix **A** is non-singular, therefore invertible.

## IV. Two Linearization Methods

Since the power flow is a non-linear problem, it is necessary to linearize the equations of the constant power nodes, which relate the voltage of the *i*-th node to the current of all the lines connected to it as expressed in

$$V_i \cdot \left( \sum_j I_j \right) + P_i = 0 . \tag{13}$$

Two methods of linearizing (13) are given in this paper.

### A. Linearization as Current Source

The first method is found by rewriting (13) dividing both parts of the equation by $V_i$, as shown in (14). In this way the nodal information is stored in one single variable, which can be conceptualized as a current source as shown in Fig. 5, providing

$$\sum_j I_j + \frac{P_i}{V_i} = 0\,. \tag{14}$$

An initial guess $V_i^{(0)}$ is used to start the iteration process and find a current source as in

$$I_{Ci}^{(0)} = \frac{P_i}{V_i^{(0)}}\,. \tag{15}$$

The current source defined in (15) can be included in the linear equations for the current node balance and, once the system is solved, a new value $V_i^{(1)}$ is found. Convergence is checked for all node voltages against an arbitrary tolerance.

### B. Linearization as Current and Impedance in Parallel

The second linearization method tested is based on the concept of negative incremental impedance for a constant power behavior in the I-V framework [12]. This type of linearization guarantees convergence for a higher number of network combinations when compared to the previous linearization method (e.g. a network with only constant power and constant impedance nodes). In this case the constant power node is linearized as a node with constant current source and impedance placed in parallel, as shown in Fig. 5. From this, we know that (16) holds true for the current:

$$I_S = -I_C + \frac{V_S}{Z}\,. \tag{16}$$

Where $V_S$ is the voltage at the power converter node, $I_C$ is the value of the current source and $I_S$ the total current actually delivered by the converter.

From the concept of negative incremental impedance it is possible to find that

$$\frac{1}{Z} = \frac{dI_S}{dV_S} = \frac{d}{dV}\left(-\frac{P}{V_S}\right) = \frac{P}{V_S^2}\,. \tag{17}$$

If a correct solution value of the voltage $V_S$, which will be called $V_0$, is guessed, it is possible to find that

$$I_S = -\frac{P}{V_0} = -I_C + \frac{V_0}{Z}\,. \tag{18}$$

Substituting (17) into (18), we obtain the following equation for the current injected by the current source

$$I_C = 2\frac{P}{V_0}\,. \tag{19}$$

With this equation we are back at the behavior described in equation (16), but in this case we have defined values for both $I_C$ and $Z$, which depend on $P$ (known node information) and $V_S$, that needs to be found with an iterative process. In order to do so, $I_C$ and $Z$ are then both used in the computation imported into the matrix **A** as defined in (8).

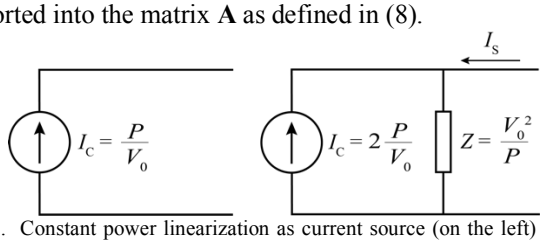


Fig. 5. Constant power linearization as current source (on the left) and as current source with impedance in parallel (on the right).

### C. Comparison of the Linearization Methods

A direct comparison between the two linearization methods previously described can be now carried out. In fact, the linearization as simple constant current source requires the vector **K** to be updated at every iteration, since the value of the linearized current varies. On the other hand, the linearization method as constant current and impedance requires that both matrix **A** and vector **K** are updated at every iteration step. In the latter case, the inverse of matrix **A** needs to be computed as well at every iteration step. This operation makes the first iteration method less computationally intensive, for each iteration, compared to the second one. However, linearizing as current source and impedance has proven to give acceptable results in a lower number of iterations, compared to the linearization as only current source.

Fig. 6 shows the results from the example previously shown in Fig. 2. It is possible to see the number of iterations needed to solve the small three-nodes two-lines network is between 2 and 3. This makes the developed method comparable to the Newton-Raphson in terms of number of iterations, as seen in Fig. 3.

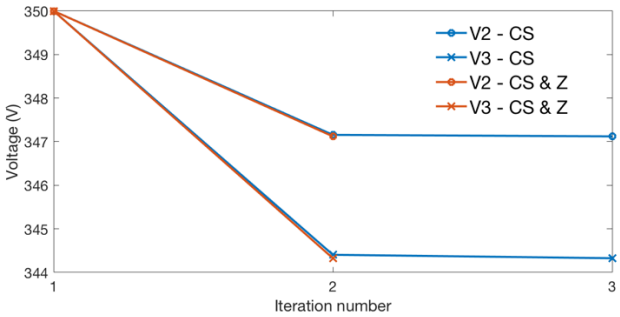


Fig. 6. State variable (voltage) trajectory for the two node voltages with the two linearization methods proposed.

However, some special cases can be drawn since it is not possible to find a solution for every combination of nodes in the system. If all nodes are constant power nodes, the computation will not converge to a solution, regardless of the type of linearization used. Moreover, a system with only constant current nodes is also not solvable, because the matrix **A** would be singular and therefore not invertible. This holds true for any computational method, since the power flow, in general, requires at least one constant voltage (or slack) node to balance the losses along the lines [6], [9], [11].

## V. Application To The IEEE European Low-Voltage Test Feeder

The implementation of the power flow method presented in this paper on the IEEE European Low-Voltage test feeder gives the opportunity to test it for a more realistic network

topology, with more realistic cable data and load shapes over one full day, with a one-minute accuracy.

### *A. Description of the test feeder*

The European Low-Voltage Test Feeder is a 416 line-to-line voltage radial system, based on a topology found in the United Kingdom [13]. The test network is provided by the IEEE Test Feeders Working Group and contains information about bus coordinates, line codes, loads, load shapes, source and transformer at the MV-LV interface. In particular, about the topology, the network is provided with 906 nodes (buses) and 905 lines (branches). The number of loads is 55. It is clear that the topology can be simplified in order to have faster computation, without affecting the results [14].

The simplification approach is the following: if one node is connected to only other two nodes (one preceding and one successive), then that node can be deleted and the resistance of the two lines can be summed up. On the other hand, if one node is connected to three or more other nodes, then that node is maintained and it will behave as a passive node (not generating nor absorbing active power). In Fig. 7 the simplified version of the test feeder, with 111 nodes and 112 lines, is shown with different types of nodes.

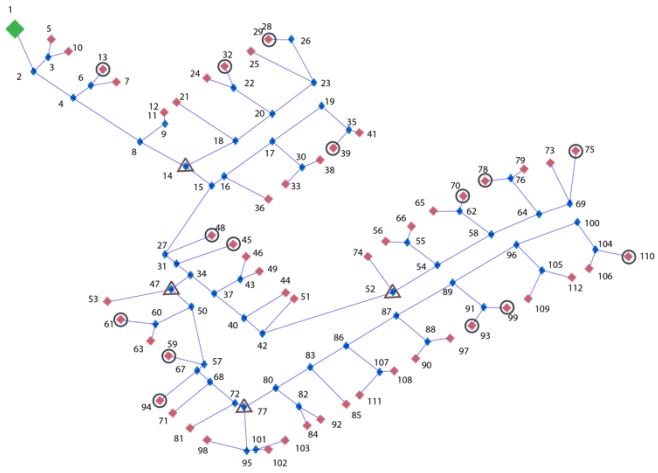

Fig. 7. IEEE European Low-Voltage Test Feeder simplified topology, with node numbers and node behaviors: constant voltage (in green), constant power loads (in red), constant impedance heating (circle) and droop-control batteries (triangle).

Node 1, in green, represents the MV-LV connection with the transmission system. This type of connection is generally implemented with a power converter (ac-to-dc or dc-to-dc) with a constant voltage setting [11], but a droop control can be implemented as an alternative.

In addition to the load-shape provided by IEEE, a constant impedance load of 48 Ω was added in parallel in order to simulate the behavior of electric resistive heating. The load was added between 6:30 and 7:30 in the morning and between 18:30 and 19:30 in the evening, as typical heating times.

Four grid-sized battery systems with droop control are also present in the network, as shown in Fig. 7. The reference voltage and droop coefficient are reported in Table I.

TABLE I
Batteries reference voltage point and droop coefficient

| Voltage reference | Droop coefficient |
|---|---|
| 350 V | 0.2 |

Many different choices for the constant voltage at the substation are available in literature and have been implemented in experimental setups [15]. For the purpose of this test, a level of 350 V has been used as suggested in recent literature studies [4]. A voltage level of 350 V line-to-ground dc voltage can be adopted in bipolar architectures to achieve higher voltage levels in a modular way. For example, industrial loads might require higher power and be therefore supplied with 700 V or 1400 V. This allows to keep the distribution network voltage level under the standard definition of low voltage, which is set at 1500 V [4].

### *B. Application of the proposed power flow method*

One of the major concerns in dc distribution grids is whether the voltage levels will remain within limits all along the feeder. In absence of distributed generation it is expected that, in any load condition, the voltage will show a decreasing fashion moving from the substation towards the end of the feeder. Fig. 8 below shows the node voltage shapes for one day simulation.

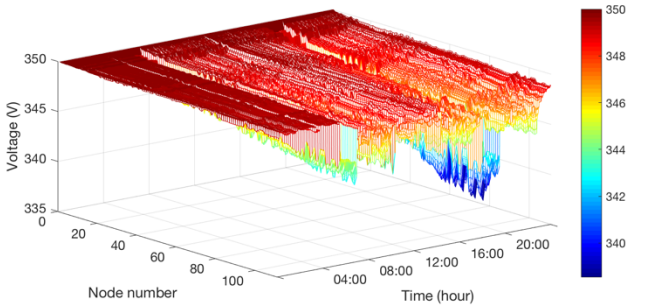


Fig. 8. Node voltage shapes for the IEEE test feeder (one day of simulation).

It is clear that the higher the load levels, the lower will be the voltage in the nodes. A voltage fluctuation of ±5% is generally accepted by international standards for power quality, and it is expected the same will be applied for dc systems. The steady-state analysis shows that indeed the minimum value of 332.5 V is not reached. The node which is affected the most by the voltage dips is node 106, one of the electrically furthest nodes from the MV-LV connection.

Another important power flow result is represented by the line currents along all the lines of the distribution network. For grid planning and congestion analysis purposes, it is in fact interesting to evaluate the current levels and what are the most stressed line in the grid. The current shapes for the one-day simulation are shown in Fig. 9.

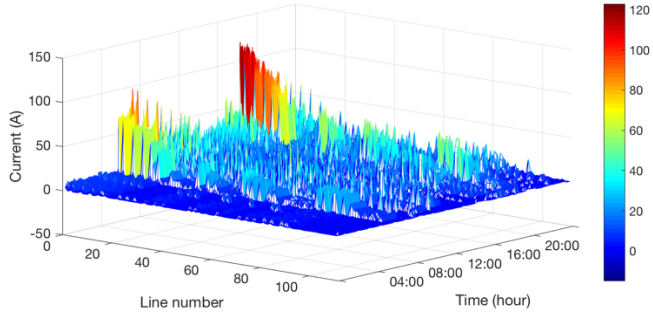


Fig. 9. Line currents for the IEEE test feeder (one of day simulation).

As expected, the highest current levels are found when the load demand is higher and towards the root of the low voltage feeder, since most of the power is retrieved from the medium

voltage grid. The highest current level found in the simulation is 122.89 A through the line connecting nodes 1 and 2, i.e. the one connecting to the medium voltage converter. Negative current is present due to the battery systems in the network, which introduce bi-directional flows.

One last direct output of the power flow calculation are the power losses along the distribution lines. The cumulative losses for one day of simulation are depicted in Fig. 10. Clearly, the higher the power demand in the system, the higher the line losses will be. The description of distribution line losses is a relevant outcome of the power flow analysis since it can be used to assess the grid impact of distributed loads and generators such as electric vehicles (EVs), photovoltaic panels and small wind turbines.

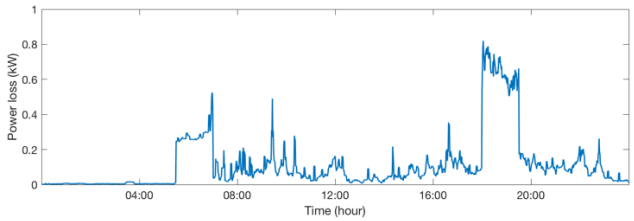


Fig. 10. Cumulative power losses in the distribution lines on one day of simulation for the IEEE test feeder.

Table II shows the average computation time - over 20 samples - needed to run the power flow algorithm in MATLAB for the 1440 time steps provided for the IEEE European Low-Voltage Test Feeder. The two types of linearization show rather different results. This can be explained by the fact that linearizing as current source and impedance requires an update of matrix **A** and, as a result, the inversion of this matrix at every iteration step. It has been determined that the sole inversion amounts for around 48% of the computation time. The computer used is a MacBook Pro with 2.6 GHz Intel Core i5.

TABLE II
Average computational time for one day of simulation

| Type of linearization | Average computation time |
|---|---|
| Current source | 3.8068 s |
| Current source and impedance | 5.7037 s |

## VI. Conclusions

It was found that a method based on Kirchhoff's equations and Ohm's law can be developed in order to solve the dc power flow problem taking into account diverse node behaviors. Three elementary linear behaviors have been identified: constant voltage, constant current and constant impedance. It has also been shown that the non-linear behavior of the constant power nodes can be linearized as a combination of the elemental behaviors. Two types of linearization of the constant power nodes have been presented in this paper: the first one linearizes the constant power node as a constant current source by guessing the value of the node voltage; the second type is obtained by linearizing the I-V behavior of the node with the concept of negative incremental impedance. The method is applied by finding the oriented incidence matrix of the network and classify the different nodes depending on their behavior and state. This approach allows to find a solution also for meshed or looped topologies.

The IEEE European Low-Voltage Test Feeder was used to evaluate the power flow tool. In order to adapt the test feeder to the dc framework, the topology is simplified in order to reduce the number of nodes and lines, without affecting the results. The line model is reduced to a simply resistive one-line graph. The data on power consumption of the households is adapted in order to be input into the power flow solver and the MV-LV connection is set at 350 V. The test feeder is provided with a one-minute time-series for the power consumption, thus different steady-state calculations are needed to simulate one day of grid. To prove the adaptability to different node behaviors, resistive heating with constant impedance and batteries with droop control have been also implemented in the network. With the method developed, only around 5 seconds were found sufficient to run one day of simulation. This shows that the computational method developed is fast and efficient, and that it can be used for diverse analyses.

## VII. References

[1] J. Wiseman, "The great energy transition of the 21st century: The 2050 zero-carbon world oration," *Energy Research & Social Science,* 2017.

[2] D. Manz, R. Walling, N. Miller, B. LaRose, R. D'Aquila and B. Daryanian, "The grid of the future: Ten trends that will shape the grid over the next decade", *IEEE Power and Energy Magazine*, vol. 12, no.3, pp. 26-36, 2014.

[3] International Energy Agency, "World Energy Outlook", 2017.

[4] L. Mackay, N. H. van der Blij, L. Ramirez Elizondo and P. Bauer, "Toward the universal dc distribution system", *Electric Power Components and Systems*, vol. 45, no. 10, pp. 1032-1042, 2017.

[5] L. Qi, J. Pan, L. Liljestrand, M. Backman, A. Antoniazzi, L. Raciti and M. Riva, "DC power distribution: New opportunities and challenges", in *IEEE Second International Conference on DC Microgrids (ICDCM)*, pp. 40-46, 2017.

[6] A. Gomez Expósito and F. L. Alvarado, "Load Flow", in *Electric Energy Systems: Analysis and Operation*, CRC Press, 2009.

[7] R. Teixeira Pinto, "Multi-Terminal DC Networks. System Integration, Dynamics and Control," Ph.D. dissertation, Dept. Electrical Sustainable Energy, Delft University of Technology, 2014.

[8] N. H. van der Blij, L.M. Ramirez-Elizondo, M. T. J. Spaan and P. Bauer, "A state-space approach to modelling dc distribution systems", *IEEE Transactions on Power Systems*, vol. 33, no.1, pp. 943-950, 2018.

[9] C. Jayarathna, P. Binduhewa, J. Ekanayake and J. Wu, "Load flow analysis of low voltage dc networks with photovoltaic", in *9th International Conference on Industrial and Information Systems (ICIIS)*, pp. 1-6, 2014.

[10] T. K. Vrana, J. Beerten, R. Belmans and O. Bjarte Fosso, "A classification of dc node voltage control methods for hvdc network", *Electric Power Systems Research*, vol.103, pp. 137-144, 2013.

[11] A. Garces, "Uniqueness of the power flow solutions in low voltage direct current grids", *Electric Power Systems Research*, vol. 151, no. 3, pp. 149-153, 2017.

[12] N. H. van der Blij, L.M. Ramirez-Elizondo, P. Bauer and M. T. J. Spaan, "Design guidelines for stable dc distribution systems," in *IEEE Second International Conference on DC Microgrids (ICDCM),* pp. 279–284, 2017.

[13] K. P. Schneider, B. Mather, B. C. Pal, C. W. Ten, G. Shirek, H. Zhu, J. Fuller, J. L. R. Pereira, L. Ochoa, L. Araujo, R. Duncan, M. Stifter, S. Paudyal, T. McDermott and B. Kersting, "Analytic considerations and design basis for the IEEE distribution test feeders", *IEEE Transactions on Power Systems*, vol. 33, no. 3, pp. 3181-3188, 2018.

[14] A. Ovalle, A. Hably and S. Bacha, *Grid Optimal Integration of Electric Vehicles: Examples with Matlab Implementation*, Springer International Publishing, 2018.

[15] S. Anand and B. G. Fernandes, "Optimal voltage level for dc microgrids", in *36th Annual Conference on IEEE Industrial Electronics Society (IECON)*, pp. 3034-3039, 2010.

# Bibliography


[1] J. Wiseman. The great energy transition of the 21st century: The 2050 zero-carbon world oration. *Energy Research & Social Science*, 2017.

[2] International Energy Agency. World Energy Outlook, 2017.

[3] D. Manz, R. Walling, N. Miller, B. LaRose, R. D'Aquila, and B. Daryanian. The grid of the future: Ten trends that will shape the grid over the next decade. *IEEE Power and Energy Magazine*, 12(3):26–36, May 2014.

[4] L. Mackay, N. H. van der Blij, L. Ramirez-Elizondo, and P. Bauer. Toward the universal dc distribution system. *Electric Power Components and Systems*, 45(10):1032–1042, 2017.

[5] Netherland Agency - Ministry of Economic Affairs, Agriculture and Innovation. Decentralized DC Power Networks. Experimenting with Intelligent Networks. Technical report, 2012.

[6] M. Tabari and A. Yazdani. A mathematical model for stability analysis of a dc distribution system for power system integration of plug-in electric vehicles. *IEEE Transactions on Vehicular Technology*, 64(5):1729–1738, May 2015.

[7] M. Barnes and A. Beddard. Voltage source converter hvdc links the state of the art and issues going forward. *Energy Procedia*, 24(Supplement C):108 – 122, 2012. Selected papers from Deep Sea Offshore Wind R&D Conference, Trondheim, Norway, 19-20 January 2012.

[8] L. Qi, J. Pan, L. Liljestrand, M. Backman, A. Antoniazzi, L. Raciti, and M. Riva. Dc power distribution: New opportunities and challenges. In *2017 IEEE Second International Conference on DC Microgrids (ICDCM)*, pages 40–46, June 2017.

[9] P. Fairley. Dc versus ac: The second war of currents has already begun [in my view]. *IEEE Power and Energy Magazine*, 10(6):104–103, Nov 2012.

[10] T. Dragievi, X. Lu, J. C. Vasquez, and J. M. Guerrero. dc microgrids part ii: A review of power architectures, applications, and standardization issues. *IEEE Transactions on Power Electronics*.

[11] L. Mackay, T. G. Hailu, G. C. Mouli, L. Ramírez-Elizondo, J. A. Ferreira, and P. Bauer. From dc nano- and microgrids towards the universal dc distribution system - a plea to think further into the future. In *2015 IEEE Power Energy Society General Meeting*, pages 1–5, July 2015.

[12] L. Meng, Q. Shafiee, G. F. Trecate, H. Karimi, D. Fulwani, X. Lu, and J. M. Guerrero. Review on control of dc microgrids and multiple microgrid clusters. *IEEE Journal of Emerging and Selected Topics in Power Electronics*, 5(3):928–948, Sept 2017.

[13] N. H. van der Blij, L. M. Ramirez-Elizondo, M. Spaan, and P. Bauer. A state-space approach to modelling dc distribution systems. *IEEE Transactions on Power Systems*, PP(99):1–1, 2017.

[14] PowerFactory - DIgSilent. `https://www.digsilent.de/en/load-flow-analysis.html`, 2018. Accessed: 2018-05-21.

[15] GridLAB-D Simulation Software. `https://www.gridlabd.org`, 2018. Accessed: 2018-05-21.

[16] M. L. Crow. *Computational Methods for Electric Power Systems*. CRC Press, 2010.

[17] A. Gomez Exposito, A. J. Conejo, and C. Canizares. *Electric Energy Systems: Analysis and Operation*. CRC Press, 2009.

[18] R. Texeira Pinto. *Multi-Terminal DC Networks. System Integration, Dynamics and Control*. PhD thesis, Delft University of Technology, 2014.

[19] L. Gan and S. H. Low. Optimal power flow in direct current networks. *IEEE Transactions on Power Systems*, 29(6):2892–2904, Nov 2014.

[20] P. Schavemaker and L. van der Sluis. *Electrical Power Systems Essentials*. John Wiley and sons, 2017.

[21] N. H. van der Blij, L. M. Ramirez-Elizondo, P. Bauer, and M. T. J. Spaan. Design guidelines for stable dc distribution systems. In *2017 IEEE Second International Conference on DC Microgrids (ICDCM)*, pages 279–284, June 2017.

[22] A. K. Marten and D. Westermann. A novel operation method for meshed hvdc overlay grids and corresponding steady state and dynamic power flow calculation principle. In *10th IET International Conference on AC and DC Power Transmission (ACDC 2012)*, pages 1–6, Dec 2012.

[23] W. M. Lin and J. H. Teng. Phase-decoupled load flow method for radial and weakly-meshed distribution networks. 143(1):39–42, Jan 1996.

[24] C. Jayarathna, P. Binduhewa, J. Ekanayake, and J. Wu. Load flow analysis of low voltage dc networks with photovoltaic. In *2014 9th International Conference on Industrial and Information Systems (ICIIS)*, pages 1–6, Dec 2014.

[25] G. T. Heydt. The next generation of power distribution systems. *IEEE Transactions on Smart Grid*, 1(3):225–235, Dec 2010.

[26] R. A. Aguirre and D. X. S. Bobis. Improved power flow program for unbalanced radial distribution systems including voltage dependent loads. In *2016 IEEE 6th International Conference on Power Systems (ICPS)*, pages 1–6, March 2016.

[27] J. Ekanayake, K. Liyanage, J. Wu, A. Yokohama, and N. Jenkins. *Smart Grid: Technology and Applications*. John Wiley and sons, 2012.

[28] A. Mahmoudi and S. H. Hosseinian. Direct solution of distribution system load flow using forward/backward sweep. In *2011 19th Iranian Conference on Electrical Engineering*, pages 1–6, May 2011.

[29] Jen-Hao Teng. A direct approach for distribution system load flow solutions. *IEEE Transactions on Power Delivery*, 18(3):882–887, July 2003.

[30] B. K. Babu and S. Maheswarapu. An efficient power flow method for distribution system studies under various load models. In *2016 IEEE Annual India Conference (INDICON)*, pages 1–6, Dec 2016.

[31] A. Garces. Uniqueness of the power flow solutions in low voltage direct current grids. *Electric Power Systems Research*, 151(3):149–153, July 2017.

[32] I. Ciornei, M. Albu, M. Sanduleac, and A. F. Martinez Palomino. Power flow formulation for lvdc microgrids with nonlinear load models. In *2017 IEEE Second International Conference on DC Microgrids (ICDCM)*, pages 445–451, June 2017.

[33] T. K. Vrana, J. Beerten, R. Belmans, and O. Bjarte Fosso. A classification of dc node voltage control methods for hvdc grids. *Electric Power Systems Research*, 103:137–144, October 2013.

[34] R. Teixeira Pinto, P. Bauer, S. F. Rodrigues, E. J. Wiggelinkhuizen, J. Pierik, and B. Ferreira. A novel distributed direct-voltage control strategy for grid integration of offshore wind energy systems through mtdc network. *IEEE Transactions on Industrial Electronics*, 60(6):2429–2441, June 2013.

[35] J. Lei, T. An, Z. Du, and Z. Yuan. A general unified ac/dc power flow algorithm with mtdc. *IEEE Transactions on Power Systems*, 32(4):2837–2846, July 2017.

[36] J. Beerten, S. Cole, and R. Belmans. Generalized steady-state vsc mtdc model for sequential ac/dc power flow algorithms. *IEEE Transactions on Power Systems*, 27(2):821–829, May 2012.

[37] E. Planas, J.Andreu, J. I. Garate, I. Martinez, and E. Ibarra. Ac and dc technology in microgrids: A review. *Renewable and Sustainable Energy Reviews*, 43:726–749, March 2015.

[38] J. J. Justo, F. Mwasilu, J. Lee, and J. W. Jung. Ac-microgrids versus dc-microgrids with distributed energy resources: A review,. *Renewable and Sustainable Energy Reviews*, 24:387–405, August 2013.

[39] D. Salomonsson and A. Sannino. Load modelling for steady-state and transient analysis of low-voltage dc systems. *IET Electric Power Applications*, 1(5):690–696, Sept 2007.

[40] T. Dragievi, X. Lu, J. C. Vasquez, and J. M. Guerrero. DC Microgrids Part I: A Review of Control Strategies and Stabilization Techniques. *IEEE Transactions on Power Electronics*, 31(7):4876–4891, July 2016.

[41] R. L. Burden, J. D. Faires, and A. M. Burden. *Numerical Analysis - 10th Edition*. Brooks Cole, 2015.

[42] IEEE Power and Energy Society test feeder working group resources. `http://sites.ieee.org/pes-testfeeders/resources/`, 2016. Accessed: 2018-03-24.

[43] K. P. Schneider, B. Mather, B. C. Pal, C. W. Ten, G. Shirek, H. Zhu, J. Fuller, J. L. R. Pereira, L. Ochoa, L. Araujo, R. Duncan, M. Stifter, S. Paudyal, T. McDermott, and B. Kersting. Analytic considerations and design basis for the ieee distribution test feeders. *IEEE Transactions on Power Systems*, PP(99), 2017.

[44] A. Ovalle, A. Hably, and S. Bacha. *Grid Optimal Integration of Electric Vehicles: Examples with Matlab Implementation*. Springer International Publishing, 2018.

[45] S. Anand and B. G. Fernandes. Optimal voltage level for dc microgrids. In *IECON 2010 - 36th Annual Conference on IEEE Industrial Electronics Society*, pages 3034–3039, Nov 2010.

[46] MathWorks - Improvements to tic and toc Functions for Measuring Absolute Elapsed Time Performance in MATLAB. `https://tinyurl.com/yc6o9jhc`, 2011. Accessed: 2018-04-17.

[47] A. Kumar and S.C. Srivastava. Ac power transfer distribution factors for allocating power transactions in a deregulated market. *IEEE Power Engineering Review*, 22(7):42–43, July 2002.

[48] A. Hoke, R. Butler, J. Hambrick, and B. Kroposki. Steady-state analysis of maximum photovoltaic penetration levels on typical distribution feeders. *IEEE Transactions on Sustainable Energy*, 4(2):350–357, April 2013.

[49] J. Ying Yong, V. K. Ramachandaramurthy, K. Miao Tan, and N. Mithulananthan. A review on the state-of-the-art technologies of electric vehicle, its impacts and prospects. *Renewable and Sustainable Energy Reviews*, 49:365–385, September 2015.

[50] K. Clement-Nyns, E. Haesen, and J. Driesen. The impact of charging plug-in hybrid electric vehicles on a residential distribution grid. *IEEE Transactions on Power Systems*, 25(1):371–380, Feb 2010.

[51] Panasonic. *Photovoltaic module N330 HIT VBHN330SJ47*, 2018.

[52] O. Isabella, K. Jager, A. Smets, R. van Swaaij, and M. Zeman. *Solar Energy: The Physics and Engineering of Photovoltaic Conversion, Technologies and Systems*. UIT Cambridge Ltd., 2016.

[53] Dutch PV Portal 2.0 - TU Delft. `https://pvportal-2.ewi.tudelft.nl`, 2018. Accessed: 2018-04-21.

[54] C. Gavriluta, J. I. Candela, C. Citro, J. Rocabert, A. Luna, and P. Rodríguez. Decentralized primary control of mtdc networks with energy storage and distributed generation. *IEEE Transactions on Industry Applications*, 50(6):4122–4131, Nov 2014.

[55] Alfen TheBattery Specifications. `https://alfen.com/en/energy-storage/thebattery-specifications`, 2018. Accessed: 2018-04-30.